

BORIC ACID INDUCED TRANSCRIPTOMIC CHANGES IN HEPG2 CELL LINE
AT GROWTH INHIBITORY CONCENTRATIONS

A THESIS SUBMITTED TO
THE GRADUATE SCHOOL OF INFORMATICS OF
THE MIDDLE EAST TECHNICAL UNIVERSITY
BY

AYŞEGÜL TOMBULOĞLU

IN PARTIAL FULFILLMENT OF THE REQUIREMENTS FOR THE DEGREE OF
DOCTOR OF PHILOSOPHY
IN
MEDICAL INFORMATICS

MARCH 2023

Approval of the thesis:

**BORIC ACID INDUCED TRANSCRIPTOMIC CHANGES IN HEPG2 CELL
LINE AT GROWTH INHIBITORY CONCENTRATIONS**

Submitted by AYŞEGÜL TOMBULOĞLU in partial fulfillment of the requirements for the degree of **Doctor of Philosophy in Health Informatics Department, Middle East Technical University** by,

Prof. Dr. Banu Günel Kılıç
Dean, **Graduate School of Informatics**

Assoc. Prof. Dr. Yeşim Aydın Son
Head of Department, **Health Informatics**

Assoc. Prof. Dr. Yeşim Aydın Son
Supervisor, **Health Informatics Dept., METU**

Examining Committee Members:

Prof. Dr. Nülüfer Tülin Güray
Biological Sciences Dept., METU

Assoc. Prof. Dr. Yeşim Aydın Son
Health Informatics Dept., METU

Asst. Prof. Dr. Aybar Can Acar
Health Informatics Dept., METU

Assoc. Prof. Dr. Bala Gür Dedeoğlu
Biotechnology Dept., Ankara University

Assoc. Prof. Dr. Nurcan Tunçbağ
Chemical and Biological Engineering Dept., Koc
University

Date: 31.03.2023

I hereby declare that all information in this document has been obtained and presented in accordance with academic rules and ethical conduct. I also declare that, as required by these rules and conduct, I have fully cited and referenced all material and results that are not original to this work.

Name, Last name: Ayşegül Tombuloğlu

Signature : _____

ABSTRACT

BORIC ACID INDUCED TRANSCRIPTOMIC CHANGES IN HEPG2 CELL LINE AT GROWTH INHIBITORY CONCENTRATIONS

Ayşegül Tombuloğlu

Ph.D, Department of Health Informatics

Supervisor: Assoc. Prof. Dr. Yeşim Aydın Son

March 2023, 91 pages

Boron is a micronutrient with many physiological roles. Although high levels of *in vitro* exposure to boric acid (BA), the physiologically abundant form of Boron, have been associated with cytotoxicity in several studies, relatively little is known about the cytotoxic mechanisms of BA. Herein, the gene expression profiles of BA treatment of HepG2 cells at three growth-inhibitory concentrations, IC₅₀, IC₂₅, and IC_{12.5}, were investigated with microarray technology. The analyses revealed key biological processes, pathways and regulatory processes elicited by *in vitro* BA treatment at growth-inhibitory doses. The pathway-level transcriptomic changes were consistent for all three levels of BA with some nuances. Regardless of the concentration, *cell cycle* and *apoptosis* were significantly overrepresented in the downregulated and upregulated lists of genes, respectively. These terms were less prominently enriched at the IC_{12.5} level. Furthermore, contrary to the higher concentrations, *DNA repair* was not significantly enriched at IC_{12.5}. At all three concentrations, *in vitro* BA treatment stimulates a marked increase in the expression of UDP-glucuronosyltransferase genes. All transcriptomic profiles exhibited significantly altered metabolism, especially lipid/steroid metabolism, despite some subtle differences concerning concentration. BA-associated regulation events were investigated through network analyses at all concentrations. Overall, BA-induced transcriptomic changes at growth-inhibitory concentrations pointed toward a senescence-like fate with early-apoptotic markers. Deregulation of DNA repair processes was noticeable at higher doses and might be linked to concentration-dependent genotoxicity examined in a previous study.

Keywords: Boric acid, Growth inhibition, Microarray, Network Analysis, HepG2

ÖZ

HEPG2 HÜCRE HATTINDA BÜYÜME KISITLAYICI DERİŞİMLERDE BORİK ASİT İLE OLUŞAN TRNSKRİPTOMİK DEĞİŞİKLİKLER

Ayşegül Tombuloğlu

Doktora, Sağlık Bilişimi Departmanı

Tez Yöneticisi: Doç. Dr. Yeşim Aydın Son

Mart 2023, 91 sayfa

Bor, birçok fizyolojik rolü olan bir mikrobeseindir. Bor'un fizyolojik formu olan borik aside (BA) yüksek düzeyde *in vitro* maruziyet, çeşitli çalışmalarda sitotoksisite ile ilişkilendirilmiş olsa da BA'nın sitotoksik mekanizmaları hakkında bilinenler nispeten azdır. Bu çalışmada, HepG2 hücrelerinin üç büyüme kısıtlayıcı derişimde (IC_{50} , IC_{25} ve $IC_{12.5}$) BA muamelesiyle ilişkili gen ekspresyon profilleri mikrodizin teknolojisi ile incelenmiştir. Büyüme kısıtlayıcı dozlarda *in vitro* BA muamelesi ile ortaya çıkan temel biyolojik süreçler, yolaklar ve düzenleyici süreçler analizlerle ortaya çıkarılmıştır. Yolak seviyesindeki transkriptomik değişiklikler, bazı nüanslarla birlikte üç BA seviyesinin tümü için tutarlıdır. Derişimden bağımsız olarak, *hücre döngüsü* ve *apoptoz*, sırasıyla aşağı regüle-edilen ve yukarı regüle edilen gen listelerinde önemli ölçüde fazla temsil edilmiştir. Bu terimler, $IC_{12.5}$ seviyesinde daha az belirgin bir şekilde yoğunlaşmıştır. Ayrıca, daha yüksek derişimlerin aksine, *DNA onarımı* $IC_{12.5}$ 'te önemli ölçüde yoğunlaşmamıştır. Her üç derişimde de *in vitro* BA muamelesi, UDP-glukuronosiltransferaz genlerinin ifadesinde belirgin bir artışı tetiklemiştir. Tüm transkriptomik profiller, derişimle ilgili bazı ince farklılıklara rağmen, önemli ölçüde değişen metabolizma, özellikle lipid/steroid metabolizması sergilemiştir. Ağ analizi, çeşitli Bor ile ilişkili düzenleyici olayları ortaya çıkarmıştır. Genel olarak, büyüme önleyici konsantrasyonlarda BA kaynaklı transkriptomik değişiklikler, erken apoptotik belirteçlerle senesens benzeri bir hücre kaderine işaret etmektedir. DNA onarım düzensizliği, daha yüksek dozlarda belirgindir ve önceki bir çalışmada araştırılan derişime-bağıli genotoksisite ile bağlantılı olabilir.

Anahtar Kelimeler: Borik asit, Büyüme kısıtlaması, Mikrodizin, Ağ Analizi, HepG2

ACKNOWLEDGEMENTS

I would like to express my deepest gratitude to my thesis advisor Assoc. Prof. Dr. Yeşim Aydın-Son for her tremendous contribution to my work with endless kindness and patience. I feel indebted for the long years of guidance and support she provided in my academic and personal challenges, which made it possible for me to complete this dissertation.

I am deeply grateful to Prof. Dr. Nülüfer Tülin Güray and Assoc. Prof. Dr. Nurcan Tunçbağ for a fruitful collaboration experience, guidance, enriching insights, and comments during my studies. I owe many thanks for their understanding in the face of setbacks; and for their friendly, open-minded approach while discussing and evaluating the thesis progress.

For valuable teamwork and meticulous performance of the biological experiments, I would like to express my heartfelt gratitude to Hülya Çöpoğlu and Eda Akyıldız.

I would like to thank the institutions and organizations that made this study possible during extraordinary challenges at the national and global levels. Special thanks should go to, The Turkish Technological Research Council for funding the project numbered 119Z551 via the 1002-Short Term Support Module; The METU Scientific Research Funds for project number YLT-704-2018-2696, moreover the providers of services on an affordable budget; The Boston University Microarray and Sequencing Resource Team for the microarray hybridization service, The BL-Turkey Team for the RNA transport service, and The Ankara University Biotechnology Institute Team for the previous microarray hybridizations.

I also sincerely thank The Middle East Technical University and The Informatics Institute for providing me with the graduate assistantship and great opportunities, the administrative staff of the institute for the flawless and sociable implementation of the procedures, The CanSyl Lab, particularly Asst. Prof. Dr. Aybar Can Acar, for his kind support with the computational facilities; Assoc. Prof. Dr. Bala Gür Dedeoğlu for the guidance in microarray services.

I owe many thanks to Umut Şener, whose company was of great importance to my well-being throughout the years; to the members of Aydın-Son Lab and the assistants of the institute who provided social and academic exchanges; and to Dr. Adem Yaşar Mülayim whose assistance with many technical hurdles was crucial in the last stage of the dissertation.

Finally, I would like to thank my family and relatives for all kinds of help and commemorate my grandparents, who passed away during my Ph.D. years. I would like to mention the unique place of my mother, who supported me generously in my difficult struggles with understanding, patience, and love.

TABLE OF CONTENTS

ABSTRACT	iv
ÖZ	v
ACKNOWLEDGEMENTS	vi
TABLE OF CONTENTS	viii
LIST OF TABLES	x
LIST OF FIGURES.....	xi
LIST OF ABBREVIATIONS	xiii
CHAPTERS	
1. INTRODUCTION.....	1
1.1 Significance of Boron in industry and biotechnology	2
1.2 Toxicology of Boron compounds.....	4
1.3 Molecular mechanisms of Boron toxicity	7
2. METHODS	11
2.1 Microarray Dataset	11
2.2 Quality Control and Preprocessing of Microarray Data.....	12
2.3 Identification of Differentially Expressed Genes	12
2.3.1 Differentially Expressed Genes at IC ₅₀ Level.....	12
2.3.2 Differentially Expressed Genes at IC ₂₅ and IC _{12.5} levels	13
2.3.3 Statistical validation	13
2.4 Heatmap Visualization	14
2.5 Pathway and Gene Ontology Enrichment Analyses and Visualization.....	14
2.6 Motif Analysis	14
2.7 Reconstruction of the PANDA Networks and Module Discovery.....	14

2.8	Calculation of the Optimal Coregulatory Subgraphs	15
3.	RESULTS	17
3.1	Microarray Data Quality	17
3.2	Identification of Differentially Expressed Genes	17
3.2.1	Differentially Expressed Genes at Half-maximal Inhibitory Concentration (IC ₅₀).....	17
3.2.2	Differentially Expressed Genes at Lower Inhibitory Concentrations (IC ₂₅ and IC _{12.5}).....	18
3.2.3	Statistical Validation of the Primary Findings.....	20
3.3	Enrichment Analyses.....	20
3.3.1	IC ₅₀ level	20
3.3.2	IC ₂₅ level	23
3.3.3	IC _{12.5} level	25
3.4	Network Analysis	26
3.4.1	IC ₅₀ level	26
3.4.2	IC ₂₅ level	32
3.4.3	IC _{12.5} level	37
3.5	Intersection of Coregulation Subgraphs.....	42
4.	DISCUSSION	43
	REFERENCES	53
	APPENDIX.....	69
	CURRICULUM VITAE	91

LIST OF TABLES

App. Table 1: RNA concentrations and quality metrics before Microarray hybridizations	69
App. Table 2: A summary of the statistical tests used for validation	80

LIST OF FIGURES

Figure 1: Volcano plot showing the transcripts identified at IC ₅₀ level	18
Figure 2: Volcano plots showing the transcripts identified at IC _{12.5} (top-figure) and IC ₂₅ (bottom-figure) levels	19
Figure 3: Top 10 Significantly enriched GO categories in HepG2 cells treated with boric acid at IC ₅₀ level (Published at Tombuloglu et al., 2020).....	21
Figure 4: Top 10 significantly enriched KEGG pathways in HepG2 cells treated with boric acid at IC ₅₀ level (Published at Tombuloglu et al., 2020).....	22
Figure 5: Enrichment terms network built for HepG2 cells treated with boric acid at IC ₅₀ level (Published at Tombuloglu et al., 2020).....	23
Figure 6: Top 10 significantly enriched GO categories in downregulated transcripts of HepG2 cells treated with boric acid at IC ₂₅ level.....	24
Figure 7: Top 10 significantly enriched GO categories in upregulated transcripts of HepG2 cells treated with boric acid at IC ₂₅ level.....	24
Figure 8: Top 10 significantly enriched GO categories in downregulated transcripts of HepG2 cells treated with boric acid at IC _{12.5} level.....	25
Figure 9: Top 10 significantly enriched GO categories in upregulated transcripts of HepG2 cells treated with boric acid at IC _{12.5} level	25
Figure 10: The CIRS-IC ₅₀ representing the regulatory interactions with increasing scores relative to the control (Z score < -1.96)	28
Figure 11: The WIRS-IC ₅₀ representing the regulatory interactions with decreasing edge scores relative to the control (Z score >1.96)	29
Figure 12: Selected <i>de novo</i> mini-modules of the IC ₅₀ -BA-regulatory network and the representative biological processes enriched within the list of module's gene targets....	31
Figure 13: The CIRS-IC ₂₅ representing the regulatory interactions with increasing scores relative to the control (Z score < -1.96)	33
Figure 14: The WIRS-IC ₂₅ representing the regulatory interactions with decreasing edge scores relative to the control (Z score >1.96)	34
Figure 15: Selected <i>de novo</i> mini-modules of the IC ₂₅ -BA-regulatory network and the representative biological processes enriched within the list of module's targets	36
Figure 16: The CIRS-IC _{12.5} representing the regulatory interactions with increasing scores relative to the control (Z score < -1.96)	38
Figure 17: The WIRS-IC _{12.5} representing the regulatory interactions with decreasing edge scores relative to the control (Z score >1.96)	39
Figure 18: Selected <i>de novo</i> mini-modules of the IC _{12.5} -BA-regulatory network and the representative biological processes enriched within the list of module's gene targets....	41

Figure 19: The intersecting coregulatory subgraph. The diamonds are the terminal nodes and the ellipticals are the Steiner nodes. The inset line graph depicts the logFC values of BA at three concentrations.	42
App. Figure 1: Boxplots of microarray log-signal intensities a, b) Raw and RMA normalized intensities of IC ₅₀ and control samples (Dataset 1) c, d) Raw, RMA normalized intensities of IC ₂₅ , IC _{12.5} and control samples (Dataset 2)	70
App. Figure 2: Cluster dendrograms of a) IC ₅₀ and control samples (Dataset 1) b) IC ₂₅ , IC _{12.5} and control samples (Dataset 2)	71
App. Figure 3: MA plots of a) IC ₅₀ and control samples (Dataset 1) b) IC ₂₅ , IC _{12.5} and control samples (Dataset 2).....	72
App. Figure 4: PCA plots of a) IC ₅₀ and control samples (Dataset 1) b) IC ₂₅ , IC _{12.5} and control samples (Dataset 2).....	73
App. Figure 5: Parameter selection at the construction of optimal coregulatory subgraphs	74
App. Figure 6: Heatmap of the top 2500 genes with the highest variance in fRMA normalized microarray samples	75
App. Figure 7: Heatmap of the known housekeeping genes of fRMA normalized microarray samples	76
App. Figure 8: Optimal coregulatory graph at IC ₅₀ , o: Steiner, \diamond : Terminal, LFC: [-3.4,4]	77
App. Figure 9: Optimal coregulatory graph at IC ₂₅ , o: Steiner, \diamond : Terminal, LFC: [-3.5,5.6]	78
App. Figure 10: Optimal coregulatory graph at IC _{12.5} , o: Steiner, \diamond : Terminal, LFC: [-3, 4.2]	79
App. Figure 11: Map of downregulated gene lists found in the statistical tests	81
App. Figure 12: Map of upregulated gene lists found in the statistical tests	82
App. Figure 13: Boxplots of microarrays after vsn+quantile normalization	83
App. Figure 14: Volcano plots obtained from VSN+quantile normalized datasets.....	84
App. Figure 15: Boxplots of IC _{12.5} dataset after rma normalization (standalone eBayes test).....	85
App. Figure 16: Boxplots of IC ₂₅ dataset after rma normalization (standalone eBayes test)	86
App. Figure 17: Boxplots of IC ₅₀ dataset after rma normalization (standalone eBayes test)	87
App. Figure 18: Volcano plot of the eBayes test results of IC _{12.5}	88
App. Figure 19: Volcano plot of the eBayes test results of IC ₂₅	89
App. Figure 20: Volcano plot of the eBayes test results of IC ₅₀	90

LIST OF ABBREVIATIONS

BA	Boric Acid
RNA	Ribonucleic acid
ATP	Adenosine triphosphate
NAD	Nicotinamide triphosphate
FAD	Flavin adenine dinucleotide
mRNA	Messenger RNA
B	Boron
O	Oxygen
LD₅₀	Median lethal dose
cADPR	Cyclic ADP ribose
PCR	Polymerase chain reaction
cDNA	Complementary DNA
RMA	Robust multiarray
IC₅₀	Inhibitory Concentration 50%
IC₂₅	Inhibitory Concentration 25%
IC_{12.5}	Inhibitory Concentration 12.5%
ANOVA	Analysis of Variance
logFC	Log fold-change
LFC	Log fold-change
BH	Benjamini-Hochberg
fRMA	Frozen RMA
DEG	Differentially Expressed Genes
FDR	False discovery rate
GO	Gene Ontology
MF	Molecular function
BP	Biological process
CC	Cellular component
KEGG	Kyoto Encyclopedia of Genes and Genomes
DNA	Deoxyribonucleic acid
TF	Transcription factor
CIRS	Consolidating Interaction Regulatory Subnetwork
WIRS	Weakening Interaction Regulatory Subnetwork

PCA Principal component analysis
NAFLD Non-alcoholic fatty liver disease

CHAPTER 1

INTRODUCTION

Boron (B) is the fifth element in the periodic table and is one of the most widely distributed elements in the world. In nature, it does not exist in elemental form but is included in the composition of minerals as borate. Boron minerals are of strategic importance for Turkey since 62% of the global borax mines are localized in Turkey, and Boron-based products contribute significantly to the export revenues (Poslu & Arslan, 1995)

Boron has been attributed biological and evolutionary significance due to its chemical properties. It can form various biomolecular interactions mainly by forming complexes with cis-diol groups. In this way, Boron crosslinks polysaccharides in plant cell walls and phenolic byproducts. Moreover, it can bind ribose in central molecules like RNA, ATP, NAD, and FAD (Power & Woods, 1997). Borates might also contribute to regulating enzymatic reactions by chelating with histidine and serine in the active site of serine proteases (Hunt, 1998).

Through the ability to form relatively stable cis-diol bonds, borates might have catalyzed ribose formation and contributed to nucleic acid evolution. Moreover, borates might have catalyzed the formation of precursors of central biomolecules like amino acids and carboxylic acids (Saladino et al., 2011).

Boron might be central to the RNA and amino-acid metabolism demonstrated in diverse experimental settings. Yeast responds to Boron toxicity by undergoing metabolic alterations in the synthesis of RNA and amino-acid (Ulusik, Kaya, Fomenko, et al., 2011; Ulusik, Kaya, Unlu, et al., 2011). In an acellular assay, 10 mM boric acid led to a massive increase in mRNA synthesis (Dzondo-Gadet et al., 2002). Boric acid might also inhibit the second step of RNA splicing in a reversible and concentration-dependent manner (Shomron & Ast, 2003).

Boron is an essential micronutrient in plants, some bacteria, algae, frogs, and fish. World Health Organization classified it as “potentially essential” for humans. Despite a broad spectrum of evidence regarding the beneficial health effects of Boron, its essentiality in humans and higher animals remains controversial due to methodological limitations (Sosa-Baldivia A et al., 2016).

Many researchers assume boric acid is the naturally occurring form of Boron within the body. Boric acid is eliminated from the human body with a half-life of approximately 21 hours when taken by intravenous injection or orally. Since breaking the B-O bond requires very high energy, boric acid is removed from the body and filtered through the kidneys without any metabolic changes (Murray, 1998).

Boron products are widely consumed, yet our knowledge about the mechanisms of Boron toxicity is limited. Mechanistic understanding of Boron toxicity is important for the safety of employees of the Boron industry and those who consume Boron-containing products. In this chapter, the growing techno-industrial significance of Boron will be briefly covered, and current literature on the toxicity and the molecular mechanisms elicited by Boron-based chemicals will be explored.

1.1 Significance of Boron in industry and biotechnology

Boron is used in the manufacture of glass, pottery, perborates, wood conservatives, fire extinguishers, paper, and agricultural products (Schubert, 2003). Besides its use in a broad spectrum of industrial commodities, Boron has many potential applications as an input to novel products (Ciani & Ristori, 2012). According to a survey between 1981-1983, nearly 500000 workers were exposed to boric acid of approximately 140000 tonnes. In 1991, the estimated amount of Boron compounds produced was about 3 million tonnes (Moorman et al., 2000). Boron compounds have attracted much attention in recent decades as potential drug and biomedical product components. An example is the cancer drug that treats multiple myeloma and mantle cell lymphoma with the active compound bortezomib (Chen et al., 2011). *Boron Neutron Capture Therapy* is a promising method to eliminate tumors around the neck and the head with minimal damage to surrounding healthy tissues (Ahmad & Alsaad, 2007). The ability of Boron compounds to interact with the carbohydrates integrated within the cell membrane makes them good candidates for the functionalization of nano-transport systems in gene therapy (Piest & Engbersen, 2011). As an antimicrobial agent, Boron compounds are being studied for the prevention of contamination of urine (Appannanavar et al., 2013; Lum & Meers, 1989), the therapy of *trichomonas vaginalis* (Brittingham & Wilson, 2014) and otomycosis (Del Palacio et al., 2002). Anti-genotoxic effect against numerous chemicals (Turkez et al., 2012), dietary benefits in health and development (Hunt, 2012), anti-inflammatory effect (Cao et al.,

2008), roles in wound healing (Benderdour et al., 2000), and cellular differentiation (Apdik et al., 2015; Ying et al., 2011) are among the many uses of Boron.

Boron-derived chemicals possess substantial therapeutic potential due to biochemical characteristics (Hunter, 2009; Soriano-Ursúa et al., 2014). Recently, new drugs were discovered by scanning a library of chemicals in which Boron was added sporadically (Hunter, 2009). Studies indicate the protective role of Boron supplementation in daily diet on prostate cancer and cervical cancer (Cui et al., 2004; Korkmaz et al., 2007; Müezzinoğlu et al., 2011). Anti-proliferative effect of boric acid/borax has been demonstrated with DU-145, LNCaP, and HepG2 cell lines (Barranco & Eckhert, 2004; Wei et al., 2016).

The wide range of uses and potential applications in medical fields lead to numerous studies on Boron toxicity (Dieter, 1994; Duydu et al., 2011; El-Dakdoky & Abd El-Wahab, 2013; Farfán-García et al., 2016; Ku et al., 1993; Scialli et al., 2010; Soriano-Ursúa et al., 2014; Tavit Sabuncuoglu et al., 2008; Weir & Fisher, 1972). On the other hand, biomolecular toxicity mechanisms of Boron in animals have yet to be studied extensively.

1.2 Toxicology of Boron compounds

Since many Boron-containing compounds are processed to boric acid in the body as a final product that is not further metabolized due to the high energy required to break the B-O bond, many toxicity studies focus on boric acid than other Boron containing compounds (Murray, 1998). At high doses, boric acid is detrimental to many mammalian organisms. In various rat strains, LD₅₀ of boric acid was determined to be 3000mg/kg-5000mg/kg, and LD₅₀ of borax is 4500mg/kg-6000mg/kg (Weir & Fisher, 1972). An increase in incidences of death was observed in rats fed with diets supplemented with boric acid (Dieter, 1994). In CD1 mice, LD₅₀ of boric acid was found to be 2150mg/kg, whereas various Boron-containing compounds exhibited LD₅₀ values ranging between 460mg/kg and 2600mg/kg (Soriano-Ursúa et al., 2014).

The most remarkable effects of boric acid treatment in animals at chronically and sub-chronically toxic doses are developmental and reproductive. Dose-associated reproductive toxicity was observed in rats fed with food containing varying doses of boric acid for nine weeks. Doses in the 3000-4500 ppm range lead to restricted sperm formation. In the 6000-9000 ppm range, irreversible testicular atrophy occurred (Ku et al., 1993). Developmental abnormalities were seen in the progeny of rats and mice fed with food supplemented with 0.1%-0.4% boric acid during their pregnancy. Boric acid was associated with increased prenatal deaths and decreased pup body weights. Expansion of lateral ventricles in the brain and shortened rib XIII are among the abnormal developmental manifestations of a high-level boric-acid diet in these animals (Heindel et al., 1992).

Boric acid has been identified as one of the four chemicals that should be prioritized in reproductive toxicity studies due to the heavy industrial use and the adverse reproductive effects observed in animal experiments (Moorman et al., 2000). In many studies involving employees exposed to high doses of Boron, no notable adverse effects on reproduction were found. In a survey carried out with 542 workers, any significant association could not be found between Boron exposure and fertility (Whorton et al., 1994). Any difference in reproductive performance and semen quality was not observed for 75 workers in China subjected to high Boron levels (Scialli et al., 2010). In another study, the blood concentration of Boron in workers was measured as 499.2 ppb, which is far below the levels causing unwanted effects in animal studies (W. A. Robbins et al., 2010). In an investigation on Boron-exposed workers in Bandırma, any association of Boron exposure with any criteria of reproductive toxicity could not be drawn (Duydu et al., 2011).

On the other hand, in a large study carried out with 63 industrial workers, 38 people residing in an environment with high Boron levels and 44 people residing in a location with low Boron levels, significant statistical associations were found between the ratio of Y chromosome to X chromosome, sex frequency in newborn babies and Boron levels in various biological fluids (Robbins et al., 2008). Another study also examined a low Y:X chromosomal ratio in workers. Boron concentration in blood, semen, or urine, however, was not correlated with the ratio of sex chromosomes (Scialli et al., 2010). Although the mechanisms of reproductive effects induced by Boron are not studied extensively, findings indicate that boric acid leads to infertility in male animals by decelerating DNA synthesis (El-Dakdoky & Abd El-Wahab, 2013).

The genotoxic effect of Boron-containing compounds has been the subject of many studies, findings of which differ according to the type of the compound, applied dose, and the biological system. At low doses, rather than causing DNA damage, some borates can heal the damage caused by genotoxic species to a certain extent. When applied to lymphocytes, potassium tetraborate reduced oxidative damage at 1.25, 2.5, and 5 mg/ml concentrations (Çelikezen et al., 2014). In many studies boric acid acted as antioxidant reversing the genotoxic effects of chemicals such as paclitaxel (Turkez et al., 2010), aflatoxin (Turkez & Geyikoglu, 2010), titanium dioxide (Turkez, 2008), vanadium tetroxide (Geyikoglu & Turkez, 2008), lead, cadmium (Ustündağ et al., 2014), arsenic, bismuth, cadmium and mercury (Turkez et al., 2012).

Boric acid did not induce sister chromatid exchange when applied to human lymphocytes; chromosomal aberrations occurred only in high concentrations such as 400-1000 µg/ml (Arslan et al., 2008). Acute exposure to Boron and boric acid in zebrafish has led to dose-dependent genotoxic effects (Gülsoy et al., 2015). According to the micronucleus test chromosomal damage ratio was higher in the lymphocytes of workers exposed to Boron trifluoride and Boron trichloride than in workers who were not exposed to these chemicals (Winker et al., 2008). The bacterial mutagenicity of thirteen different Boronic acids was assessed with the Ames test. Twelve of thirteen Boron-containing compounds were positive in bacterial chemical mutagenicity (O'Donovan et al., 2011). However, four of the nine Boronic acids yielded positive results in genotoxicity tests performed with eukaryotic cells. Moreover, weak mutagenic effects were observed in mammalian cultures involving various borax ores (Landolph, 1985).

According to several case reports, boric acid poisonings result in kidney failure if not treated quickly enough (Corradi, Brusasco, Palermo, & Belvederi, 2010; Ideura et al., 1998; Schmutz & Gillet-Terver, 2003; Webb, Stowman, & Patterson, 2013). In these poisonings, rapid excretion of the boric acid through the urine before any damage to the kidney tissues is critical. Oliguria and anuria are seen in many patients as a result of the poisoning (Wong et al., 1964). Autopsies of children poisoned with high-dose boric acid did not reveal kidney glomerular changes. However, toxic nephrosis symptoms such as cloudy swelling, fat degeneration, and congestion were observed (Young et al., 1949). A 57-year-old man in Japan was poisoned after consuming disinfectants containing large amounts of boric acid and suffered kidney failure. Percutaneous renal biopsy performed 30 days later in the patient treated with hemodialysis showed signs of necrosis and degeneration in the renal proximal tubule epithelium (Ideura et al., 1998).

The link between Boron and chronic renal disease needs to be better understood due to a lack of studies. Boron is involved in vitamin D metabolism and both may be linked to chronic kidney disease (Swaminathan, 2013). It has been suggested that exposure to Boron and Boron-containing compounds may cause chronic kidney disease in Southeast Asia (Pahl et al., 2005). In a large-scale study in which boric acid was administered to rats at the subacute level, it was shown that Boron accumulates in the kidney tissue and causes histopathological results in the kidneys depending on the dose and time. Boron at the subacute level causes deterioration, particularly in proximal tubule tissue (Tavil Sabuncuoglu et al., 2008). In another study, tissue integrity, proximal tubule, and glomerulus damage were observed in the kidneys of rats who were fed 375 mg of boric acid per kg per day. It was observed that consuming Omega-3 and an equal amount of boric acid reduced kidney tissue damage (Nacar et al., 2014). In rats, it has been discovered that long-term low-dose Boron ingestion also has a harmful impact that vitamin C can counteract (Abdel-Hamied, 2015). Acute boric acid exposure in trout caused pathological changes such as glomerular edema, glomerulonephritis, deterioration of tubular epithelium, and hyaline deposition in the tubular lumen (Topal et al., 2015).

Boron is distributed similarly with little to no accumulation in soft tissues. It accumulates mainly in bones. In rats fed 9000 ppm boric acid for seven and 28 days, in addition to accumulation within the bones, the highest amount of B deposition was detected in the kidneys and adrenal tissues among the soft tissues (Moseman, 1994). Boron accumulation in tissues was investigated after intraperitoneal injection of Boronophenylalanine (BPA), sodiumborocaptate (BSH), and boric acid chemicals into rats. The highest amount of Boron among soft tissues was found in the kidney. For all three chemicals, the amount of Boron detected in the kidneys is higher than the amount of Boron in the blood (Chou et al., 2009). In dogs given 55 mg of BSH per kilogram, the Boron concentration reached its highest values in the kidneys and liver at the 2nd, 6th, and 12th hours (Kraft et al., 1994). The highest Boron accumulation in soft tissues was again in the kidneys in rats given 2-

25 mg of Boron daily for six weeks. The Boron concentration measured in the kidney for each dose is 1.5-2 times the plasma concentration (Samman et al., 1998).

In animal studies investigating the toxicities of boric acid at acute, chronically, and sub-chronically toxic levels, changes in kidney weight are commonly observed in animals fed with boric acid at various doses. Male and female rats fed 4500 ppm boric acid for 27 weeks showed a decrease in kidney/adrenal tissue weights compared to the control group. In rats that consumed 400 mg of boric acid for 45 days, kidney weights on the 10th and 30th days were lower than the control, but this effect was not observed on the 45th day (Tavil Sabuncuoglu et al., 2008). In various studies the kidney weights of pregnant animals consuming boric acid were observed to be higher than the control group in postnatal measurements (Heindel et al., 1992; Price et al., 1996).

The SLC4 family of proteins includes mammalian homologs of BOR1, known as the Boron transport protein in plants. These proteins, known as sodium bicarbonate transporters, are extensively expressed in the kidneys and regulate cellular pH (Frommer & von Wirén, 2002; Romero, 2005). NaBC1 is one of the mammalian homologs of the borate transport protein in plants. It is most expressed in the salivary gland and renal tubule. There is evidence that NaBC1 has functions in Boron transport, homeostasis, cell growth, and proliferation (Park et al., 2004a). However, according to the results of another study, this protein does not play a role in Boron transport (Ogando et al., 2013). SLC4A11 knock-out mouse mutant manifested changes in urine density and excretion (Gröger et al., 2010). The expression rate of SLC4A2 and SLC4A3 genes from the SLC4 family increased in HEK293 cells exposed to boric acid (Akbas & Aydin, 2012). Boron-supplemented feeding led to changes in NaBC1 expression in the small intestine and kidney in developing pigs (Liao et al., 2011).

1.3 Molecular mechanisms of Boron toxicity

Studying the mechanisms of chemical toxicity is becoming more important in risk assessment studies. Investigating action profiles of chemicals at the genome level is a new and popular area of research. Gene expression patterns in cell behavior might be more meaningful in toxicity inference than sole quantitative measurements of cell damage (Roberts et al., 1997).

Studies on Boron-dependent testicular toxicity have demonstrated that boric acid dose-dependently decreases the rate of DNA synthesis in germ cells and causes infertility in male animals. The anticarcinogenic potential of boric has been the subject of many investigations with many cancerous cell lines. Boric acid has been observed to suppress proliferation in different prostate cell lines without activating apoptotic pathways. The proliferation-suppressing effect is proportional to the *in vitro* concentration of boric acid

(Barranco & Eckhert, 2004). Boric acid binds to the cADPR molecule in the DU- 145 prostate cell line, reducing the calcium ion concentration in the luminal region of the endoplasmic reticulum (Kim, Hee, Norris, Faull, & Eckhert, 2006). It has been shown that boric acid at a concentration of 10 μ M inhibits proliferation by activating the EIF2 α pathway associated with endoplasmic reticulum stress (Kobylewski et al., 2016). When the osteoblastic cell line NOS-1 was cultured in a medium containing 0.1 mM boric acid, calcium ion flux across the cell membrane was increased. In this way, the Boron supplementation in the culture medium has been observed to increase osteoblastic activity (Capati et al., 2016). Boric acid has apoptotic effects at 1 mM concentration in healthy lymphocyte cells and the HL-60 acute leukemia cell line (Canturk et al., 2016). Treatment of HEPG2 cells with 4 mM borax has been reported to suppress proliferation by increasing the expression of apoptosis-related genes such as p53, Bcl-2, and Bax (Wei et al., 2016).

Microarray experiments have been performed on various species to understand better the molecular mechanisms underlying the biological responses to Boron deficiency or abundance.

Gene expression patterns of *Saccharomyces cerevisiae* cultured in a medium with high levels of Boron were scrutinized using microarrays. Microarray data analysis revealed that protein and amino acid metabolism gene were among the most differentially regulated genes in response to Boron stress (Kaya et al., 2009). Other genes were clustered in functional categories such as cell organization, signaling, electron transport, energy, transcription, and stress. Researchers identified ATR1 protein as a Boron efflux pump essential for tolerating yeast Boron stress. The transcription factor *gcn4* orchestrated the activity of ATR1 and *gcn2* mediated inhibition of protein synthesis in Boron-stress (Ulusik, Kaya, Fomenko, et al., 2011).

High concentrations of environmental Boron lead to plant toxicity, manifesting in arrested root growth. Microarrays customized for *A. thaliana* to investigate Boron toxicity revealed increased expression of genes involved in cell wall modification and genes acting in the ABA signaling pathway, which is essential in root growth. Expression levels of genes involved in water transport, food transport, and glucosinolate biosynthesis declined in response to Boron toxicity. Transcriptomic patterns accompanying toxic Boron levels are similar to mechanisms of water stress (Aquea et al., 2012). In another microarray study with a barley species sensitive to Boron toxicity, pathways associated with environmental stress were uncovered (Oz et al., 2009). In the roots of *A. thaliana* grown at Boron deficient conditions, 12 genes had over a 3-fold expression level. One of the genes known as NIP5 is a membrane protein and was validated with qRT-PCR (Takano et al., 2006). Microarrays designed for tobacco were hybridized with mRNA samples obtained at five different time intervals to understand the effects of Boron deprivation on a time course. Expression levels of 124 expressed sequence tags changed significantly in at least one of the intervals. Altered levels of expression were also confirmed with an independent

microarray experiment. Homology analysis showed that 33 genes are homologs of proteins with known functions. Among these are genes essential in metabolism, transcription, and protein modification (Kobayashi et al., 2004).

This study will examine the transcriptomic profile of HepG2 cells exposed to Boron using high-throughput technology. Gene lists obtained as a result of microarray analysis will be explored with network analysis which will facilitate the elucidation of toxicity mechanisms using the scientific knowledge in databases. Network analysis might also reveal clues about the physiological effects of BA.

CHAPTER 2

METHODS

2.1 Microarray Dataset

Microarray experiments were designed to study the gene expression changes in the HepG2 cell line as a response to boric acid treatment at different growth-inhibitory concentrations. The cell culture experiments were conducted at Güray Lab, METU Biological Sciences. HepG2 cells were grown at 3×10^5 cells/ml density within 35 mm cell culture dishes and treated with either 0.1% DMSO (control group) or boric acid dissolved in 0.1% DMSO (treatment group). The cells were cultured for 24 hours. Two separate sets of experiments were carried out to investigate the effects of boric acid treatment at three different concentrations. In the first experiment set, HepG2 cells were treated with 24 mM boric acid, the half maximal inhibitory concentration (IC_{50}). Total RNA samples were harvested from treated cells ($n=3$) and untreated cells ($n=3$) by Qiagen RNeasy total RNA isolation kit (Qiagen, Germany). The quality and amount of RNA samples were checked using Biodrop Nanodrop (United Kingdom). The absorbance ratio of 260/280 for all the RNA samples was in the 1.8-2.0 range, and the RNA integrity number was higher than 8.0. cDNA was prepared from RNA samples and subsequent microarray hybridizations at Ankara University Biotechnology Center. The samples were processed and hybridized to GeneChip® Human Gene-1.0-st. Affymetrix arrays according to the manufacturer's protocols.

In a later set, the cells were treated with boric acid at IC_{25} and $IC_{12.5}$ levels. Total RNA samples were harvested from cells treated with 12 mM boric acid (IC_{25} , $n=3$), 6 mM boric acid ($IC_{12.5}$, $n=3$), and untreated cells ($n=3$) by Thermo Scientific GeneJET RNA isolation kit (Thermo Scientific, USA). The RNA samples' quality and concentration were checked using Biodrop Nanodrop (United Kingdom). The absorbance ratio of 260/280 for all the RNA samples was in the 1.8-2.0 range. The samples were stored at -80°C . Samples were transferred to the Boston University Microarray Processing Unit in dry ice. Quality control and concentration measurements of the samples were repeated after the delivery.

The A260/A280 ratios were in the range of 1.8-2.0. Although some of the A260/A230 measurement ratios were slightly lower than the expected range (2.0-2.5), these were considered sufficient to continue hybridization (App. Table 1). Hybridizations of each sample were carried out with Affymetrix Human 1.0 ST microarray chip at Boston University Microarray Processing Unit.

As a result of the experiments, two sub-datasets jointly containing 15 CEL files were obtained. All subsequent analyses and plot visualizations were performed in R using R base and Bioconductor packages unless stated otherwise.

2.2 Quality Control and Preprocessing of Microarray Data

In order to check for the quality metrics of the datasets, Affymetrix online quality control module's source code was downloaded, and the quality control procedures were performed (Eijssen et al., 2013). Among many tests and quality metrics, the following were mainly used to evaluate the data quality. The relative technical quality of the microarrays was assessed with the RLE (Relative Log Expression) and NUSE (Normalized Unscaled Standard Error) metrics. The log-signal distributions of the raw microarray data and the RMA-normalized microarray data were examined by box plots. MA plots were used to investigate the signal-dependent technical quality of both raw and RMA-normalized microarray data.

The Limma package (Smyth, 2005) of Bioconductor was used for the preprocessing step. The data were normalized and summarized using RMA. Brainarray cdf hugene10sthsensgcdf version 23 (Dai et al., 2005) mapped the probe sets to Ensembl transcript codes. For network analyses, hugene10sthsensgcdf (Dai et al., 2005) was used.

2.3 Identification of Differentially Expressed Genes

2.3.1 Differentially Expressed Genes at IC₅₀ Level

Differentially expressed transcripts in HepG2 cells treated with boric acid at IC₅₀ level were found using eBayes moderated t-test from the limma package (Smyth, 2005). Statistically significant transcripts (BH adjusted $p < 0.05$) with a log₂-fold-change larger than two were selected as differentially expressed transcripts. The transcripts selected according to the filtering criteria were visualized with a Volcano plot. Upregulated and downregulated gene sets were determined by mapping the selected transcripts to official gene symbols using Biomart database October 2018 archive.

2.3.2 Differentially Expressed Genes at IC₂₅ and IC_{12.5} levels

User guide of the limma package (Smyth, 2005) was used to conduct ANOVA analysis to investigate the changes in transcript expressions depending on boric acid concentration. Then, statistically significant changes were determined for each treatment level using an eBayes t-test (according to predetermined contrasts). In this test, transcripts with a BH-corrected p-value less than 0.05 and showing a 2-fold logarithmic change in both directions were accepted as the changing list. The selected transcripts in each treatment group were visualized using Volcano plots. By determining the official gene symbols corresponding to the selected transcripts using Biomart database October 2018 archive, the downregulated gene list and the upregulated gene list were determined for each level.

2.3.3 Statistical validation

Follow-up tests were conducted to ensure the reliability and validity of the statistical tests used to find DEG lists at consecutive levels. Two separate procedures were used to determine the lists of upregulated and downregulated transcripts. At first, eBayes t-tests were carried out separately for each RMA-processed dataset of each inhibitory concentration. Secondly, the raw microarray data were preprocessed first using vsnrma, including background correction, vsn normalization, and summarization with median polish. Then quantile normalization was carried out. The two-step preprocessing procedure was necessary to combine data into a unified dataset with individual samples with similar distributions. One-way ANOVA and eBayes t-tests were conducted to determine transcriptomic changes within three levels according to three planned contrasts (IC₅₀-Control, IC₂₅-Control, IC_{12.5}-Control). Two distinct methods of multiple test adjustment were used to determine the differentially expressed transcript lists. The method 'separate' BH adjustment procedure was carried out for each planned contrast separately. In the global method, the BH adjustment was made by considering all the tests in all planned contrasts.

Results were compared with the previous findings to check for validity and any potential problems with the computation. To visualize how resulting lists relate to each other, upregulated and downregulated lists were first transformed into binary matrices, which were used to calculate cosine distance. Then correlation maps were built separately for upregulated and downregulated lists based on calculated cosine metrics.

2.4 Heatmap Visualization

All datasets were combined and normalized with fRMA (McCall et al., 2010), a variant of RMA that can compensate for the batch effect. The top 2500 genes having the highest variance within the integrated dataset were visualized using the software at the website heatmapper.ca (Babicki et al., 2016). Heatmap was also plotted with the fRMA normalized log-signals of the known housekeeping genes as a control.

2.5 Pathway and Gene Ontology Enrichment Analyses and Visualization

DAVID Bioinformatics platform tools (Huang et al., 2007) were used to identify pathways and gene ontologies enriched within the genes of interest. Upregulated and downregulated genes identified were submitted separately to the DAVID Online Bioinformatics Platform. Pathways and GO categories with Benjamini-Hochberg adjusted $FDR < 0.05$ were determined as significantly enriched pathways.

The joint list of differentially expressed genes from the IC₅₀ dataset was fed into the DAVID functional enrichment tool to conduct a subsequent enrichment analysis. Significant functional annotations for KEGG and Reactome pathways, GO-MF terms, GO-BP terms, and KEGG and Reactome pathways were remapped onto a broader integrated network using EnrichmentMap (Bader et al., 2014; Merico et al., 2010) and WordCloud (Oesper et al., 2011).

2.6 Motif Analysis

To obtain the motif list of transcription factors, the DNA sequences located at [-750, 250] position of the transcripts according to the transcription start site were downloaded from the Ensembl database, and the motif sequences were downloaded from the HOCOMOCO database (Kulakovskiy et al., 2013). The DNA sequences in the [-750, 250] position, were scanned with the FIMO program (Grant et al., 2011). Motif data, including possible transcription factor-gene relationships, were obtained for every transcript.

2.7 Reconstruction of the PANDA Networks and Module Discovery

PANDA analysis (Glass et al., 2013) was carried out using the pandaR package using the default settings. As the initial step, regulatory networks were obtained for each treatment condition and the respective controls. RMA normalized expression datasets, protein-

protein interaction data of transcription factors (Ravasi et al., 2010), and motif data from the previous step were provided as inputs. A separate analysis was carried out for each condition (IC_{12.5}, IC₂₅, IC₅₀, and both control groups). At the end of the analysis, a regulatory network, a coregulatory network, and an updated TF interaction table were obtained.

To obtain the condition-specific networks (difference networks), the difference in the scores of regulatory edges from the control and treatment networks was calculated. The difference network was centered and scaled to fit a normal distribution. The final Z-scores greater than 1.96 and lower than -1.96 are selected as the meaningful edges to obtain Consolidating Interaction (with higher regulation scores in treatment, $Z < -1.96$) and Weakening Interaction (with lower regulation scores in treatment $Z > 1.96$) Regulatory Networks.

The final networks were also filtered to involve only the selected gene list. As a result, two networks were obtained for each concentration, namely, Consolidating Interaction Regulatory Subgraphs (CIRS) and Weakening Interaction Regulatory Subgraphs (WIRS) with selected genes.

The ALPACA package (Padi & Quackenbush, 2018) revealed the differential modular structure of the resulting networks. The ALPACA algorithm was run with the combined regulatory edges of the control and treatment networks. The resulting communities were further narrowed down according to the differential modularity score, including the top 5 TFs and 50 target genes. Using a modified version of the liststogo function from the package, enrichment analyses were carried out with the lists of the top 50 target genes to find significant GO_BP and KEGG terms. The communities with significant terms (BH adj. $p < 0.05$) were kept while others were eliminated. The representative biological processes were chosen according to the following process. Among the terms changing in a 5-fold range of the minimal adjusted p-value, the term with the highest Odds Ratio was selected as the representative module process. For ease of interpretation, the organ-level terms were ruled out. The resulting communities were colored according to the module number and were visualized using the Cytoscape (Shannon et al., 2003).

2.8 Calculation of the Optimal Coregulatory Subgraphs

The forest module of OMICS-Integrator software (Tuncbag et al., 2016) was used to calculate optimal subgraphs from the coregulatory networks obtained with the PANDA algorithm. The input files were prepared with R, while the forest runs were performed within the Jupyter Notebook with Python 3 libraries. Omics-Integrator2 was installed from Github the example code was modified to carry out parameter sweeps with coregulatory networks for each condition.

Lists of DEG were provided as terminals with absolute log-fold-change values as the prizes. The first differential PANDA coregulatory network which was provided as the input network was obtained by calculating the difference between the treatment coregulatory network and the appropriate control coregulatory network. Probabilities were estimated from the centered and scaled edge weights of the differential coregulatory network using the formula $p=2*\text{pnorm}(-\text{abs}(E))$ where E represents normalized edge weights. Those edges with $p<0.1$ were selected as the input network, and estimated p-values were given as costs.

A total of 30 parameter sets were provided within the algorithm with beta values of 0.1, 0.25, 0.5, 1, 5, 10; omega values of 0.05, 0.5, 1, 2, 5, and a G value of 3. The parameter set beta=10, omega=5, G=3 for all three coregulatory networks retrieved the maximal coverage of terminals and many Steiner nodes (App. Figure 5). The resulting subgraph obtained with this parameter set was selected as the optimal coregulatory subgraph.

An intersection network was also built from the shared nodes in multiple coregulatory networks. The node size was determined based on the commonality in the three networks. The nodes were colored according to Average logFC, and the logFC values at each condition were added as a line graph inset within the nodes.

CHAPTER 3

RESULTS

3.1 Microarray Data Quality

The relative technical qualities of the microarray samples are comparable and valid (App. Figure 1-4). After RMA normalization, arrays show similar log-signal distribution (App. Figure 1). MA plots were used to investigate the signal-dependent technical quality of raw and RMA-normalized microarray data. Arrays have very little signal-related bias which disappeared after RMA normalization (App. Figure 3). The general structure of the data set and the clustering patterns of the samples were examined by PCA, dendrogram, and correlation graph methods before and after RMA normalization (App Figure 2,4). The clustering of the experimental groups in these plots was as expected after the RMA normalization. Microarray quality control analyses showed the sufficient quality of the microarray dataset and the suitability of the RMA normalized dataset for analysis.

3.2 Identification of Differentially Expressed Genes

3.2.1 Differentially Expressed Genes at Half-maximal Inhibitory Concentration (IC₅₀)

The eBayes moderated t-test was used to identify transcripts with variable expression levels in boric acid-treated HepG2 cells at the IC₅₀ level. 7116 transcripts had significantly different expression levels (BH adjusted $p < 0.05$) and more than two log-fold-change in expression in treated cells. 2805 transcripts were upregulated, and 4311 were downregulated among differentially expressed transcripts. The differentially expressed transcripts can be discerned as the blue points in the Volcano Plot (Figure 1). The

transcripts were mapped to official gene IDs using Biomart database October 2018 archive.

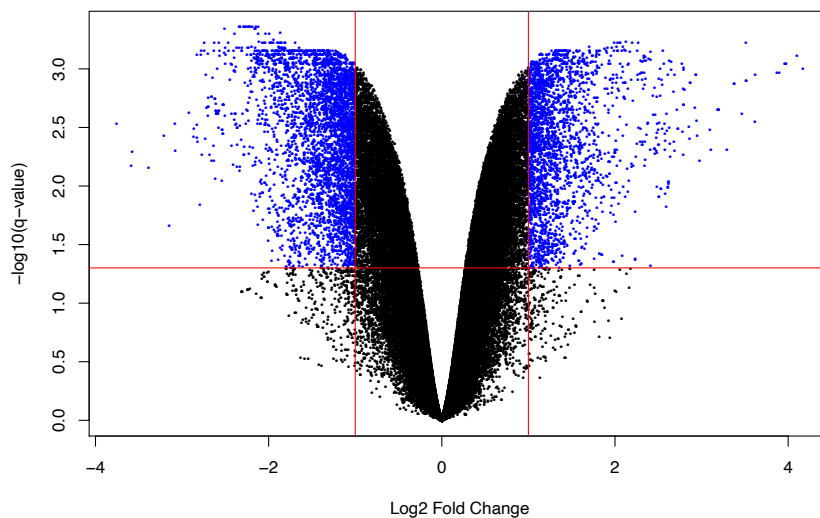


Figure 1: Volcano plot showing the transcripts identified at IC_{50} level

3.2.2 Differentially Expressed Genes at Lower Inhibitory Concentrations (IC_{25} and $IC_{12.5}$)

Data were analyzed with one-way ANOVA; then, statistically significant transcripts that changed at each boric acid concentration were determined by eBayes t-test. 13815 transcripts corresponding to 2469 genes at the $IC_{12.5}$ level, and 19643 transcripts corresponding to 3550 genes at the IC_{25} level were determined as the differentially expressed transcripts (BH adjusted $p < 0.05$ and $\logFC > 1$).

Volcano plots show that microarray hybridizations successfully elucidate the transcript profile whose expression is altered due to boric acid. Transcripts above the red lines (BH adjusted $p < 0.05$, $\logFC > 1$) were selected as the group whose expression changed (Figure 2). The transcripts were mapped to official gene IDs using Biomart database October 2018 archive.

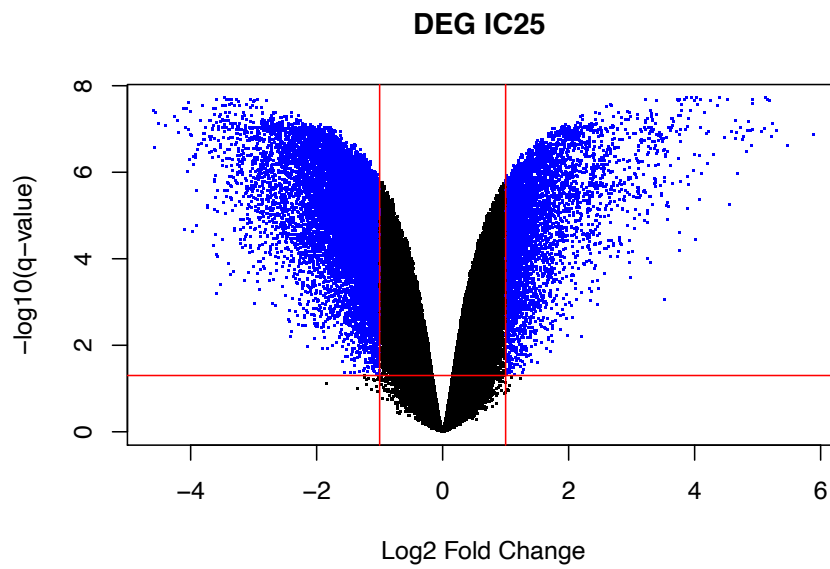
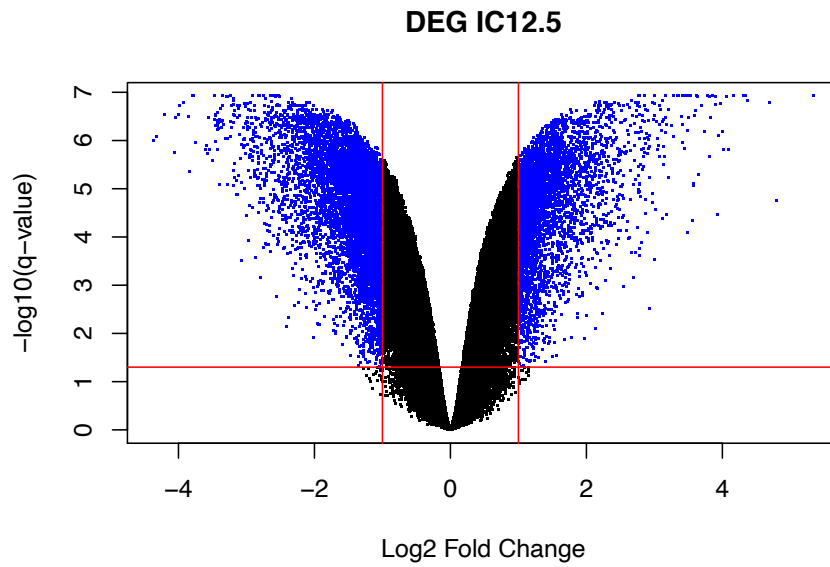


Figure 2: Volcano plots showing the transcripts identified at IC_{12.5} (top-figure) and IC₂₅ (bottom-figure) levels

3.2.3 Statistical Validation of the Primary Findings

To check for the reliability and the validity of the primary results, the statistical tests used to obtain the list of differentially expressed transcripts were reperformed using different methodologies.

In this study, ANOVA was used to test the effect of two inhibitory levels of BA (IC_{12.5}, IC₂₅) on HepG2 cells using the second microarray dataset. After ANOVA, DEG lists for each level were obtained via eBayes t-tests through planned contrasts. Testing each concentration level separately with eBayes without fitting a linear model yielded very similar number of upregulated or downregulated transcripts. Furthermore, the correlation map showed that the results of separate eBayes t-tests were nearly identical with the planned contrasts after ANOVA (App Figure 11, 12).

In a separate statistical validation procedure, all the microarray data were combined into one dataset using a proper preprocessing method. The effect of BA level was investigated using ANOVA and the DEG lists at each level were then obtained with eBayes t-tests on the planned contrasts. This procedure yielded substantially lower number of upregulated and downregulated transcripts for all three levels (App. Table 2). Despite the smaller volume of the findings in this procedure, the relative sizes and the contents of the DEG lists at three levels were similar with the other tests (App. Figure 11, 12, App. Table 2). Performing the BH multiple test thresholding separately for each contrast or globally including all subsequent tests did not have an observable effect on the results (App. Table 2).

Overall, the primary findings in this study were robust to changes in the chosen statistical methodologies.

3.3 Enrichment Analyses

Enrichment analyses were performed independently for each DEG list to understand better the transcriptomic changes in response to boric acid at the growth inhibitory concentrations. Over-represented pathways or GO terms have been identified for upregulated or downregulated transcript lists.

3.3.1 IC₅₀ level

250 GO terms and 58 pathways were significantly enriched in downregulated transcripts, while 116 GO terms and 11 pathways were significantly enriched in upregulated transcripts. The most highly enriched biological processes in the downregulated transcript collection were *DNA replication* and the *cell cycle*. *Nucleoside binding* and chromosome-

related terms are the most strongly enriched terms in down-regulated transcripts. As biological processes, *xenobiotic glucuronidation*, *regulation of molecular function*, *regulation of phosphorus metabolism*, and *intracellular signaling* are among the top significantly enriched GO terms associated with upregulation. As molecular functions, *glucuronosyltransferase activity*, *protein heterodimerization activity*, *enzyme inhibitor activity*, *enzyme binding*, and *small molecule binding* terms are among the top significantly enriched GO terms associated with upregulation (Figure 3).

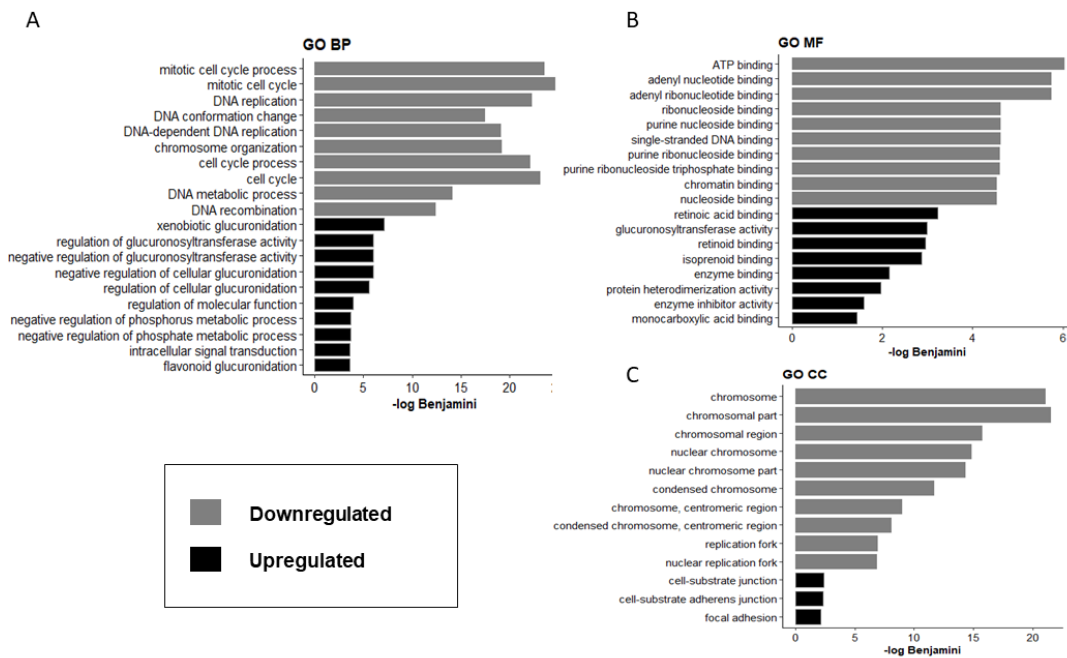


Figure 3: Top 10 significantly enriched GO categories in HepG2 cells treated with boric acid at IC₅₀ level (Published at Tombuloglu et al., 2020).

In addition to gene ontologies, the top 20 enriched pathways from the Reactome and KEGG pathways (Figure 4) included DNA repair mechanisms like *homologous DNA repair*, *nucleotide excision repair*, *mismatch repair*, and pathways related to DNA synthesis like *activation and assembly of the pre-replicative complex* are among the list of enriched pathways in the transcriptional response that is downregulated in conjunction with *DNA replication* and the *cell cycle*. Primary downregulated responses include

metabolic pathways, *steroid and cholesterol production*, and transcription factor SREBF-regulated pathways. Many metabolic pathways, such as the pathways for drug metabolism, chemical carcinogenesis, and p53 signaling, were discovered as enriched upregulated pathways with the highest relevance (Figure 4).

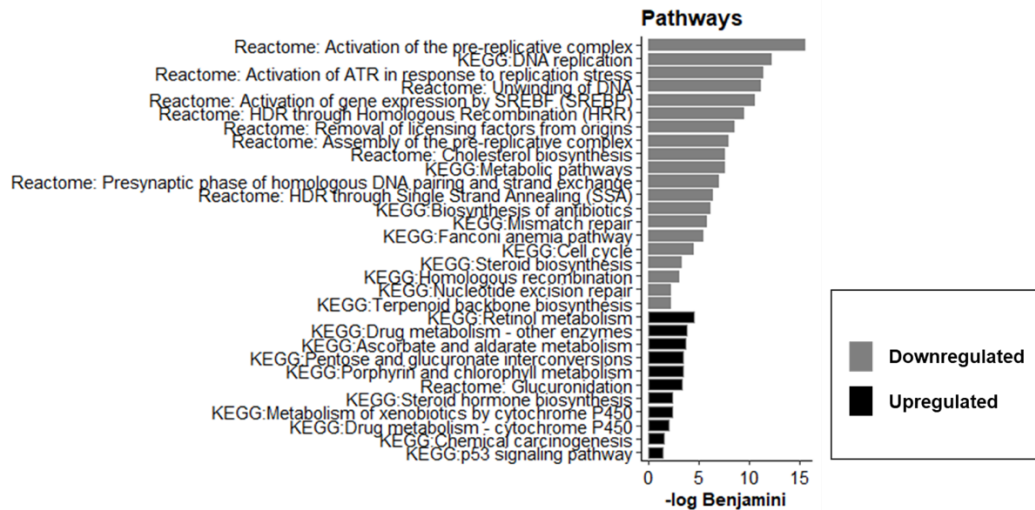


Figure 4: Top 10 significantly enriched KEGG pathways in HepG2 cells treated with boric acid at IC₅₀ level (Published at Tombuloglu et al., 2020)

A second functional enrichment analysis was conducted with the entire list of differentially expressed transcripts to comprehend the biological processes triggered by boric acid treatment and the relationships between enrichment results. The results were then visualized in a network constructed using EnrichmentMap (Bader et al., 2014; Merico et al., 2010). The network was made up of nodes corresponding to significantly enriched terms connected by the edges signifying similarities in the transcript content of the node (Figure 5 published at Tombuloglu et al., 2020).

WordCloud is a helpful tool for finding and labeling functional clusters in a network (Oesper et al., 2011). Nine major functional clusters were determined (Figure 5). A considerable degree of similarity exists across these clusters, which can be confirmed via the strong connections between the four of them: *DNA repair*, *cell cycle*, *nucleotide binding*, and *DNA organization*. Downregulated transcripts predominately comprise the functional transcript sets in these four categories (Figure 5).

Since lipid and amino acid metabolism are closely related, common transcripts likely participate in both processes. The total betweenness of the transcript sets involved in *Xenobiotic metabolism* is considerably greater than other clusters in the enrichment-terms network. The elevated glucuronyltransferase transcripts that reflect glucuronidation-

related terms are observed as dark red nodes at the center of the *Xenobiotic Metabolism* Cluster (Figure 5).

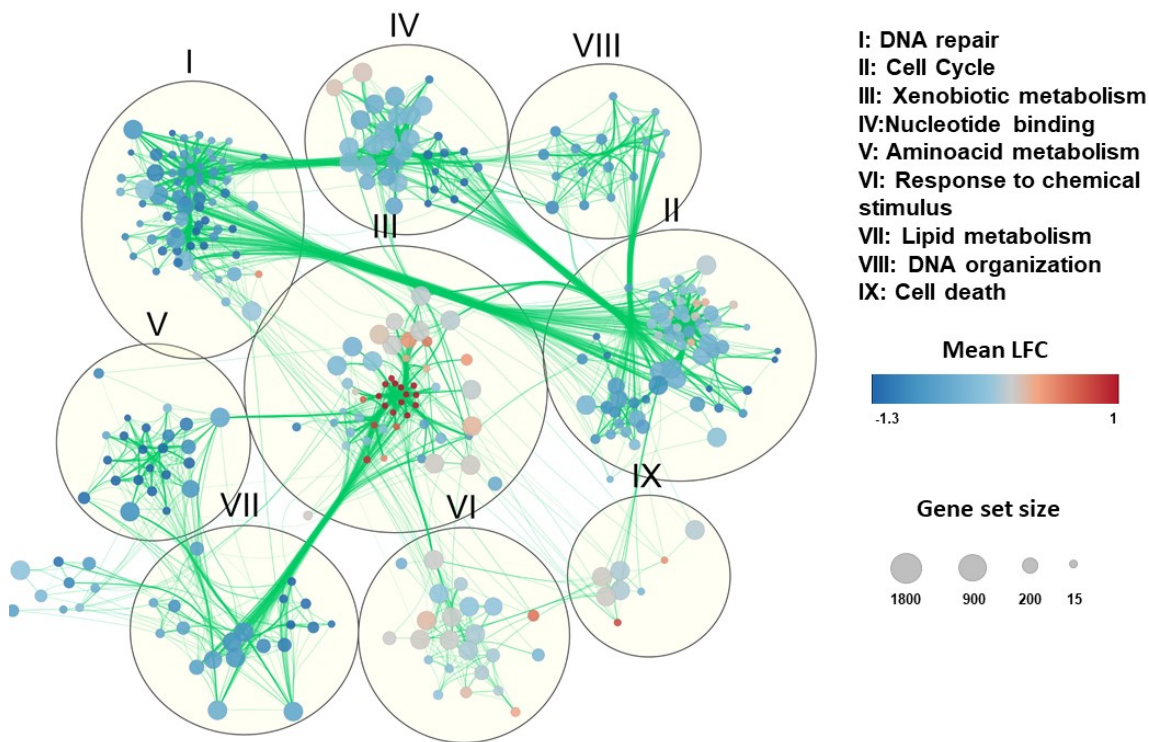


Figure 5: Enrichment terms network built for HepG2 cells treated with boric acid at IC₅₀ level (published at Tombuloglu et al., 2020)

3.3.2 IC₂₅ level

Among the top ten enriched GO categories associated with the BA treatment at the IC₂₅ level, terms related to *cell cycle* for the downregulated genes (Figure 7), terms related to *xenobiotic metabolism* and *apoptotic process* were noticeable (Figure 8). In the whole enrichment results of the downregulated genes, terms related to *DNA repair* were present which is similar with the IC₅₀ case.

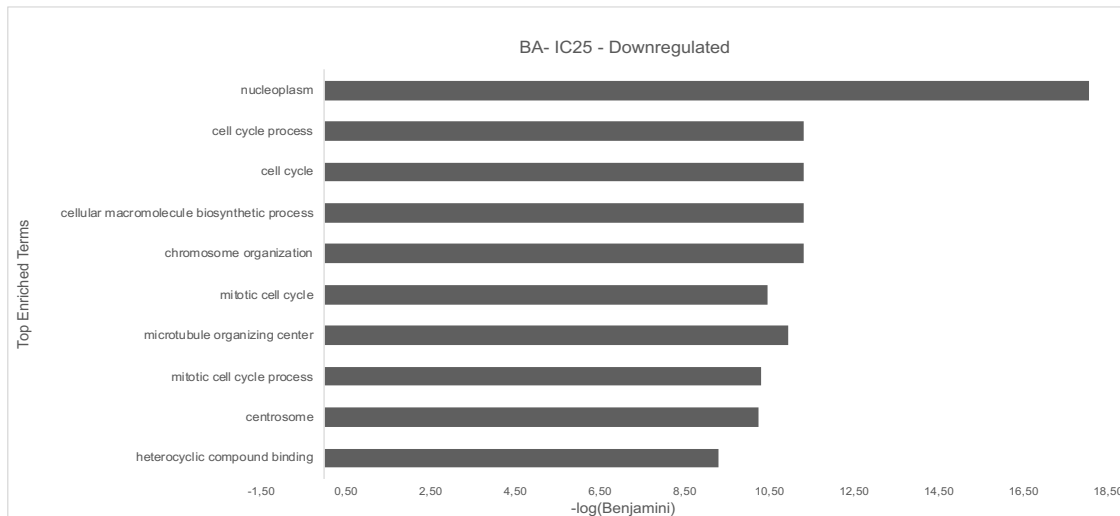


Figure 6: Top 10 significantly enriched GO categories in downregulated transcripts of HepG2 cells treated with boric acid at IC₂₅ level

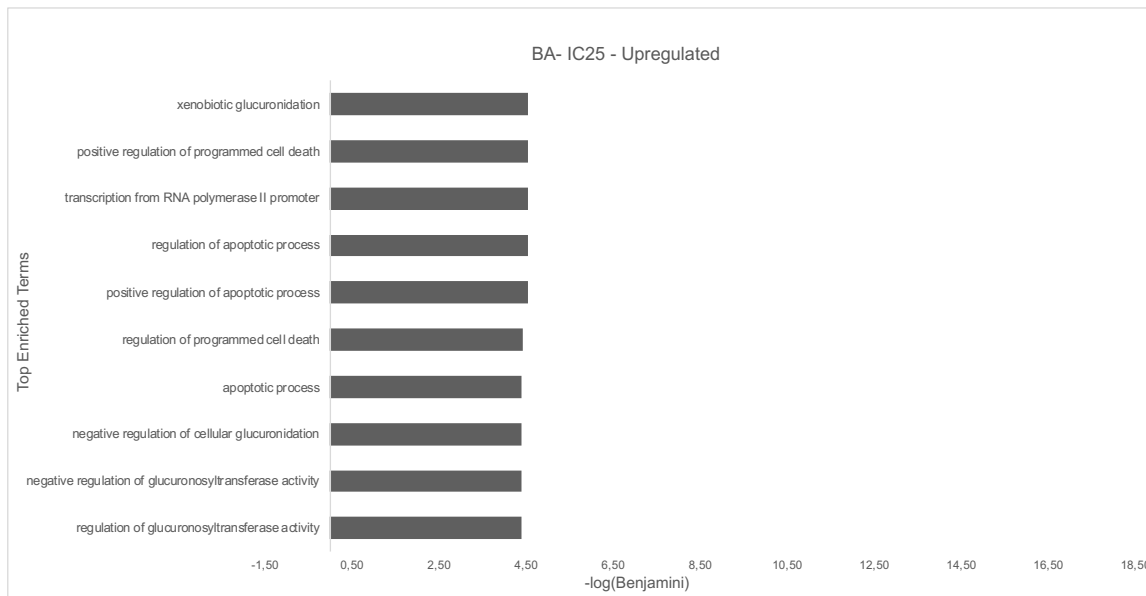


Figure 7: Top 10 significantly enriched GO categories in upregulated transcripts of HepG2 cells treated with boric acid at IC₂₅ level

3.3.3 IC_{12.5} level

The most noticeable categories among the top 10 results of the enrichment analysis at the IC_{12.5} level, were the ones related to metabolism, including *lipid metabolism* and *amino acid* for the downregulated genes (Figure 9) and *xenobiotic metabolism* for the upregulated genes (Figure 10). Similar with the IC₅₀ and IC₂₅ cases, cell cycle processes were also overrepresented within the downregulated gene list (Figure 9). Unlike higher concentrations, *DNA repair* term was not found within the whole enrichment results of the downregulated genes (data not shown).

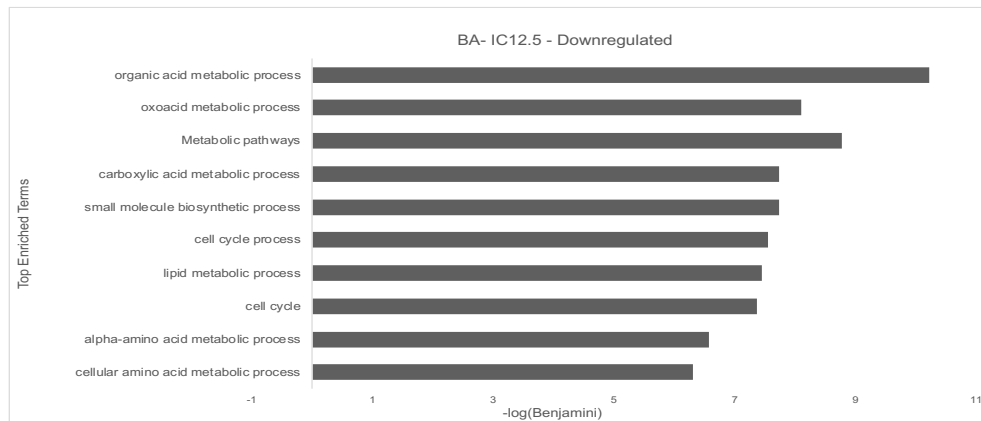


Figure 8: Top 10 significantly enriched GO categories in downregulated transcripts of HepG2 cells treated with boric acid at IC_{12.5} level

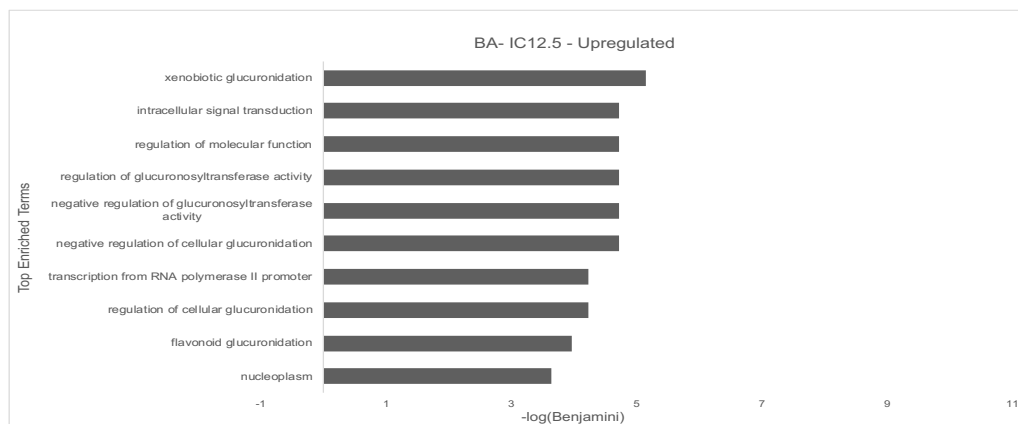


Figure 9: Top 10 significantly enriched GO categories in upregulated transcripts of HepG2 cells treated with boric acid at IC_{12.5} level

3.4 Network Analysis

The reconstructed regulatory networks depict the differential TF-gene relations that change in BA treatment conditions compared to the control. At each dose of BA, two subnetworks were obtained to visualize the interaction of the DEG with the targeting TFs: one with increasing TF-target interaction scores and one with decreasing TF-target scores. Increasing TF-target interaction scores indicate consolidation of the regulatory relations; hence the subnetworks comprised of such TF-target relations will be called *Consolidating Interaction Regulatory Subnetwork (CIRS)*. Similarly, decreasing scores represent the weakening of the TF-target relations. The subnetworks with declining scores will be called *Weakening Interaction Regulatory Subnetworks (WIRS)*.

Evaluating the changes in network topology with the differential network approach is problematic due to the abundance of uncertain edges, the presence of dual-signed scores, and the loss of contextual meaning when concentrating on the perturbed interactions while ignoring common ones. Moreover, using conventional modularity maximization techniques may fail to detect smaller communities with biological relevance. Therefore, the differences in regulatory network structure were investigated with ALPACA, specifically designed to deal with these challenges (Padi & Quackenbush, 2018). The novel modules with significant enrichment scores were studied in detail. Coregulatory networks were also presented as biologically relevant subgraphs depicting the gene coexpression relations iteratively revised with information from the regulatory interactions and minimized with *Prize Collecting Steiner Forest* algorithm (Tuncbag et al., 2016).

Together, network analyses helped identify critical molecular interactions associated with the growth inhibitory BA concentrations.

3.4.1 IC₅₀ level

The CIRS-IC₅₀ consists of 2160 edges representing the interactions between 156 transcription factors (TFs) and 236 target genes comprising 120 upregulated and 116 downregulated genes. In this subgraph, CTCFL with 75 outgoing edges has the highest number of altered interactions with the DEG, followed by IRF3 which has 74 outgoing edges (Figure 10).

The WIRS-IC₅₀ consists of 2144 edges portraying the interactions between 147 TFs with 76 upregulated and 150 downregulated genes. Interestingly, IRF3 has the highest number of weakening interactions with the DEG with 89 outgoing edges. Two densely connected components can be discerned in both subgraphs. In the CIRS-IC₅₀, most target genes are localized within the first component, and upregulated genes were overrepresented. The

second component has relatively few target-genes majority of which are downregulated. In the WIRS-IC₅₀, a large proportion of the DEG, mostly downregulated, were confined within the first component. In contrast, a few DEG, most of which are upregulated, were found within the second component (Figure 11).

SREBF genes, SREBF1 and SREBF2, which were downregulated at the IC₅₀ level and were predicted as key regulatory molecules in the previous enrichment analyses, are located as TFs within the second connected component of the CIRS-IC₅₀ and WIRS-IC₅₀ (Figure 10, 11).

The coregulatory subgraph involved the DEG represented as diamonds and Steiner nodes represented as ellipses. Any biological processes other than the known ones could not be identified with the novel nodes (App. Figure 8).

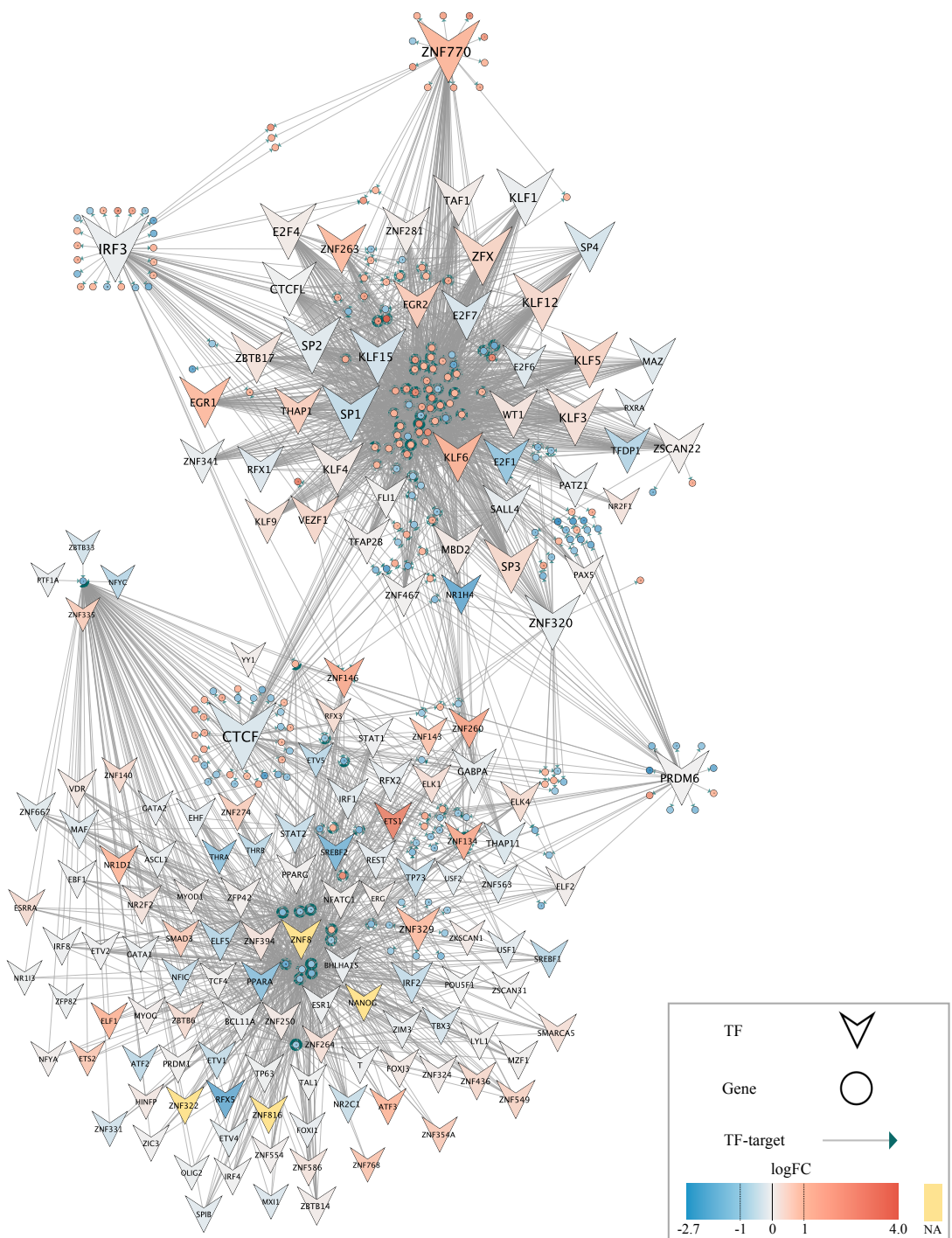


Figure 10: The CIRS-IC₅₀ representing the regulatory interactions with increasing scores relative to the control (Z score < -1.96)

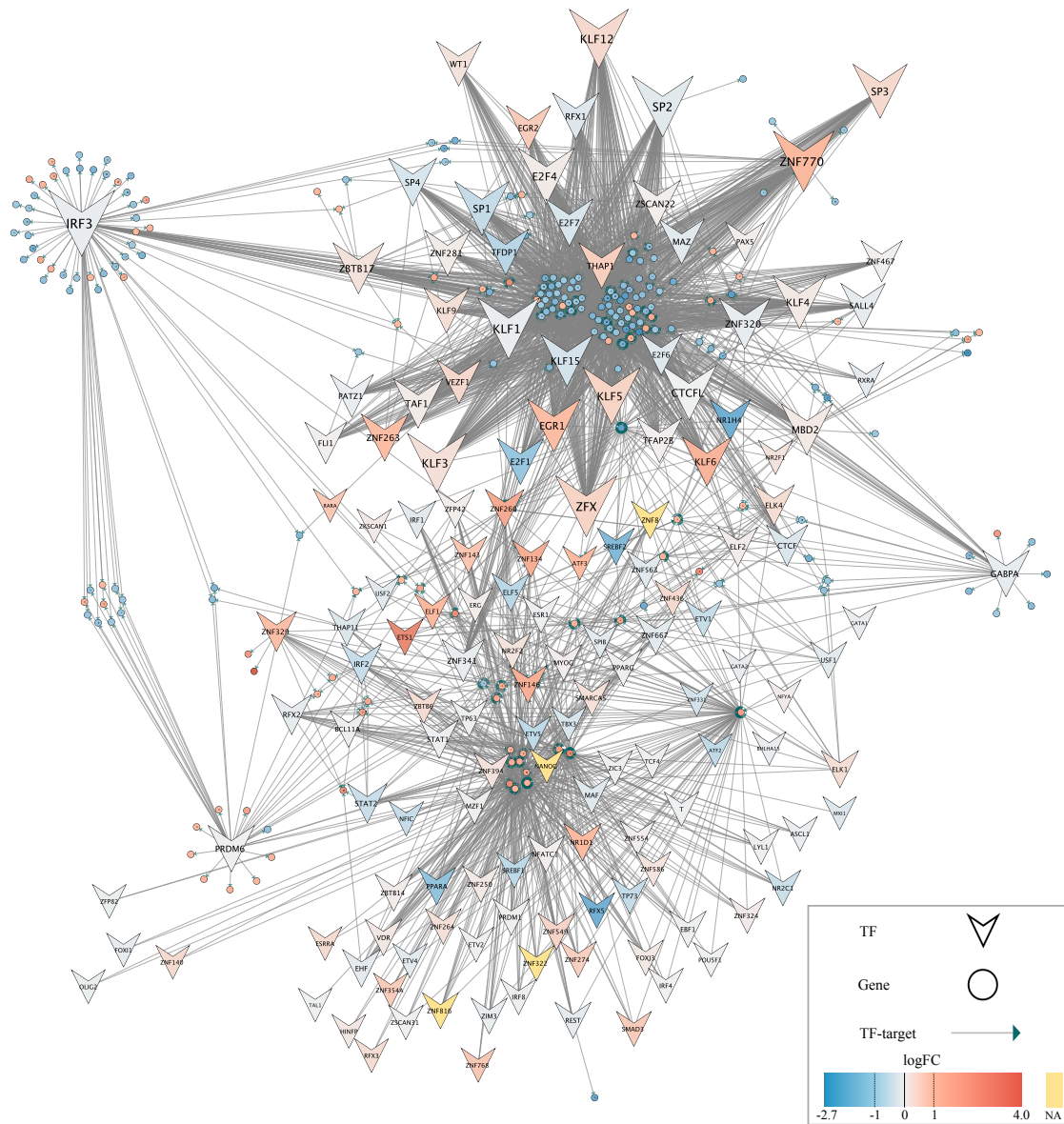


Figure 11: The WIRS-IC₅₀ representing the regulatory interactions with decreasing edge scores relative to the control (Z score >1.96)

Analyzing the differential modular structure of the IC₅₀ regulatory network revealed a total of 25 network communities changing in reaction to BA treatment at the IC₅₀ level. The communities were refined using the differential modularity scores to obtain mini modules involving the top 5 transcription factors and 50 target genes. Among the 25 mini-modules, 13 were significantly enriched for cellular processes and pathways. Representative terms were chosen by considering both the adjusted p-value and the Odds-ratio. The three most significant terms (adj. p<0.002) enriched within the modules were *Keratinization* (black module), *RNA secondary structure unwinding* (purple module), and *Response to type I interferon* (orange module) (Figure 12). These were followed by the chosen terms (adj. p<0.05), *Excretion* (dark yellow module), *Fat digestion and absorption* (green module), *Endocytosis* (brown module), *Steroid hormone biosynthesis* (yellow-green module), *Taurine metabolic process* (golden yellow module), *Catecholamine secretion* (dark purple module), *Phosphatidylinositol phosphorylation* (pink module), *Fc epsilon RI signaling pathway* (cyan module) and the least significantly enriched *Lysine degradation* (turquoise module) (Figure 12).

The selected modules were highly interconnected through intermediary nodes acting as TF in one module and target in another (Figure 12). The purple module associated with RNA secondary structure unwinding had the TFs (TFAP2B, RFX1, MBD2, CTCF, and CTCFL) with the highest outdegree of the subgraph, targeting 56 nodes (Figure 12). These were followed by the four TFs of the brown subgraph (RARA, ZNF121, THRA, and PAX5) with an outdegree of 55 and IRF3 of the turquoise module with an outdegree of 54 (Figure 12).

Most members within the selected modules were not found among differentially expressed genes (Figure 12). Some differentially expressed TFs (BH adj. p<0.05) within the subgraph are ZNF260 (LFC=1.55), ZNF146 (LFC=1.38) within the golden module, ZNF121(LFC=1.02), THRA (LFC= -1.15) within the brown module and SREBF2(LFC= -1.5) within the yellow-green module (Figure 12).

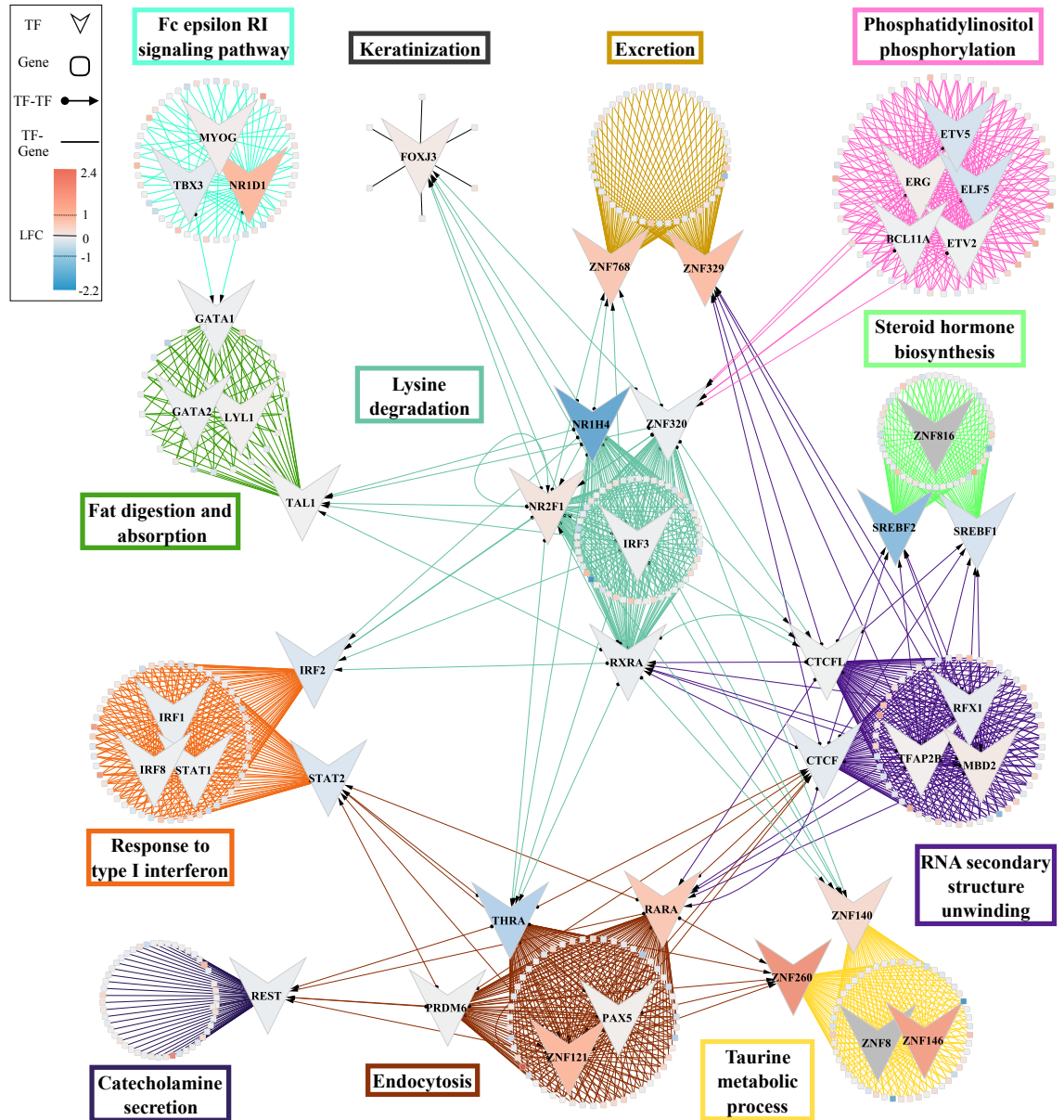


Figure 12: Selected *de novo* mini-modules of the IC₅₀-BA-regulatory network and the representative biological processes enriched within the list of module's gene targets.

3.4.2 IC₂₅ level

The CIRS-IC₂₅ is a subgraph comprising 9336 edges representing interactions between 147 transcription factors and 530 target DEG. 323 of the target genes were downregulated and 207 were upregulated. Among the TFs, SP1 and ZNF320 have the highest number of consolidating interactions with 250 and 244 outgoing edges (Figure 13). On the other hand, the WIRS-IC₂₅ subgraph, which contains 9757 edges, shows the interactions between 150 TFs and 184 upregulated, 384 downregulated genes. ZNF320 which has 391 outgoing edges, is the TF with the highest number of weakening interactions with the DEG in this subgraph (Figure 14).

In the coregulatory subgraph DEG were represented as diamonds and the Steiner nodes as ellipses. Any biological processes other than the known ones could not be identified with the novel nodes (App. Figure 9).

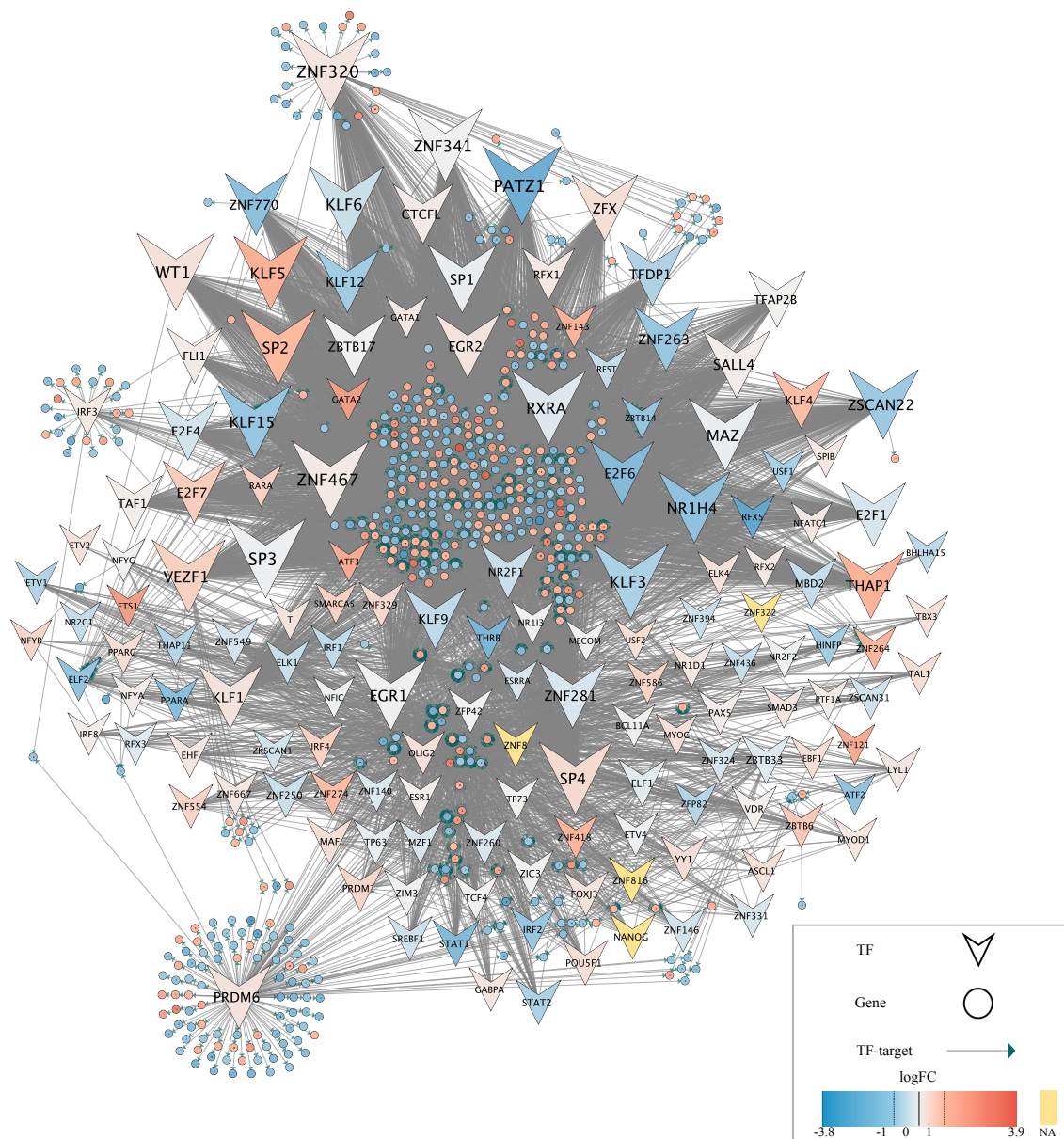


Figure 13: The CIRS-IC₂₅ representing the regulatory interactions with increasing scores relative to the control (Z score < -1.96)

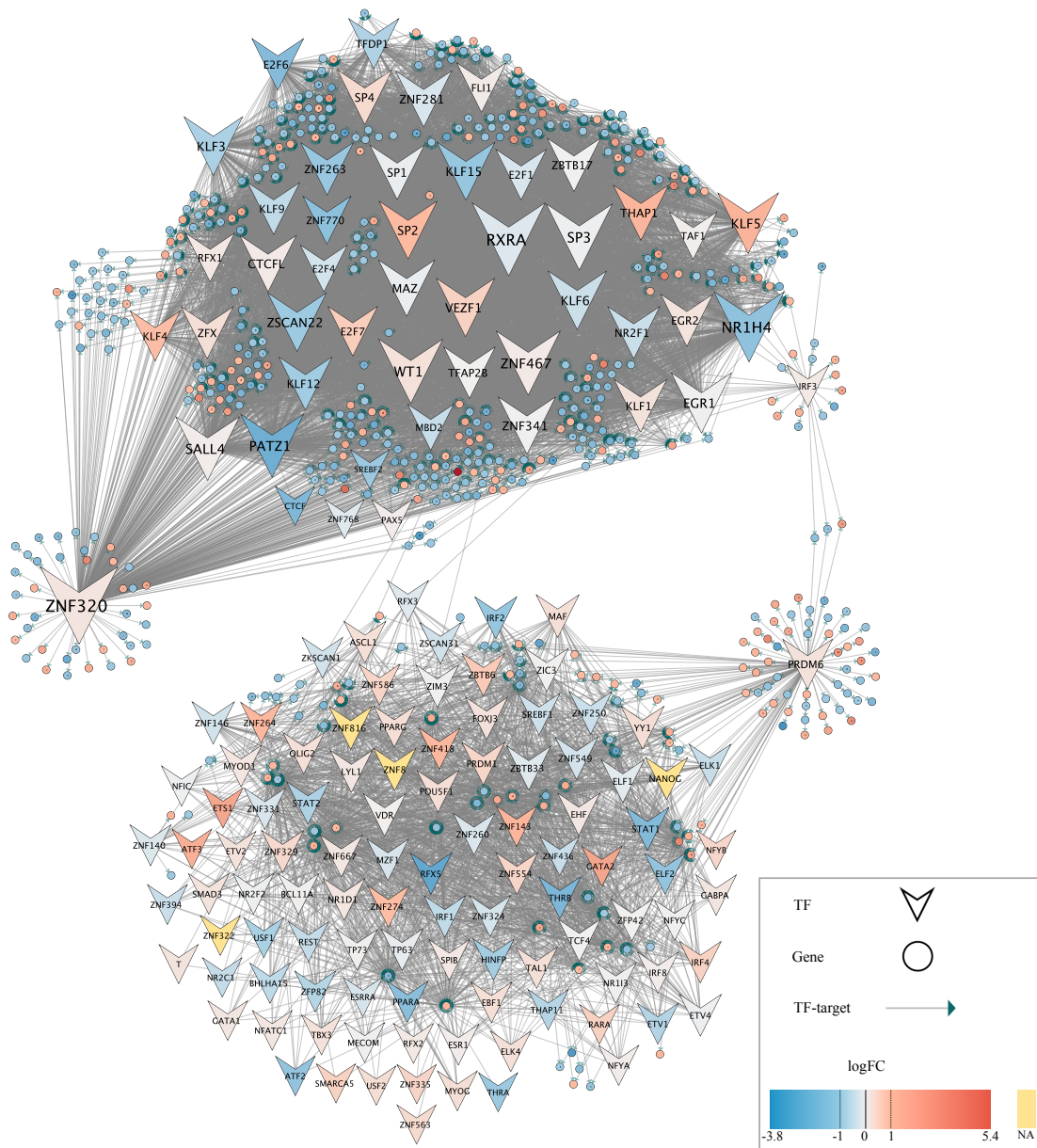


Figure 14: The WIRS-IC₂₅ representing the regulatory interactions with decreasing edge scores relative to the control (Z score >1.96)

Upon conducting an analysis of the differential modularity of the IC₂₅ network, 42 communities were found to be differentiating in response to BA treatment at this level. Further refinement of these communities resulted in mini modules, each consisting of the top 5 transcription factors and 50 target genes. Ten mini modules significantly enriched for various cellular processes and pathways were selected for further investigation. Notably, the most significant terms (adj. $p < 0.002$) included *Response to Type I interferon (orange module)*, *Keratinization (black module)*, and *Negative regulation of calcium ion-dependent exocytosis (dark purple module)* (Figure 15). The remaining significant terms (adj. $p < 0.05$) are as follows: *C-terminal protein methylation (cyan)*, *Drug metabolism - cytochrome P450 (yellow-green module)*, *Fat digestion and absorption (green module)*, *Arginine and proline metabolism (yellow module)*, *Taurine metabolic process (golden yellow module)*, *Angiotensin-activated signaling pathway (dark green module)*, *N-Glycan biosynthesis (dark yellow module)*, and *Response to salt (lilac)* (Figure 15).

Of particular interest was the module associated with N-Glycan biosynthesis, which had the highest number of outgoing edges. The transcription factors of the dark yellow module, namely PATZ1, VEZF1, ZBTB17, MAZ, and SP4, targeted not only the genes within the module but also the TFs of seven other modules (Figure 15).

Many intermediary nodes acted as both transcription factors and targets in two different modules. However, unlike the IC₅₀ modular subgraph, the modules were not fully connected through intramodular interactions via intermediary nodes. The TFs of the lilac and black modules had no interaction with other TFs in other modules. A small proportion of high-confidence intermodular TF-gene interactions was shown as gray edges to reveal how such modules might be interrelated with other modules. TFs of the central dark yellow module also have regulatory interactions with high differential modularity with the genes of these modules (Figure 15).

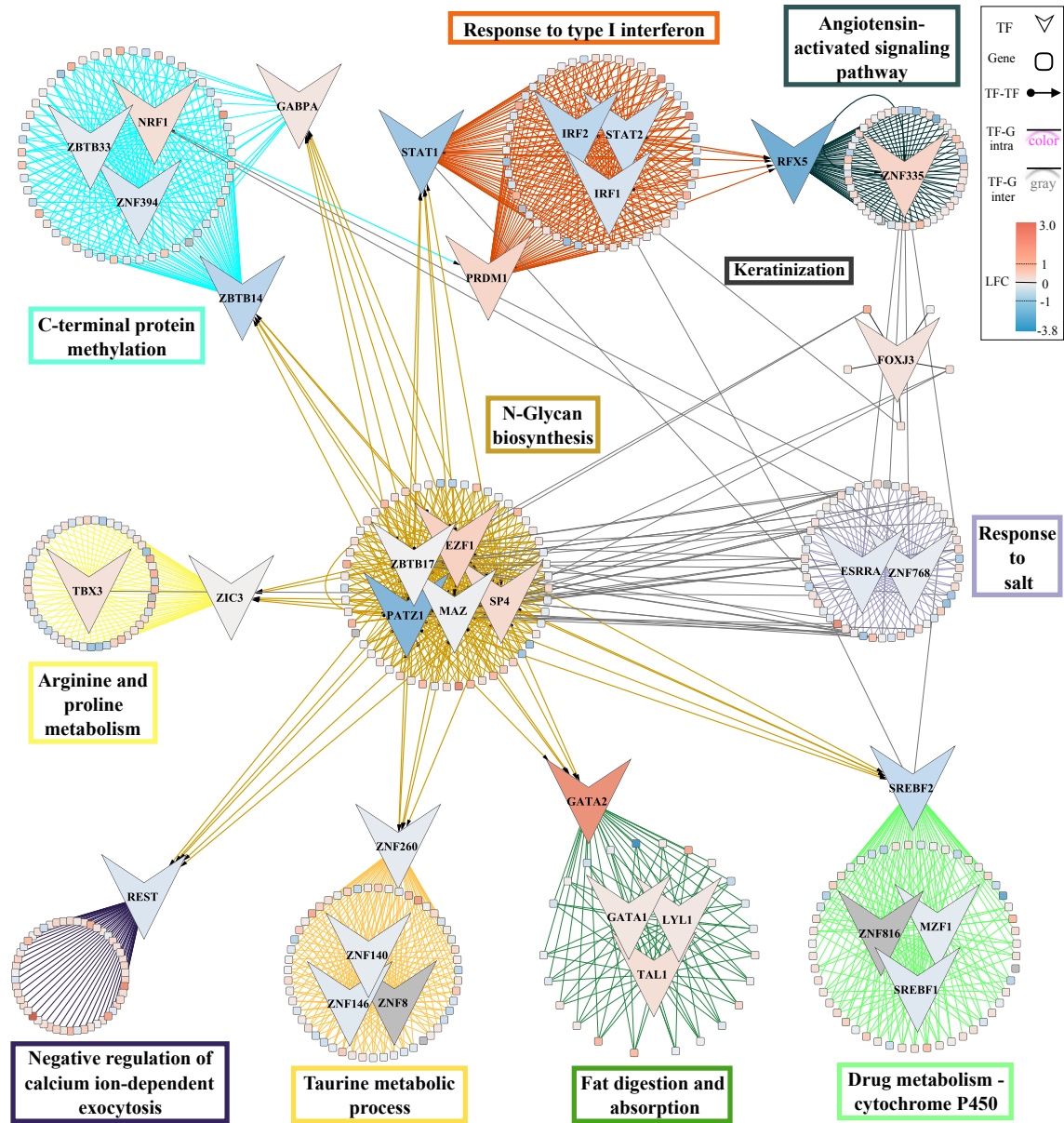


Figure 15: Selected *de novo* mini-modules of the IC₂₅-BA-regulatory network and the representative biological processes enriched within the list of module's targets

3.4.3 IC_{12.5} level

Within the subgraph CIRS-IC_{12.5}, there are 6045 edges that represent interactions between 127 transcription factors and 281 DEG which include 154 downregulated genes and 127 upregulated genes. SP3 and KLF3 exhibit the highest outdegrees in the subgraph with 205 and 192 outgoing edges respectively (Figure 16). Meanwhile, the WIRS-IC_{12.5} subgraph, consisting of 6997 edges, displays the interactions between 135 transcription factors and 361 genes, 178 upregulated and 183 downregulated. Within this subgraph, SP3 with 205 targeting interactions has the highest outdegree followed by SP1 with 192 interactions with DEG (Figure 17).

In the coregulatory subgraph DEG were represented as diamonds and the Steiner nodes as ellipses. Any biological processes other than the known ones could not be identified with the novel nodes (App. Figure 10).

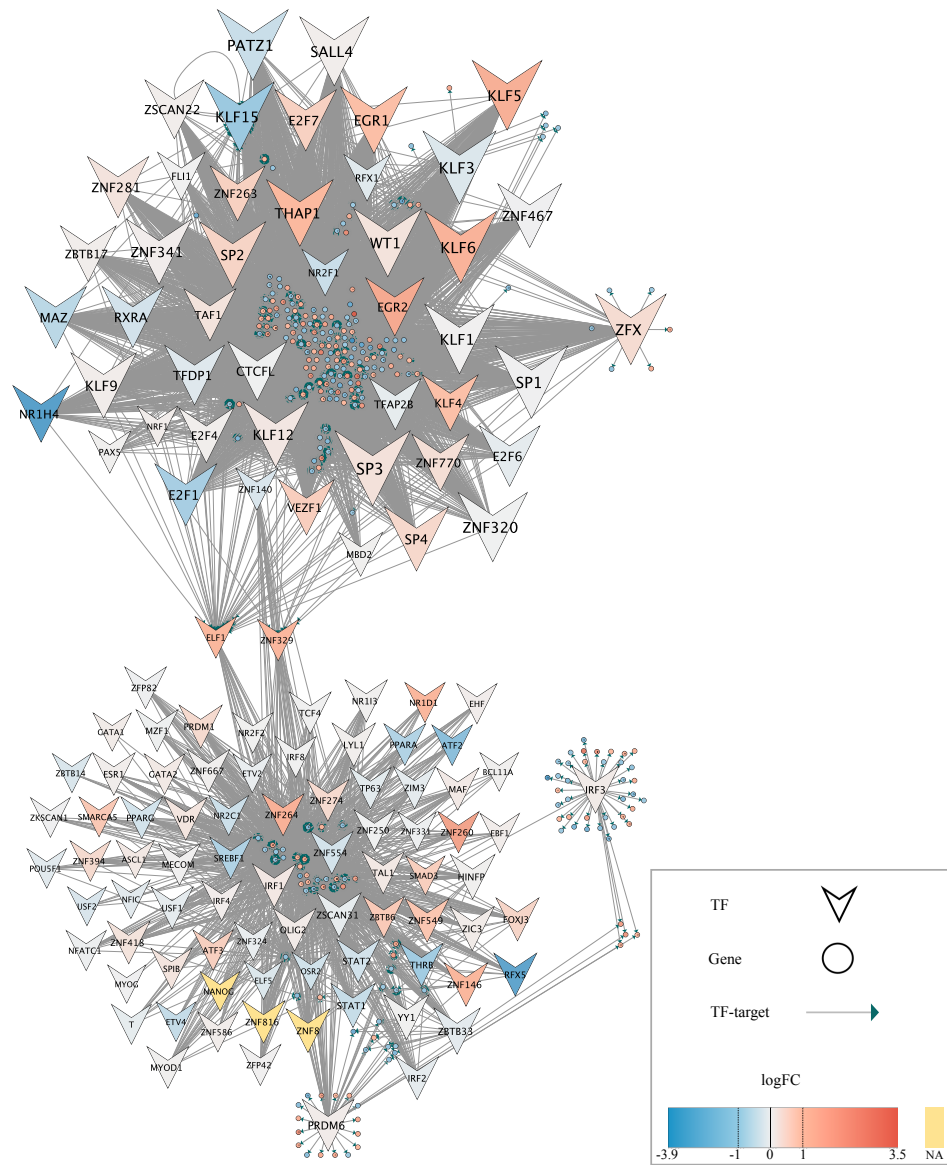


Figure 16: The CIRS-IC_{12.5} representing the regulatory interactions with increasing scores relative to the control (Z score < -1.96)

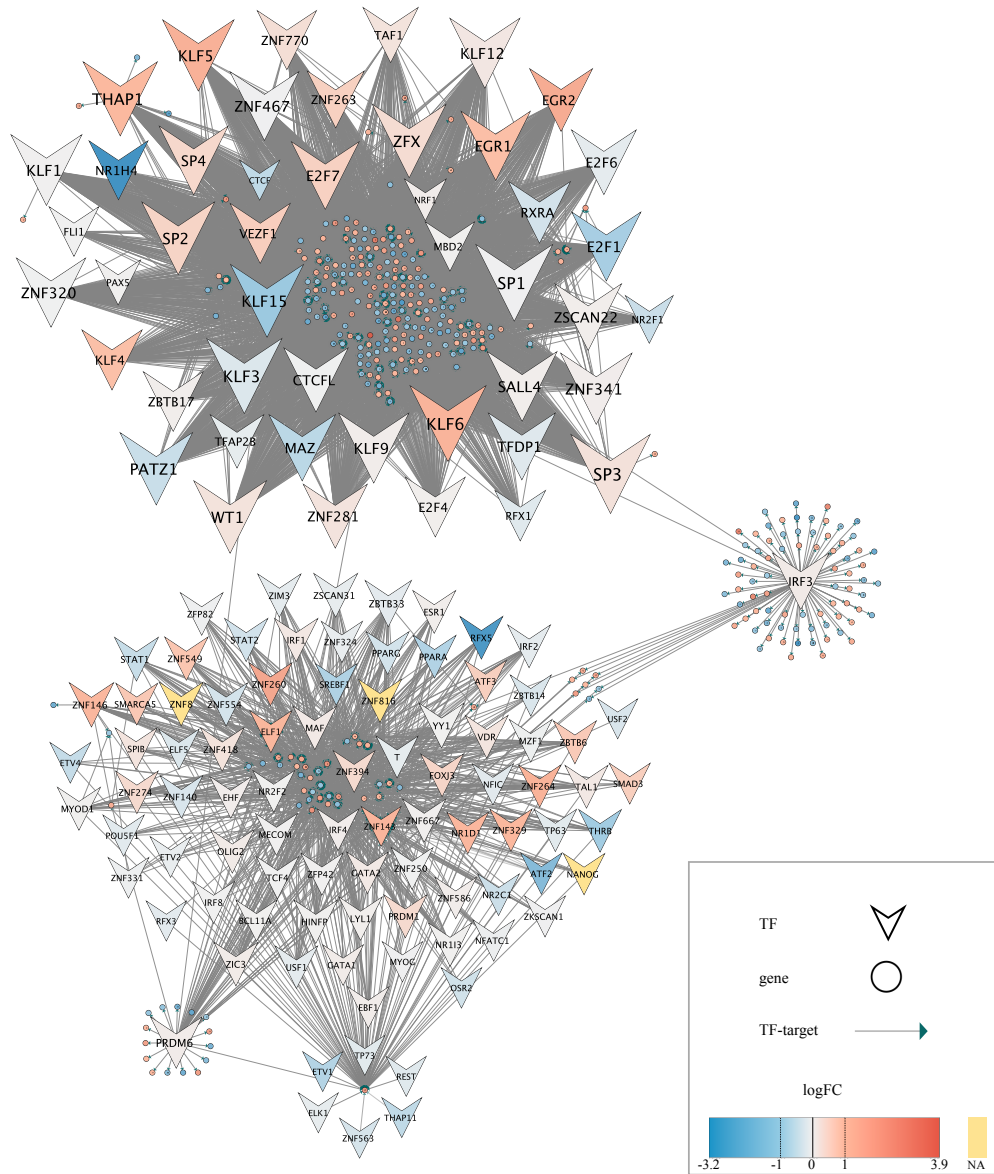


Figure 17: The WIRS-IC_{12.5} representing the regulatory interactions with decreasing edge scores relative to the control (Z score >1.96)

The IC_{12.5} network was similarly analyzed to find communities with high differential modularity scores, which were then minimized to contain the top 5 TFs and top 50 genes. Fundamental regulatory interactions were investigated by focusing on the mini modules enriched for cellular processes. A total of 35 communities were discovered, and 13 modules were selected for further study.

At the IC_{12.5} level, the most significant three terms (adj. $p < 0.003$) associated with the selected modules were *Response to type I interferon (orange module)*, *Spliceosome (pink module)*, and *Fat digestion and absorption (green module)* (Figure 18). Other representative terms (adj. $p < 0.05$) in the order of significance (adj. $p < 0.05$) are *Negative regulation of calcium ion-dependent exocytosis (deep purple module)*, *Taurine metabolic process (golden yellow module)*, *Negative regulation of cAMP-dependent protein kinase activity (beige module)*, *Steroid hormone biosynthesis (yellow-green module)*, *PPAR signaling pathway (olive module)*, *Inositol phosphate metabolism (pink module)*, *RNA secondary structure unwinding (purple module)*, *Monoubiquitinated protein deubiquitination (cyan module)*, *TGF-beta signaling (brown module)*, *Positive regulation of mRNA splicing, via spliceosome (lilac module)* (Figure 18).

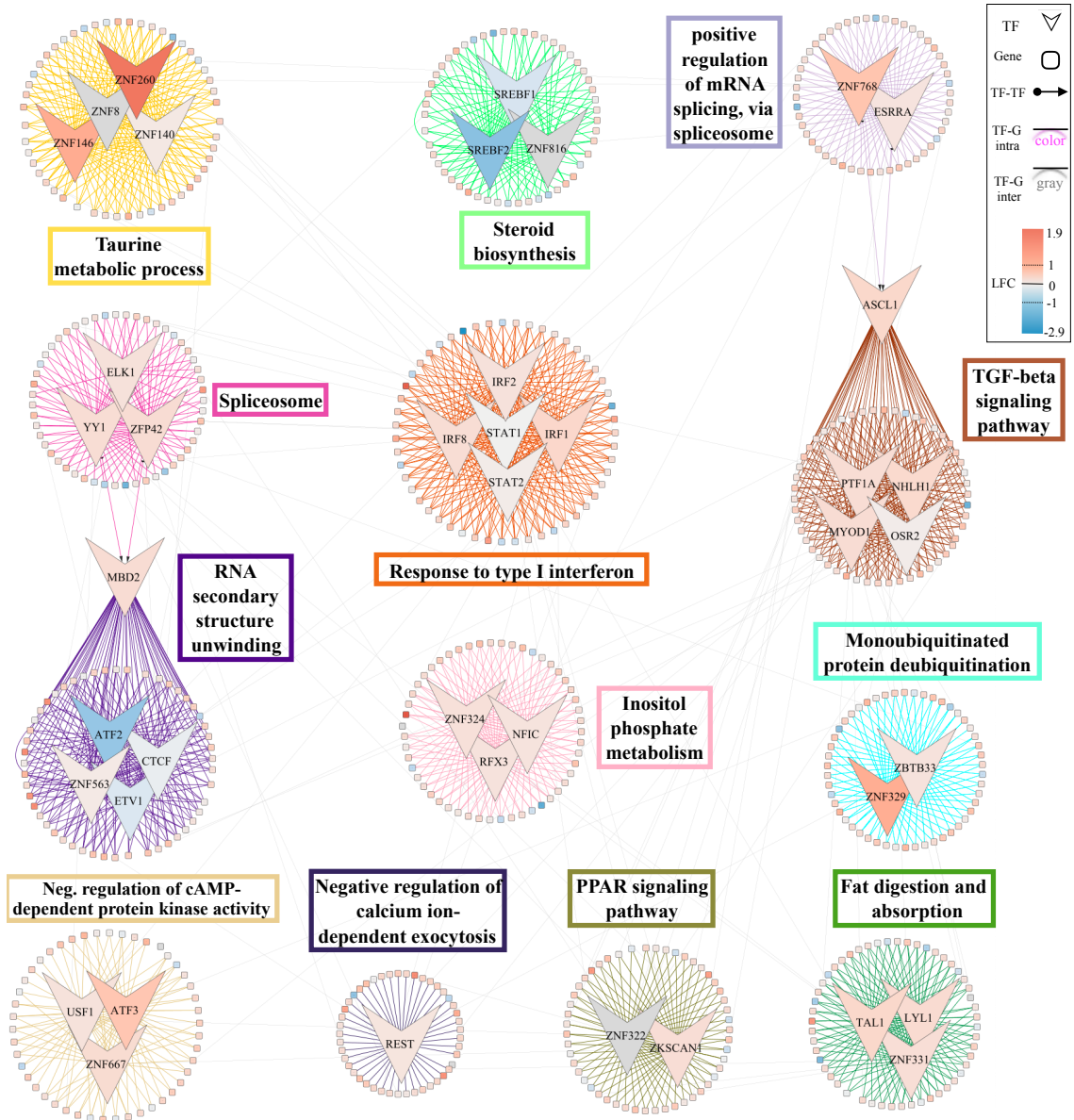


Figure 18: Selected *de novo* mini-modules of the IC_{12.5}-BA-regulatory network and the representative biological processes enriched within the list of module's gene targets

3.5 Intersection of Coregulation Subgraphs

An intersection subgraph (Figure 19) was built from the nodes observed within at least two of the coregulatory subgraphs (App. Figure 8-10). The terminal nodes which represent DEG are shown as diamond whereas Steiner nodes which are nodes discovered by the algorithm are shown as elliptical. The nodes common to all coregulatory subgraphs were depicted as the larger nodes. The log FC values at each level was shown as an inset line graph within these nodes. In general, common nodes had all positive or negative LFC values regardless of the BA treatment level. The node colors represent the average LFC values. It is notable that the gene *ARRDC4* and *AQP3* were very highly upregulated at all levels of BA treatment. Among the common nodes many were transmembrane proteins or had regulatory functions.

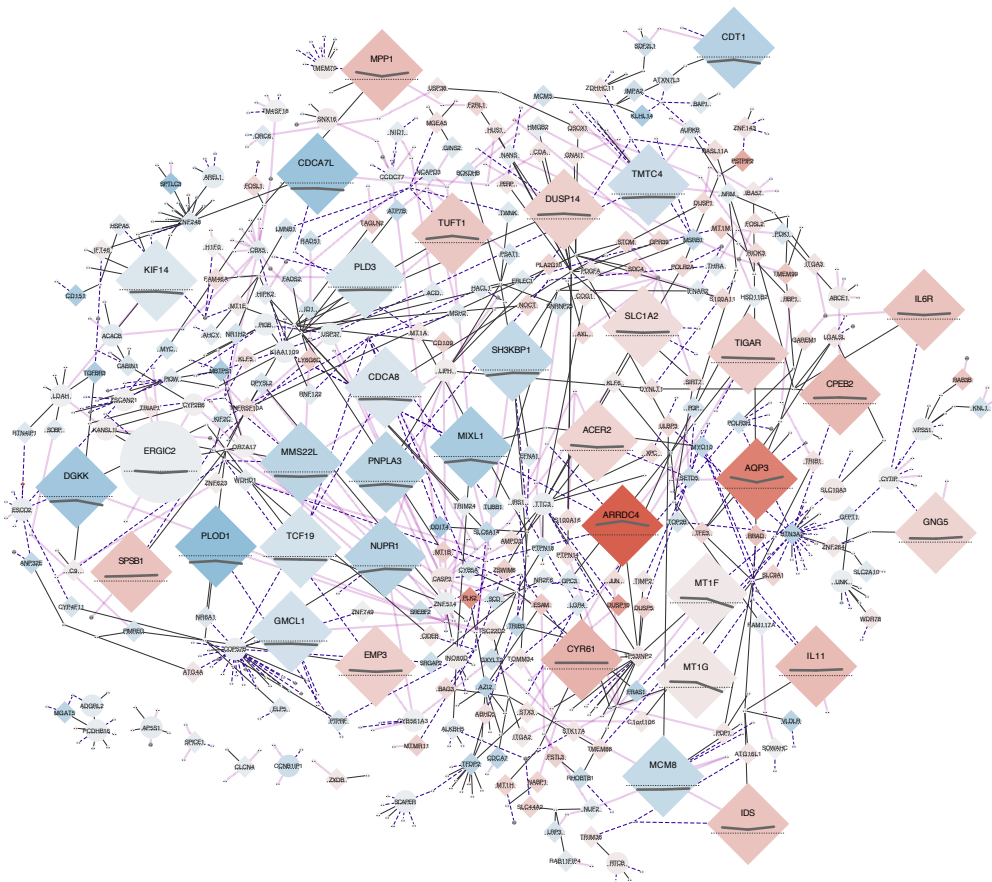


Figure 19: The intersecting coregulatory subgraph. The diamonds are the terminal nodes and the ellipses are the Steiner nodes. The inset line graph depicts the logFC values of BA at three concentrations.

CHAPTER 4

DISCUSSION

Boric acid is the physiologically available form of Boron, and accumulating evidence demonstrates its role in many biological processes (Barranco & Eckhert, 2004; Park et al., 2004). Although essential to the diet, high concentrations of boric acid might be hazardous to health (Hunt, 2012; Murray, 1998).

Previously, the dose-dependent toxicity and growth inhibition was monitored by treating HepG2 cells with boric acid at varying amounts. The half-maximum inhibitory concentration of boric acid was estimated to be 24 mM, while a boric acid concentration as low as 5 mM was sufficient to inhibit HepG2 cell growth (Tombuloglu et al., 2020). Several *in vitro* studies reported minimal growth inhibitory concentrations of boric at a comparable level. Minimal growth inhibitory concentration was estimated as 5 mM for Hek and HeLa (Park et al., 2004), 8 mM for cell lines with skin origin (Apdik et al., 2015), and 6.25 mM for DU-145 cell line (Hacioglu et al., 2020). While a prominent growth inhibition is observed at such doses, boric acid treatment can also promote cell proliferation when administered at micromolar quantities (Park et al., 2004).

This work examined the transcriptomic changes accompanying boric acid treatment of HepG2 cells at three inhibitory concentrations and revealed potential molecular mechanisms. Half-maximal inhibitory concentration (IC_{50}) is the concentration at which the cell growth is reduced at 50%. At IC_{50} concentration, boric acid treatment of HepG2 cells also led to a significant increase in genotoxic markers, which was bare, although not significantly observed at IC_{25} or lower doses. $IC_{12.5}$ concentration is 6 mM, close to the level at which growth inhibitory effects of boric acid start to occur (Tombuloglu et al., 2020).

The transcriptomic profile changed significantly in response to boric acid treatment at all three inhibitory concentrations. At IC_{50} level inhibition, there is a marked overexpression

of apoptotic genes, including the genes in the p53 signaling pathway, and a large downregulation of genes involved in the cell cycle, DNA repair, chromosomal architecture, and metabolic pathways. These genes include many markers of early apoptosis and cellular senescence (Figure 3,4). Additionally, there was a high enrichment of the pathway phrase "*Activation of ATR in response to replication stress*" (Data not shown). ATR signal pathway is known to promote a response to DNA breaks described by a halt in the cell cycle or the activation of apoptotic mechanisms. This response may result in cellular senescence when the damage ceases to be fixed (Toledo et al., 2008).

At the IC₂₅, and IC_{12.5} and concentrations similar gene enrichment terms were obtained when the downregulated and upregulated genes were submitted as distinct lists. At the IC_{12.5} concentration, cell cycle-related terms (Figure 8,9) are enriched with a lower score than at the IC₂₅ concentration (Figure 6,7). In contrast, metabolic regulation-related terms remain prominent in the list (Figure 8,9). In addition, cell death regulatory terms are enriched with a higher score in the gene list with an increased expression at the IC₂₅ level (Figure 6,7).

Although elevated apoptotic genes suggest activation of early-stage apoptosis, these transcriptional alterations suggest senescence-linked cell cycle arrest as a plausible mechanism of boric acid-induced growth suppression in the HepG2 cell line. A recent hypothesis proposes that downregulated DNA repair mechanisms may be a characteristic of senescent cells and contribute to or worsen DNA damage. According to the hypothesis, E2F functions as a major regulator of senescence by regulating the transcription of DNA repair genes (Collin et al., 2018). Downregulated DNA damage pathways constitute a significant cluster among enriched terms in the transcriptional profile of cells treated with boric acid at IC₅₀ dose (Figure 4). Additionally, it was shown that the list of downregulated transcripts of IC₅₀ BA treatment dataset was considerably enriched for the E2F-triggered transcription pathway (data not shown). In HepG2 cells treated with boric acid, these transcriptional patterns may be an additional sign of senescence and perhaps have a causal role in DNA damage.

At half-maximal inhibitory concentration, transcriptional reprogramming toward a senescence-like profile was observed. As in many examples reported in the literature (Collin et al., 2018; Kachhap et al., 2010; Mitsiades et al., 2003). DNA damage may occur through sensitization of cells due to downregulated DNA repair-associated response that is correlated with chromosomal organization and cell cycle processes (Figure 5). Direct binding of boric acid to DNA might also be influential, as boric acid has been found to interact with DNA, resulting in the denaturation of the strands in a concentration-dependent way (Ozdemir et al., 2014).

Pathways with decreased expression of DNA repair observed at the IC₅₀ level were also observed at the IC₂₅ level (data not shown) but not at the IC_{12.5} level (data not shown). DNA repair deregulation also observed at IC₂₅ concentration in this study, might be the primary mechanism behind Boron-associated DNA damage, as several studies show an association between imprinted DNA repair genes with DNA damage and senescence (Collin et al., 2018; Kachhap et al., 2010; Mitsiades et al., 2003).

Recently, inhibition of histone deacetylases and consequent chromosomal instability was proposed as a universal molecular mechanism among eukaryotes underlying double-strand DNA breaks in response to high Boron stress. Boric acid, at hazardous levels, caused histone hyperacetylation in *Arabidopsis thaliana*, which is required for chromosomal integrity and shielding DNA from reactive chemicals. A functional 26S proteasome was required to counteract the high Boron-induced hyperacetylation and genotoxicity (Sakamoto et al., 2018).

Histone deacetylase inhibitors may elicit transcriptional suppression of DNA damage response/repair pathways by decreasing the activity of the E2F transcription factor and increasing sensitivity to DNA damage (Kachhap et al., 2010). Furthermore, healthy cells could repair DNA damage caused by histone deacetylase inhibitors, but cancer cells were unable, giving HDACs an edge in tumor-targeted therapy (Lee et al., 2010).

Inhibition of histone deacetylases may be the primary mechanism behind the DNA damage and senescent-like transcriptional profile of boric acid-treated HepG2 cells considering the concentration-dependent transcriptional responses noticed in our investigation. Histone deacetylation might be a common mechanism throughout eukaryotes leading to B-induced effects. In that case, the cancer-targeted activity of histone deacetylases could explain the anti-carcinogenic benefits of dietary Boron and the increased susceptibility of carcinogenic cell lines to cytotoxic effects of Boron compared to healthy cell lines (Barranco & Eckhert, 2004; Canturk et al., 2016). Similarities in gene expression patterns between histone deacetylase inhibitors and bortezomib might indicate enzyme inhibition as the principal mechanism of action for boric acid's cytotoxic profile.

Aside from the transcriptional alterations associated with boric acid-related cytotoxicity, boric acid treatment at the IC₅₀ level resulted in metabolic reprogramming, including downregulated amino acid metabolism, lipid metabolism transcripts, and upregulated xenobiotic metabolism transcripts (Figure 3,4). It is important to note that Boron is a hypothetical metabolic regulator in various organisms (Hunt, 1996). A relationship between Boron stress and amino acid metabolism was discovered in yeast, and a dysregulated amino acid regulatory mechanism was hypothesized to contribute to Boron toxicity (Ulusik, Kaya, Fomenko, et al., 2011). Boric acid-related downregulation of steroid and lipid metabolism pathways, as demonstrated in this work, is particularly

noteworthy given the rising interest in Boron's role as a regulator of lipid metabolism. Dietary Boron has been linked to improved plasma lipid profiles (Donoiu et al., 2018) and the prevention of fatty liver (Basoglu et al., 2010).

Boron is also known to have a role in the metabolism of steroid hormones. Boron consumption has been demonstrated to affect estrogen and testosterone plasma levels (Nielsen et al., 1987). Boron may modulate steroid metabolism by catalyzing the addition of hydroxyl groups to hormones or by binding to hormones and preventing them from degradation (Touillaud et al., 2005). Another hypothesis is that Boron interacts with transport proteins, interfering with the binding of steroid hormones (Bello et al., 2018).

The gene expression profiling identified SREBF-regulated expression as a prominent pathway enriched among downregulated genes at IC₅₀ (Figure 4) and IC_{12.5} levels (Data not shown). Furthermore, SREBF1 and SREBF2 transcripts were shown to be considerably downregulated at all concentrations (Figure 12, 15, 18). SREBP proteins are transcription factors that control the transcription of enzymes and other proteins involved in lipid metabolism (Eberlé et al., 2004). *In vitro*, investigations with various Boron-containing substances revealed downregulated SREBF and its downstream targets (Zhao et al., 2014). These findings point to the downregulation of SREBF-mediated metabolic pathways as a critical mechanism in Boron-induced lipid or steroid metabolism changes. Notably, the upregulation of genes encoding Phase I and II metabolic enzymes was examined at growth-inhibiting boric acid levels. As these enzymes have roles in detoxification and steroid metabolism, their expression implies boron detoxification and possible links in steroid activity (McNamara et al., 2013).

Interestingly, specific modules revealed during the differential module analyses of BA-treatment networks were very similar at changing levels of BA. These modules had the same or similar TFs, and their target genes were enriched with similar or even the same biological processes.

An example is the orange modules identified at all three levels (Figure 12, 15, 18). The top 5 TFs of the orange modules included IRF1, IRF2, STAT1, and STAT2. The orange modules of the IC_{12.5} and IC₅₀ levels also included IRF8, whereas, at the IC₂₅ level, the module additionally included PRDM1. Differentially modular target genes of all three levels of BA were enriched for *Response to type I interferon*. Although the TFs were not included in the enrichment analysis, the function of the TFs aligned well with the target genes as the IRFs, STAT1, and STAT2 are known to elicit antiviral defenses via Type-I Interferon signaling (Antonczyk et al., 2019).

Such changes observed in the network's modular structure suggest interferon type-I signaling as a process induced by boric acid at growth-inhibitory concentrations.

Researchers are currently studying boron-containing chemicals' potential to suppress viruses and the molecular mechanisms underlying their antiviral properties (Trippier & McGuigan, 2010). A recent study found an unexpected link between bortezomib's antiviral role and type I interferon signaling. With the findings presented in this study, type I interferon response emerges as a boron-specific molecular response and a putative mechanism of action by which boric acid exerts its antiviral effects (Dudek et al., 2010).

Taurine metabolism associated with the golden modules and *Fat digestion/absorption* associated with the green modules were other biological processes recurrent in all three BA-treatment networks. These modules were also analogous in their regulatory node content (Figure 12, 15,18). The TFs within the golden modules consisted of ZNF260, ZNF146, ZNF140, and ZNF8 (Figure 12, 15, 18). The TFs of the green modules were GATA1, GATA2, LYL1, and TAL1 at the IC_{12.5} and IC₅₀ levels (Figure 12, 15, 18). In the IC₂₅ level, the TFs were LYL1, TAL1, and ZNF331 (Figure 12, 15, 18).

Taurine is a non-standard sulfur-containing amino acid in mammals. It is not involved in the protein structure and is the most plentiful free amino acid in many tissues, such as the heart, retina, skeletal muscle, and brain. In cells, taurine has protective roles against oxidative stress, and its compound Tau-C1 modulates anti-inflammation (Schuller-Levis & Park, 2003). High taurine levels are sustained in the liver through biosynthesis and transport, and a disturbance in the taurine homeostasis occurs in many liver diseases. Taurine alleviates hepatotoxin-induced cellular damage and is a potential therapeutic supplement in nonalcoholic hepatosteatosis (Miyazaki & Matsuzaki, 2014).

Enrichment analyses have shown that, at the transcriptomic level, cytotoxic BA concentrations evoked drug metabolism and detoxification mechanisms. Taurine metabolism, which emerged as a biological process in the network analyses, might be a prominent mechanism through which HepG2 cells counteract the effects of BA-induced cytotoxicity.

GATA1, GATA2, TAL1, and LYL1, which target green module genes (Figure 12, 15, 18) with dominant enrichment in fat assimilation, typically modulate hematopoietic stem cell differentiation (Pimkin et al., 2014). Although the role of hematopoietic transcriptional factors in a cell line of hepatic origin is unclear, RUNX1 (Bertran et al., 2021; Pimkin et al., 2014; Wilson et al., 2010), which is another master regulator and cooperates with GATA2, TAL1, and LYL1 in hematopoietic stem cells, is known to provide hepatoprotection against lipotoxicity in the early phases of nonalcoholic fatty liver disease. Runx1 also has a regulatory role in transforming fat-accumulating cells into fat burners (Hou et al., 2018).

Maintaining a balance in fat intake and export is critical for liver health, and a loss in the balance in favor of fat storage is implicated in nonalcoholic fatty liver disease (Liu et al., 2010). Although excessive storage of triglycerides in hepatocytes is a manifestation of NAFLD, according to a study, the accumulated fat is probably not inherently harmful but guards the liver against further damage (Yamaguchi et al., 2007).

Yellow-green modules, which were driven by the TFs SREBF1, SREBF2, and ZNF816, were also interesting for understanding the role of boric acid in lipid metabolism (Figure 12, 15, 18). At IC_{12.5} and IC₅₀ levels, these modules' target genes were significantly enriched for *Steroid biosynthesis* (Figure 12, 18), whereas, at the IC₂₅ level, *drug metabolism* was a more appropriate enrichment term for yellow-green target genes (Figure 15). Although the enrichment analyses only involved the target genes, the TFs were compatible with the enriched process as the SREBF1 and SREBF2 are primary regulators of steroid metabolism (Eberlé et al., 2004). ZNF816 was also predicted to be a prominent regulator within these modules; however, its role in steroid metabolism is unknown. The primary microarray analyses indicated altered metabolism of steroids and cholesterol in downregulated genes, with a putative role for SREBF-regulation in metabolic pathways (data not shown). Moreover, SREBF1 and SREBF2 had negative LFC values at all levels (Figure 12, 15, 18). The differential modules in network analyses again show SREBF-regulated transcription as a potential mechanism of boric acid-induced steroid metabolism. In the liver, SREBF1 and SREBF2 (SREBPs) regulate intracellular lipid accumulation and are implicated in the etiology of fatty liver disease (Liang et al., 2020). Particularly SREBF1 levels increase in response to insulin within the hepatocytes, leading to lipid deposition within cells. Fish oil and omega-3 within diets have hepatoprotective effects through decreasing SREBF1 expression. Furthermore, elevated levels of SREBPs have been causally linked to ER stress, hepatitis caused by HCV, and the development of liver cancer (Moslehi & Hamidi-Zad, 2018). Earlier, a boron-rich diet was effective in preventing fatty liver (Basoglu et al., 2010). Here, the decrease in SREBP expression levels induced by boric acid treatment suggests that Boron may protect against liver diseases.

BA has been many times linked to energy metabolism, and BA-supplemented diets could lead to weight reduction. The repeated appearance of network modules linked with fat assimilation and steroid biosynthesis in this work (Figure 12, 15, 18) implies boric acid treatment-related reprogramming of energy metabolism. At the IC_{12.5} level, a stronger inclination toward transcriptional changes in metabolic pathways was observable within enrichment results (Figure 8, 9). PPAR signaling, which occurred in the IC_{12.5} level regulatory network modules (Figure 18), is also noteworthy since it is a central pathway in regulating sugar and lipid balance and might also be another means of BA-dependent mechanism in the regulation of cellular energetics (Hong et al., 2019)

A REST-driven module was present in all BA treatment subgraphs of differential modularity (Figure 12, 15, 18). At IC_{12.5} and IC₂₅ levels, these dark purple modules regulated by REST had relatively high enrichment scores in *Negative regulation of Calcium exocytosis* (Figure 15, 18). At IC₅₀, the dark purple module with REST was more predisposed towards enrichment in *Catecholamine secretion* (Figure 12). REST is usually expressed in neural tissues and involved in neurogenesis (Schoenherr & Anderson, 1995). REST-regulated Ca²⁺ dependent exocytosis was demonstrated in glioblastoma cells (Prada et al., 2011). In HepG2 cells, the Ca²⁺-mediated exocytosis is controlled by cytoplasmic Ca²⁺ and cytosolic protein kinase (Bruck et al., 1994). Boric acid might mediate cellular effects through Ca²⁺ signaling by generating a dose-dependent inhibition in the Ca²⁺ discharge from the intracellular reservoirs in prostate cells (Barranco & Eckhart, 2006). Calcium signaling with other enriched terms, such as negative regulation of camp-dependent pK activity and inositol phosphate metabolism, also indicates BA-stimulated regulation of signaling events on a cellular scale (Figure 18).

Black modules of the IC₅₀-level and the IC₂₅-level networks are small modules with six or seven nodes (Figure 12, 15). Both involve FOXJ3 as the driving transcription factor (Figure 12, 15) and KRTAPs (keratin-associated proteins) as the target genes (data not shown). The black modules were associated with the keratinization process. The black modules might suggest a role for keratins implicated in various liver diseases and may play a role in signaling the response to toxicity (Zatloukal et al., 2006).

RNA metabolism is a frequent theme in the transcriptomic level changes elicited by BA at all three levels. RNA metabolism was significantly enriched within the DEG lists of IC_{12.5}, IC₂₅, and IC₅₀ (data not shown). Some terms related to RNA metabolism were significantly associated with the modules in the differential network analysis. At the IC_{12.5} and IC₅₀ levels, the target genes of the purple modules were significantly enriched in RNA secondary structure unwinding (Figure 12, 18). At the IC_{12.5} level, ATF2, MBD2, CTCF, ETV1, and ZNF563 (Figure 18); at the IC₅₀ level, MBD2, CTCF, CTCFL, RFX1, and TFAP2B (Figure 12) were the top TFs participating in the regulation of purple modules' targets. At the IC_{12.5} level, two other processes predicted in differential modules were also related to RNA metabolism. These terms were *Spliceosome* predicted in the pink module and *Positive regulation of mRNA splicing via spliceosome* in the lilac module (Figure 18). A prior study found that boric acid can hinder the second stage of mRNA splicing in a concentration-dependent and reversible way. The inhibition only occurred in the presence of boric acid but not other boric acid esters. According to the study, adding boric acid to an *in vitro* mRNA splicing reaction led to an initial elevation in the RNA splicing activity and the splicing products, which then declined steadily. At 5 mM, the amount of mRNA splicing intermediates and products were maximal. The splicing activity diminished with increasing BA concentration and was impaired at nearly 20 mM

boric acid (Shomron & Ast, 2003). Moreover, in an acellular assay, boric acid caused a ten-fold increase in the transcription products. (Dzondo-Gadet et al., 2002).

RNA secondary structure unwinding process occurred at IC_{12.5} (6 mM BA) and IC₅₀ (24 mM BA) level modules with some differences in top TFs (Figure 12, 18). Besides, at IC_{12.5}, mRNA splicing-associated terms were present in modules (Figure 18), whereas, at IC₂₅ (12 mM), any RNA-involved process could not be noticed within the differential modules (Figure 15). These patterns might reflect a similar dynamic in which the cell undergoes a transcriptional reprogramming stemming from boric acid's role in RNA metabolism and mRNA splicing events.

Boron elicits U-shaped responses in various biological processes depending on the concentration (Calabrese et al., 2023). Some U-shaped transcriptomic patterns were noticeable regarding the concentration range used in this study (Figure 19, App. Figure 6, App Figure 7). The content and the patterns of differentially expressed transcripts of IC₂₅ were lower than that of IC₅₀ and the IC_{12.5} level, given the Volcano plots and the heatmap (Figure 1, Figure 2, App. Figure 6, App Figure 7). Moreover, the order of the number of differentially expressed transcripts detected for each level was IC₂₅ > IC_{12.5} > IC₅₀. This order did not change with respect to changes in statistical testing (App. Table 2).

A possible explanation might be underlying the role of Boron in RNA metabolism. Boron boosts RNA synthesis and transcription and can affect mRNA splicing in a millimolar range (Dzondo-Gadet et al., 2002; Shomron & Ast, 2003). In an acellular experimental setting, boric acid can improve the mRNA splicing activity up to 5 mM and impair the second stage splicing after that concentration (Shomron & Ast, 2003). Furthermore, in another study, BA is reported to inflate RNA synthesis rate multiple times, up to 10 mM BA (Dzondo-Gadet et al., 2002). Similar effects might also be present in the current study. mRNA splicing has occurred as a key enriched process at 6 mM (IC_{12.5}), but modules related to mRNA splicing were not significant at larger doses (Figure 12, 15, 18). Alternative splicing and changing RNA metabolism might have led to the widening of the DEG list up to nearly IC₂₅, which might have gradually subsided after this threshold due to the splicing inhibition, ongoing transcriptomic reprogramming leading to metabolic slow-down, and senescence. However, this explanation should be regarded with caution since the observed transcriptomic U-turn might be an artifact of inevitable sources of error when comparing different experimental batches.

Out-grouping of the IC₂₅ DEG profile was also observed when the datasets were preprocessed with fRMA (App. Figure 6), which can account for the batch effect to some extent, and vsn+quantile, which effectively normalized between-array variation (App. Figure 11, 12). On the other hand, it should be noted that batch effect removal techniques do not work effectively when the unwanted source of variation coincides with the

biological condition of interest (Leek et al., 2012; Leek & Storey, 2007). In this study, differences in the handling and the calibration of the micropipettes, varying effective concentrations and differential adsorption of BA due to temperature changes might have contributed to unremovable sources of unwanted variation. Furthermore, A_{260}/A_{230} ratios which reflect the impurities in total RNA were slightly poorer for the IC₂₅ samples (App Table 1). Therefore, the level of impurities in the RNA might also have impacted the quality of the hybridizations for the IC₂₅ experimental group, and this factor might have led to artificial variation in the findings. Hence, the findings should be interpreted cautiously, considering the potential sources of error stemming from unremovable sources of unwanted variation.

It is important to note that there may be limitations to the microarray and network analyses presented. Although microarray technology is a powerful tool for analyzing transcripts at a genome-wide level, small sample sizes used for each treatment level could increase the risk of false positives and limit the generalizability of the results. Additionally, the TF motif lists obtained from the motif database may not represent all possible motifs, and the promoter region specified in the motif search could exclude some TF gene relations. As a result, the TF-gene lists provided at the beginning of the analysis may be biased toward specific biological processes. Furthermore, incomplete initial data could lead to false negatives in the network. Therefore, validating the critical molecular findings through biological assays is crucial.

The results presented here could help clarify the molecular mechanisms of the *in vitro* effects of BA and potentially provide additional clues about the molecular basis of Boron-based genotoxicity, antiviral, antiproliferative, and apoptotic effects investigated in other studies. Further investigation is needed to determine how this wide variety of effects changes with time and more doses, as well as to understand the subtleties of the underlying regulatory mechanisms.

REFERENCES

- Abdel-Hamied, K. M. (2015). Effect of long-term boron administration on the renal cortical structure of adult male albino rats and role of vitamin C coadministration. *The Egyptian Journal of Histology*, 38(1), 57–67. <https://doi.org/10.1097/01.EHX.0000459992.94295.88>
- Ahmad, A. A., & Alsaad, A. M. (2007). Adhesive B-doped DLC films on biomedical alloys used for bone fixation. *Bulletin of Materials Science*, 30(4), 301–308.
- Akbas, F., & Aydin, Z. (2012). Boric acid increases the expression levels of human anion exchanger genes SLC4A2 and SLC4A3. *Genetics and Molecular Research : GMR*, 11(2), 847–854. <https://doi.org/10.4238/2012.April.3.6>
- Antonczyk, A., Krist, B., Sajek, M., Michalska, A., Piaszyk-Borychowska, A., Plens-Galaska, M., Wesoly, J., & Bluysen, H. A. R. (2019). Direct inhibition of IRF-dependent transcriptional regulatory mechanisms associated with disease. *Frontiers in Immunology*, 10(MAY). <https://doi.org/10.3389/fimmu.2019.01176>
- Apdik, H., Doğan, A., Demirci, S., Aydın, S., & Şahin, F. (2015). Dose-dependent Effect of Boric Acid on Myogenic Differentiation of Human Adipose-derived Stem Cells (hADSCs). *Biological Trace Element Research*, 165(2), 123–130. <https://doi.org/10.1007/s12011-015-0253-3>
- Appannanavar, S., Biswal, M., Rajkumari, N., Mohan, B., & Taneja, N. (2013). Evaluation of commercial boric acid containing vials for urine culture: low risk of contamination and cost effectiveness considerations. *Indian Journal of Pathology & Microbiology*, 56(3), 261–264. <https://doi.org/10.4103/0377-4929.120386>
- Aquea, F., Federici, F., Moscoso, C., Vega, A., Jullian, P., Haseloff, J., & Arce-Johnson, P. (2012). A molecular framework for the inhibition of Arabidopsis root growth in

- response to boron toxicity. *Plant, Cell and Environment*, 35(4), 719–734. <https://doi.org/10.1111/j.1365-3040.2011.02446.x>
- Arslan, M., Topaktas, M., & Rencuzogullari, E. (2008). The effects of boric acid on sister chromatid exchanges and chromosome aberrations in cultured human lymphocytes. *Cytotechnology*, 56(2), 91–96. <https://doi.org/10.1007/s10616-007-9094-z>
- Babicki, S., Arndt, D., Marcu, A., Liang, Y., Grant, J. R., Maciejewski, A., & Wishart, D. S. (2016). Heatmapper: web-enabled heat mapping for all. *Nucleic Acids Research*, 44(1). <https://doi.org/10.1093/NAR/GKW419>
- Bader, G. D., Isserlin, R., Merico, D., & Voisin, V. (2014). Enrichment Map - a Cytoscape app to visualize and explore OMICs pathway enrichment results. *F1000Research*, 3. <https://doi.org/10.12688/f1000research.4536.1>
- Barranco, W. T., & Eckhert, C. D. (2004). Boric acid inhibits human prostate cancer cell proliferation. *Cancer Letters*, 216(1), 21–29. <https://doi.org/10.1016/j.canlet.2004.06.001>
- Barranco, W. T., & Eckhert, C. D. (2006). Cellular changes in boric acid-treated DU-145 prostate cancer cells. *British Journal of Cancer*, 94(6), 884–890. <https://doi.org/10.1038/sj.bjc.6603009>
- Basoglu, A., Baspinar, N., & Ozturk, A. S. (2010). Effects of boron administration on hepatic steatosis, hematological and biochemical profiles in obese rabbits. *Trace Elements and Electrolytes*, 27(4), 225–231. <http://www.dustri.com/nc/journals-in-english/mag/trace-elements-and-electrolytes.html%0Ahttp://ovidsp.ovid.com/ovidweb.cgi?T=JS&PAGE=reference&D=emed12&NEWS=N&AN=359834297>
- Bello, M., Guadarrama-García, C., Velasco-Silveyra, L. M., Farfán-García, E. D., & Soriano-Ursúa, M. A. (2018). Several effects of boron are induced by uncoupling steroid hormones from their transporters in blood. *Medical Hypotheses*, 118, 78–83. <https://doi.org/10.1016/j.mehy.2018.06.024>
- Benderdour, M., Van Bui, T., Hess, K., Dicko, a, Belleville, F., & Dousset, B. (2000). Effects of boron derivatives on extracellular matrix formation. *Journal of Trace Elements in Medicine and Biology: Organ of the Society for Minerals and Trace Elements (GMS)*, 14(3), 168–173.
- Bertran, L., Pastor, A., Portillo-Carrasquer, M., Binetti, J., Aguilar, C., Martínez, S., Vives, M., Sabench, F., Porrás, J. A., Riesco, D., Castillo, D. Del, Richart, C., & Auguet, T. (2021). The potential protective role of runx1 in nonalcoholic fatty liver

- disease. *International Journal of Molecular Sciences*, 22(10).
<https://doi.org/10.3390/ijms22105239>
- Brittingham, A., & Wilson, W. a. (2014). The Antimicrobial Effect of Boric Acid on *Trichomonas vaginalis*. *Sexually Transmitted Diseases*, 41(12), 718–722.
<https://doi.org/10.1097/OLQ.0000000000000203>
- Bruck, R., Nathanson, M. H., Roelofsen, H., & Boyer, J. L. (1994). Effects of protein kinase C and cytosolic Ca²⁺ on exocytosis in the isolated perfused rat liver. *Hepatology*, 20(4). <https://doi.org/10.1002/hep.1840200436>
- Calabrese, E., Pressman, P., Agathokleous, E., Dhawan, G., Kapoor, R., & Calabrese, V. (2023). Boron enhances adaptive responses and biological performance via hormetic mechanisms. In *Chemico-Biological Interactions* (Vol. 376).
<https://doi.org/10.1016/j.cbi.2023.110432>
- Canturk, Z., Tunali, Y., Korkmaz, S., & Gulbaş, Z. (2016). Cytotoxic and apoptotic effects of boron compounds on leukemia cell line. *Cytotechnology*, 68(1), 87–93.
<https://doi.org/10.1007/s10616-014-9755-7>
- Cao, J., Jiang, L., Zhang, X., Yao, X., Geng, C., Xue, X., & Zhong, L. (2008). Boric acid inhibits LPS-induced TNF- α formation through a thiol-dependent mechanism in THP-1 cells. *J Trace Elem Med Biol*, 22(3), 189–195.
<https://doi.org/10.1016/j.jtemb.2008.03.005>
- Capati, M. L. F., Nakazono, A., Igawa, K., Ookubo, K., Yamamoto, Y., Yanagiguchi, K., Kubo, S., Yamada, S., & Hayashi, Y. (2016). Boron Accelerates Cultured Osteoblastic Cell Activity through Calcium Flux. *Biological Trace Element Research*, 174(2), 300–308. <https://doi.org/10.1007/s12011-016-0719-y>
- Çelikezen, F. Ç., Turkez, H., Togar, B., & Izgi, M. S. (2014). DNA damaging and biochemical effects of potassium tetraborate. *EXCLI Journal*, 13, 446–450.
- Chen, D., Frezza, M., Schmitt, S., Kanwar, J., & P Dou, Q. (2011). Bortezomib as the first proteasome inhibitor anticancer drug: current status and future perspectives. *Current Cancer Drug Targets*, 11(3), 239–253.
<https://doi.org/10.2174/156800911794519752>
- Chou, F. I., Chung, H. P., Liu, H. M., Chi, C. W., & Lui, W. Y. (2009). Suitability of boron carriers for BNCT: Accumulation of boron in malignant and normal liver cells after treatment with BPA, BSH and BA. *Applied Radiation and Isotopes*, 67(7-8 SUPPL.). <https://doi.org/10.1016/j.apradiso.2009.03.025>

- Ciani, L., & Ristori, S. (2012). Boron as a platform for new drug design. *Expert Opinion on Drug Discovery*, 7(11), 1017–1027. <https://doi.org/10.1517/17460441.2012.717530>
- Collin, G., Huna, A., Warnier, M., Flaman, J. M., & Bernard, D. (2018). Transcriptional repression of DNA repair genes is a hallmark and a cause of cellular senescence article. *Cell Death and Disease*, 9(3). <https://doi.org/10.1038/s41419-018-0300-z>
- Cui, Y., Winton, M. I., Zhang, Z. F., Rainey, C., Marshall, J., De Kernion, J. B., & Eckhert, C. D. (2004). Dietary boron intake and prostate cancer risk. *Oncology Reports*, 11(4), 887–892.
- Dai, M., Wang, P., Boyd, A. D., Kostov, G., Athey, B., Jones, E. G., Bunney, W. E., Myers, R. M., Speed, T. P., Akil, H., Watson, S. J., & Meng, F. (2005). Evolving gene/transcript definitions significantly alter the interpretation of GeneChip data. *Nucleic Acids Research*. <https://doi.org/10.1093/nar/gni179>
- Del Palacio, A., Cuétara, M. S., López-Suso, M. J., Amor, E., & Garau, M. (2002). Randomized prospective comparative study: Short-term treatment with ciclopiroxolamine (cream and solution) versus boric acid in the treatment of otomycosis. *Mycoses*, 45(7–8), 317–328. <https://doi.org/10.1046/j.1439-0507.2002.00737.x>
- Dieter, M. P. (1994). Toxicity and carcinogenicity studies of boric acid in male and female B6C3F1 mice. *Environmental Health Perspectives*, 102(SUPPL. 7), 93–97.
- Donoiu, I., Militaru, C., Obleagă, O., Hunter, J. M., Neamțu, J., Biță, A., Scorei, I. R., & Rogoveanu, O. C. (2018). Effects of boron-containing compounds on cardiovascular disease risk factors – A review. In *Journal of Trace Elements in Medicine and Biology* (Vol. 50, pp. 47–56). <https://doi.org/10.1016/j.jtemb.2018.06.003>
- Dudek, S. E., Luig, C., Pauli, E.-K., Schubert, U., & Ludwig, S. (2010). The Clinically Approved Proteasome Inhibitor PS-341 Efficiently Blocks Influenza A Virus and Vesicular Stomatitis Virus Propagation by Establishing an Antiviral State. *Journal of Virology*, 84(18). <https://doi.org/10.1128/jvi.00533-10>
- Duydu, Y., Ba??aran, N., ??st??nda??, A., Aydin, S., ??nde??er, ??lk??, Ataman, O. Y., Aydos, K., D??ker, Y., Ickstadt, K., Waltrup, B. S., Golka, K., & Bolt, H. M. (2011). Reproductive toxicity parameters and biological monitoring in occupationally and environmentally boron-exposed persons in Bandirma, Turkey. *Archives of Toxicology*, 85(6), 589–600. <https://doi.org/10.1007/s00204-011-0692-3>

- Dzondo-Gadet, M., Mayap-Nzietchueng, R., Hess, K., Nabet, P., Belleville, F., & Dousset, B. (2002). Action of Boron at the Molecular Level Effects on Transcription and Translation in an Acellular System. *Biological Trace Element Research*, 85(1), 23–33. <https://doi.org/10.1385/BTER:85:1:23>
- Eberlé, D., Hegarty, B., Bossard, P., Ferré, P., & Foufelle, F. (2004). SREBP transcription factors: Master regulators of lipid homeostasis. In *Biochimie* (Vol. 86, Issue 11, pp. 839–848). <https://doi.org/10.1016/j.biochi.2004.09.018>
- Eijssen, L. M. T., Jaillard, M., Adriaens, M. E., Gaj, S., de Groot, P. J., Müller, M., & Evelo, C. T. (2013). User-friendly solutions for microarray quality control and pre-processing on ArrayAnalysis.org. *Nucleic Acids Research*, 41(Web Server issue). <https://doi.org/10.1093/nar/gkt293>
- El-Dakdoky, M. H., & Abd El-Wahab, H. M. F. (2013). Impact of boric acid exposure at different concentrations on testicular DNA and male rats fertility. *Toxicology Mechanisms and Methods*. <https://doi.org/10.3109/15376516.2013.764951>
- Farfán-García, E. D., Castillo-Mendieta, N. T., Ciprés-Flores, F. J., Padilla-Martínez, I. I., Trujillo-Ferrara, J. G., & Soriano-Ursúa, M. A. (2016). Current data regarding the structure-toxicity relationship of boron-containing compounds. *Toxicology Letters*, 258, 115–125. <https://doi.org/10.1016/j.toxlet.2016.06.018>
- Frommer, W. B., & von Wirén, N. (2002). Ping-pong with boron. *Nature*, 420(3), 282–283. <https://doi.org/10.1111/dom.12265>
- Geyikoglu, F., & Turkez, H. (2008). Boron compounds reduce vanadium tetraoxide genotoxicity in human lymphocytes. *Environmental Toxicology and Pharmacology*, 26(3), 342–347. <https://doi.org/10.1016/j.etap.2008.07.002>
- Glass, K., Huttenhower, C., Quackenbush, J., & Yuan, G.-C. (2013). Passing Messages between Biological Networks to Refine Predicted Interactions. *PLoS ONE*, 8(5), e64832. <https://doi.org/10.1371/journal.pone.0064832>
- Grant, C. E., Bailey, T. L., & Noble, W. S. (2011). FIMO: Scanning for occurrences of a given motif. *Bioinformatics*, 27(7). <https://doi.org/10.1093/bioinformatics/btr064>
- Gröger, N., Fröhlich, H., Maier, H., Olbrich, A., Kostin, S., Braun, T., & Boettger, T. (2010). SLC4A11 prevents osmotic imbalance leading to corneal endothelial dystrophy, deafness, and polyuria. *Journal of Biological Chemistry*, 285(19), 14467–14474. <https://doi.org/10.1074/jbc.M109.094680>

- Gülsoy, N., Yavaş, C., & Mutlu, Ö. (2015). Genotoxic effects of boric acid and borax in zebrafish, danio rerio using alkaline comet assay. *EXCLI JOURNAL*, *14*, 890–899.
- Hacioglu, C., Kar, F., Kacar, S., Sahinturk, V., & Kanbak, G. (2020). High Concentrations of Boric Acid Trigger Concentration-Dependent Oxidative Stress, Apoptotic Pathways and Morphological Alterations in DU-145 Human Prostate Cancer Cell Line. *Biological Trace Element Research*. <https://doi.org/10.1007/s12011-019-01739-x>
- Heindel, J. J., Price, C. J., Field, E. A., Marr, M. C., Myers, C. B., Morrissey, R. E., & Schwetz, B. A. (1992). Developmental toxicity of boric acid in mice and rats. *Fundamental and Applied Toxicology*, *18*(2), 266–277. [https://doi.org/10.1016/0272-0590\(92\)90055-M](https://doi.org/10.1016/0272-0590(92)90055-M)
- Hong, F., Pan, S., Guo, Y., Xu, P., & Zhai, Y. (2019). PPARs as nuclear receptors for nutrient and energy metabolism. In *Molecules* (Vol. 24, Issue 14). <https://doi.org/10.3390/molecules24142545>
- Hou, X., Zhang, Y., Li, W., Hu, A. J., Luo, C., Zhou, W., Hu, J. K., Daniele, S. G., Wang, J., Sheng, J., Fan, Y., Greenberg, A. S., Farmer, S. R., & Hu, M. G. (2018). CDK6 inhibits white to beige fat transition by suppressing RUNX1. *Nature Communications*, *9*(1). <https://doi.org/10.1038/s41467-018-03451-1>
- Huang, D. W., Sherman, B. T., Tan, Q., Kir, J., Liu, D., Bryant, D., Guo, Y., Stephens, R., Baseler, M. W., Lane, H. C., & Lempicki, R. A. (2007). DAVID Bioinformatics Resources: Expanded annotation database and novel algorithms to better extract biology from large gene lists. *Nucleic Acids Research*, *35*(SUPPL.2). <https://doi.org/10.1093/nar/gkm415>
- Hunt, C. D. (1996). Biochemical effects of physiological amounts of dietary boron. *Journal of Trace Elements in Experimental Medicine*, *9*(4), 185–213. [https://doi.org/10.1002/\(SICI\)1520-670X\(1996\)9:4<185::AID-JTRA6>3.0.CO;2-Q](https://doi.org/10.1002/(SICI)1520-670X(1996)9:4<185::AID-JTRA6>3.0.CO;2-Q)
- Hunt, C. D. (1998). Regulation of enzymatic activity. *Biological Trace Element Research*, *66*(1–3), 205–225. <https://doi.org/10.1007/BF02783139>
- Hunt, C. D. (2012). Dietary boron: Progress in establishing essential roles in human physiology. *Journal of Trace Elements in Medicine and Biology*, *26*(2–3), 157–160. <https://doi.org/10.1016/j.jtemb.2012.03.014>
- Hunter, P. (2009). Not boring at all. Boron is the new carbon in the quest for novel drug candidates. *EMBO Reports*, *10*(2), 125–128. <https://doi.org/10.1038/embor.2009.2>

- Ideura, T., Hora, K., Sato, K., Futatsugi, Y., Tachibana, N., Yamaura, S., Muramatsu, T., Akou, S., Oguchi, T., & Kiyosawa, K. (1998). A case of acute renal failure due to boric acid poisoning. *Shinshu Medical Journal*, *46*(3), 193–199.
- Kachhap, S. K., Rosmus, N., Collis, S. J., Kortenhorst, M. S. Q., Wissing, M. D., Hedayati, M., Shabbeer, S., Mendonca, J., Deangelis, J., Marchionni, L., Lin, J., Höti, N., Nortier, J. W. R., Dewese, T. L., Hammers, H., & Carducci, M. A. (2010). Downregulation of homologous recombination DNA repair genes by HDAC inhibition in prostate cancer is mediated through the E2F1 transcription factor. *PLoS ONE*, *5*(6). <https://doi.org/10.1371/journal.pone.0011208>
- Kaya, A., Karakaya, H. C., Fomenko, D. E., Gladyshev, V. N., & Koc, A. (2009). Identification of a novel system for boron transport: Atr1 is a main boron exporter in yeast. *Molecular and Cellular Biology*, *29*(13), 3665–3674. <https://doi.org/10.1128/MCB.01646-08>
- Kobayashi, M., Mutoh, T., & Matoh, T. (2004). Boron nutrition of cultured tobacco BY-2 cells. IV. Genes induced under low boron supply. *Journal of Experimental Botany*, *55*(401), 1441–1443. <https://doi.org/10.1093/jxb/erh142>
- Kobylewski, S. E., Henderson, K. A., Yamada, K. E., & Eckhert, C. D. (2016). Activation of the EIF2 α /ATF4 and ATF6 Pathways in DU-145 Cells by Boric Acid at the Concentration Reported in Men at the US Mean Boron Intake. *Biological Trace Element Research*, 1–16. <https://doi.org/10.1007/s12011-016-0824-y>
- Korkmaz, M., Uzgören, E., Bakirdere, S., Aydin, F., & Ataman, O. Y. (2007). Effects of dietary boron on cervical cytopathology and on micronucleus frequency in exfoliated buccal cells. *Environmental Toxicology*, *22*(1), 17–25. <https://doi.org/10.1002/tox.20229>
- Kraft, S. L., Gavin, P. R., Leathers, C. W., DeHaan, C. E., Bauer, W. F., Miller, D. L., Dorn, R. V., & Griebenow, M. L. (1994). Biodistribution of boron in dogs with spontaneous intracranial tumors following borocaptate sodium administration. *Cancer Research*, *54*(5), 1259–1263.
- Ku, W. W., Chapin, R. E., Wine, R. N., & Gladen, B. C. (1993). Testicular toxicity of boric acid (BA): Relationship of dose to lesion development and recovery in the F344 rat. *Reproductive Toxicology*, *7*(4), 305–319. [https://doi.org/10.1016/0890-6238\(93\)90020-8](https://doi.org/10.1016/0890-6238(93)90020-8)
- Kulakovskiy, I. V., Medvedeva, Y. A., Schaefer, U., Kasianov, A. S., Vorontsov, I. E., Bajic, V. B., & Makeev, V. J. (2013). HOCOMOCO: A comprehensive collection of

- human transcription factor binding sites models. *Nucleic Acids Research*, 41(D1). <https://doi.org/10.1093/nar/gks1089>
- Landolph, J. R. (1985). Cytotoxicity and negligible genotoxicity of borax and borax ores to cultured mammalian cells. *American Journal of Industrial Medicine*, 7(1), 31–43. <https://doi.org/10.1002/ajim.4700070105>
- Lee, J. H., Choy, M. L., Ngo, L., Foster, S. S., & Marks, P. A. (2010). Histone deacetylase inhibitor induces DNA damage, which normal but not transformed cells can repair. *Proceedings of the National Academy of Sciences of the United States of America*, 107(33), 14639–14644. <https://doi.org/10.1073/pnas.1008522107>
- Leek, J. T., Johnson, W. E., Parker, H. S., Jaffe, A. E., & Storey, J. D. (2012). The SVA package for removing batch effects and other unwanted variation in high-throughput experiments. *Bioinformatics*, 28(6). <https://doi.org/10.1093/bioinformatics/bts034>
- Leek, J. T., & Storey, J. D. (2007). Capturing heterogeneity in gene expression studies by surrogate variable analysis. *PLoS Genetics*, 3(9). <https://doi.org/10.1371/journal.pgen.0030161>
- Liang, C., Qiao, L., Han, Y., Liu, J., Zhang, J., & Liu, W. (2020). Regulatory roles of SREBF1 and SREBF2 in lipid metabolism and deposition in two chinese representative fat-tailed sheep breeds. *Animals*, 10(8). <https://doi.org/10.3390/ani10081317>
- Liao, S. F., Monegue, J. S., Lindemann, M. D., Cromwell, G. L., & Matthews, J. C. (2011). Dietary supplementation of boron differentially alters expression of borate transporter (NaBC1) mRNA by jejunum and kidney of growing pigs. *Biological Trace Element Research*, 143(2), 901–912. <https://doi.org/10.1007/s12011-010-8936-2>
- Liu, Q., Bengmark, S., & Qu, S. (2010). The role of hepatic fat accumulation in pathogenesis of non-alcoholic fatty liver disease (NAFLD). In *Lipids in Health and Disease* (Vol. 9). <https://doi.org/10.1186/1476-511X-9-42>
- Lum, K. T., & Meers, P. D. (1989). Boric acid converts urine into an effective bacteriostatic transport medium. *Journal of Infection*, 18(1), 51–58. [https://doi.org/10.1016/S0163-4453\(89\)93667-0](https://doi.org/10.1016/S0163-4453(89)93667-0)
- McCall, M. N., Bolstad, B. M., & Irizarry, R. A. (2010). Frozen robust multiarray analysis (fRMA). *Biostatistics*, 11(2). <https://doi.org/10.1093/biostatistics/kxp059>

- McNamara, K. M., Nakamura, Y., Miki, Y., & Sasano, H. (2013). Phase two steroid metabolism and its roles in breast and prostate cancer patients. In *Frontiers in Endocrinology* (Vol. 4, Issue SEP). <https://doi.org/10.3389/fendo.2013.00116>
- Merico, D., Isserlin, R., Stueker, O., Emili, A., & Bader, G. D. (2010). Enrichment map: A network-based method for gene-set enrichment visualization and interpretation. *PLoS ONE*, *5*(11). <https://doi.org/10.1371/journal.pone.0013984>
- Mitsiades, N., Mitsiades, C. S., Richardson, P. G., Poulaki, V., Tai, Y. T., Chauhan, D., Fanourakis, G., Gu, X., Bailey, C., Joseph, M., Libermann, T. A., Schlossman, R., Munshi, N. C., Hideshima, T., & Anderson, K. C. (2003). The proteasome inhibitor PS-341 potentiates sensitivity of multiple myeloma cells to conventional chemotherapeutic agents: Therapeutic applications. *Blood*, *101*(6), 2377–2380. <https://doi.org/10.1182/blood-2002-06-1768>
- Miyazaki, T., & Matsuzaki, Y. (2014). Taurine and liver diseases: A focus on the heterogeneous protective properties of taurine. In *Amino Acids* (Vol. 46, Issue 1). <https://doi.org/10.1007/s00726-012-1381-0>
- Moorman, W. J., Ahlers, H. W., Chapin, R. E., Daston, G. P., Foster, P. M. D., Kavlock, R. J., Morawetz, J. S., Schnorr, T. M., & Schrader, S. M. (2000). Prioritization of NTP reproductive toxicants for field studies. *Reproductive Toxicology*, *14*(4), 293–301. [https://doi.org/10.1016/S0890-6238\(00\)00089-7](https://doi.org/10.1016/S0890-6238(00)00089-7)
- Moseman, R. F. (1994). Chemical disposition of boron in animals and humans. *Environmental Health Perspectives*, *102*(SUPPL. 7), 113–117. <https://doi.org/10.1289/ehp.94102s7113>
- Moslehi, A., & Hamidi-Zad, Z. (2018). Role of SREBPs in liver diseases: A mini-review. In *Journal of Clinical and Translational Hepatology* (Vol. 6, Issue 3). <https://doi.org/10.14218/JCTH.2017.00061>
- Müezzinoğlu, T., Korkmaz, M., Neşe, N., Bakirdere, S., Arslan, Y., Ataman, O. Y., & Lekili, M. (2011). Prevalence of prostate cancer in high boron-exposed population: A community-based study. *Biological Trace Element Research*, *144*(1–3), 49–57. <https://doi.org/10.1007/s12011-011-9023-z>
- Murray, F. J. (1998). A comparative review of the pharmacokinetics of boric acid in rodents and humans. *Biological Trace Element Research*, *66*(1–3), 331–341. <https://doi.org/10.1007/BF02783146>
- Nacar, A., Selçuk, Y., Okuyan, H. M., Sefil, N. K., Deligönül, E., & Nacar, E. (2014). Borik asit uygulamasının sıçan böbrek ve testis dokusunda oluşturduğu hasara karşı

Omega-3 yağ asitlerinin koruyucu etkisinin histopatolojik olarak incelenmesi. *Dicle Tıp Dergisi*, 41(2).

Nielsen, F. H., Hunt, C. D., Mullen, L. M., & Hunt, J. R. (1987). Effect of dietary boron on mineral, estrogen, and testosterone metabolism in postmenopausal women. *FASEB Journal*, 1(5), 394–397. <https://doi.org/10.1096/fasebj.1.5.3678698>

O'Donovan, M. R., Mee, C. D., Fenner, S., Teasdale, A., & Phillips, D. H. (2011). Boronic acids-A novel class of bacterial mutagen. *Mutation Research - Genetic Toxicology and Environmental Mutagenesis*, 724(1–2), 1–6. <https://doi.org/10.1016/j.mrgentox.2011.05.006>

Oesper, L., Merico, D., Isserlin, R., & Bader, G. D. (2011). WordCloud: A Cytoscape plugin to create a visual semantic summary of networks. *Source Code for Biology and Medicine*, 6. <https://doi.org/10.1186/1751-0473-6-7>

Ogando, D. G., Jalimarada, S. S., Zhang, W., Vithana, E. N., & Bonanno, J. a. (2013). SLC4A11 is an EIPA-sensitive Na⁽⁺⁾ permeable pHi regulator. *American Journal of Physiology. Cell Physiology*, 305(7), C716-27. <https://doi.org/10.1152/ajpcell.00056.2013>

Oz, M. T., Yilmaz, R., Eyidogan, F., de Graaff, L., Yucel, M., & Oktem, H. A. (2009). Microarray Analysis of Late Response to Boron Toxicity in Barley (*Hordeum vulgare* L.) Leaves. *Turkish Journal of Agriculture and Forestry*, 33(2), 191–202.

Ozdemir, A., Gursacılı, R. T., & Tekinay, T. (2014). Non-intercalative, deoxyribose binding of boric acid to calf thymus DNA. *Biological Trace Element Research*, 158(2), 268–274. <https://doi.org/10.1007/s12011-014-9924-8>

Padi, M., & Quackenbush, J. (2018). Detecting phenotype-driven transitions in regulatory network structure. *Npj Systems Biology and Applications*, 4(1). <https://doi.org/10.1038/s41540-018-0052-5>

Pahl, M. V., Culver, B. D., & Vaziri, N. D. (2005). Boron and the Kidney. In *Journal of Renal Nutrition* (Vol. 15, Issue 4, pp. 362–370). <https://doi.org/10.1053/j.jrn.2005.05.001>

Park, M., Li, Q., Shcheynikov, N., Zeng, W., & Muallem, S. (2004). NaBC1 is a ubiquitous electrogenic Na⁽⁺⁾-coupled borate transporter essential for cellular boron homeostasis and cell growth and proliferation. *Molecular Cell*, 16(3), 331–341. <https://doi.org/10.1016/j.molcel.2004.09.030>

- Piest, M., & Engbersen, J. F. J. (2011). Role of boronic acid moieties in poly(amido amine)s for gene delivery. *Journal of Controlled Release*, *155*(2), 331–340. <https://doi.org/10.1016/j.jconrel.2011.07.011>
- Pimkin, M., Kossenkov, A. V., Mishra, T., Morrissey, C. S., Wu, W., Keller, C. A., Blobel, G. A., Lee, D., Beer, M. A., Hardison, R. C., & Weiss, M. J. (2014). Divergent functions of hematopoietic transcription factors in lineage priming and differentiation during erythro-megakaryopoiesis. *Genome Research*, *24*(12). <https://doi.org/10.1101/gr.164178.113>
- Poslu, K., & Arslan, I. (1995). Dünya bor mineralleri ve bileşikleri üretiminde Türkiye'nin yeri. *Endüstriyel Hammaddeler Sempozyumu*, 33–34.
- Power, P. P., & Woods, W. G. (1997). The chemistry of boron and its speciation in plants. *Plant and Soil*, *193*(1–2), 1–13. <https://doi.org/10.1023/A:1004231922434>
- Prada, I., Marchaland, J., Podini, P., Magrassi, L., D'Alessandro, R., Bezzi, P., & Meldolesi, J. (2011). REST/NRSF governs the expression of dense-core vesicle gliosecretion in astrocytes. *Journal of Cell Biology*, *193*(3). <https://doi.org/10.1083/jcb.201010126>
- Price, C. J., Marr, M. C., Myers, C. B., Seely, J. C., Heindel, J. J., & Schwetz, B. A. (1996). The developmental toxicity of boric acid in rabbits. *Fundamental and Applied Toxicology*, *34*(2), 176–187. <https://doi.org/10.1006/faat.1996.0188>
- Ravasi, T., Suzuki, H., Cannistraci, C. V., Katayama, S., Bajic, V. B., Tan, K., Akalin, A., Schmeier, S., Kanamori-Katayama, M., Bertin, N., Carninci, P., Daub, C. O., Forrest, A. R. R., Gough, J., Grimmond, S., Han, J.-H., Hashimoto, T., Hide, W., Hofmann, O., ... Hayashizaki, Y. (2010). An Atlas of Combinatorial Transcriptional Regulation in Mouse and Man. *Cell*, *140*(5), 744–752. <https://doi.org/10.1016/j.cell.2010.01.044>
- Robbins, W. a, Wei, F., Elashoff, D. a, Wu, G., Xun, L., & Jia, J. (2008). Y:X sperm ratio in boron-exposed men. *Journal of Andrology*, *29*(1), 115–121. <https://doi.org/10.2164/jandrol.107.003541>
- Robbins, W. A., Xun, L., Jia, J., Kennedy, N., Elashoff, D. A., & Ping, L. (2010). Chronic boron exposure and human semen parameters. *Reproductive Toxicology*, *29*(2), 184–190. <https://doi.org/10.1016/j.reprotox.2009.11.003>
- Roberts, R. a, Nebert, D. W., Hickman, J. a, Richburg, J. H., & Goldsworthy, T. L. (1997). Perturbation of the mitosis/apoptosis balance: a fundamental mechanism in

- toxicology. *Fundamental and Applied Toxicology : Official Journal of the Society of Toxicology*, 38(2), 107–115. <https://doi.org/10.1006/faat.1997.2331>
- Romero, M. F. (2005). Molecular pathophysiology of SLC4 bicarbonate transporters. *Current Opinion in Nephrology and Hypertension*, 14(5), 495–501. <https://doi.org/00041552-200509000-00013> [pii]
- Sakamoto, T., Tsujimoto-Inui, Y., Sotta, N., Hirakawa, T., Matsunaga, T. M., Fukao, Y., Matsunaga, S., & Fujiwara, T. (2018). Proteasomal degradation of BRAHMA promotes Boron tolerance in Arabidopsis. *Nature Communications*, 9(1). <https://doi.org/10.1038/s41467-018-07393-6>
- Saladino, R., Barontini, M., Cossetti, C., Di Mauro, E., & Crestini, C. (2011). The Effects of Borate Minerals on the Synthesis of Nucleic Acid Bases, Amino Acids and Biogenic Carboxylic Acids from Formamide. *Origins of Life and Evolution of Biospheres*, 41(4), 317–330. <https://doi.org/10.1007/s11084-011-9236-3>
- Samman, S., Naghii, M. R., Lyons Wall, P. M., & Verus, a P. (1998). The nutritional and metabolic effects of boron in humans and animals. *Biological Trace Element Research*, 66(1–3), 227–235. <https://doi.org/10.1007/BF02783140>
- Schoenherr, C. J., & Anderson, D. J. (1995). The neuron-restrictive silencer factor (NRSF): A coordinate repressor of multiple neuron-specific genes. *Science*, 267(5202). <https://doi.org/10.1126/science.7871435>
- Schubert, D. M. (2003). Borates in industrial use. In *Group 13 Chemistry III* (pp. 1–40). Springer.
- Schuller-Levis, G. B., & Park, E. (2003). Taurine: New implications for an old amino acid. In *FEMS Microbiology Letters* (Vol. 226, Issue 2). [https://doi.org/10.1016/S0378-1097\(03\)00611-6](https://doi.org/10.1016/S0378-1097(03)00611-6)
- Scialli, A. R., Bonde, J. P., Br??ske-Hohlfeld, I., Culver, B. D., Li, Y., & Sullivan, F. M. (2010). An overview of male reproductive studies of boron with an emphasis on studies of highly exposed Chinese workers. In *Reproductive Toxicology* (Vol. 29, Issue 1, pp. 10–24). <https://doi.org/10.1016/j.reprotox.2009.10.006>
- Shannon, P., Markiel, A., Ozier, O., Baliga, N. S., Wang, J. T., Ramage, D., Amin, N., Schwikowski, B., & Ideker, T. (2003). Cytoscape: A software Environment for integrated models of biomolecular interaction networks. *Genome Research*, 13(11). <https://doi.org/10.1101/gr.1239303>

- Shomron, N., & Ast, G. (2003). Boric acid reversibly inhibits the second step of pre-mRNA splicing. *FEBS Letters*, 552(2–3), 219–224. [https://doi.org/10.1016/S0014-5793\(03\)00928-1](https://doi.org/10.1016/S0014-5793(03)00928-1)
- Smyth, G. K. (2005). limma: Linear Models for Microarray Data. In *Bioinformatics and Computational Biology Solutions Using R and Bioconductor* (pp. 397–420). Springer-Verlag. https://doi.org/10.1007/0-387-29362-0_23
- Soriano-Ursúa, M. A., Farfán-García, E. D., López-Cabrera, Y., Querejeta, E., & Trujillo-Ferrara, J. G. (2014). Boron-containing acids: Preliminary evaluation of acute toxicity and access to the brain determined by Raman scattering spectroscopy. *NeuroToxicology*, 40, 8–15. <https://doi.org/10.1016/j.neuro.2013.10.005>
- Sosa-Baldivia A, Ibarra G, R., La Torre RR, R., G, G.-S., A, T., JD, E.-B., & L, R.-S. (2016). Five causes why boron essentiality on humans has not been confirmed: A hypothesis. *Integrative Food, Nutrition and Metabolism*, 4(1). <https://doi.org/10.15761/ifnm.1000170>
- Swaminathan, S. (2013). Nutritional Management of Renal Disease. In *Nutritional Management of Renal Disease*. Elsevier. <https://doi.org/10.1016/B978-0-12-391934-2.00023-0>
- Takano, J., Wada, M., Ludewig, U., Schaaf, G., von Wirén, N., & Fujiwara, T. (2006). The Arabidopsis Major Intrinsic Protein NIP5;1 Is Essential for Efficient Boron Uptake and Plant Development under Boron Limitation. *The Plant Cell*, 18(6), 1498–1509. <https://doi.org/10.1105/tpc.106.041640>
- Tavil Sabuncuoglu, B., Aribal Kocaturk, P., Yaman, O., Ozelci Kavas, G., & Tekelioglu, M. (2008). Effects of Subacute Boric Acid Administration on Rat Kidney Tissue. *Clinical Toxicology*, 44(3), 249–253. <https://doi.org/10.1080/15563650600584386>
- Toledo, L. I., Murga, M., Gutierrez-Martinez, P., Soria, R., & Fernandez-Capetillo, O. (2008). ATR signaling can drive cells into senescence in the absence of DNA breaks. *Genes and Development*. <https://doi.org/10.1101/gad.452308>
- Tombuloglu, A., Copoglu, H., Aydin-Son, Y., & Guray, N. T. (2020). In vitro effects of boric acid on human liver hepatoma cell line (HepG2) at the half-maximal inhibitory concentration. *Journal of Trace Elements in Medicine and Biology*. <https://doi.org/10.1016/j.jtemb.2020.126573>
- Topal, A., Oruç, E., Altun, S., Ceyhun, S. B., & Atamanalp, M. (2015). The effects of acute boric acid treatment on gill, kidney and muscle tissues in juvenile rainbow

- trout. *Journal of Applied Animal Research*, 44(1), 297–302. <https://doi.org/10.1080/09712119.2015.1031784>
- Touillaud, M. S., Pillow, P. C., Jakovljevic, J., Bondy, M. L., Singletary, S. E., Li, D., & Chang, S. (2005). Effect of dietary intake of phytoestrogens on estrogen receptor status in premenopausal women with breast cancer. *Nutrition and Cancer*, 51(2), 162–169. https://doi.org/10.1207/s15327914nc5102_6
- Trippier, P. C., & McGuigan, C. (2010). Boronic acids in medicinal chemistry: Anticancer, antibacterial and antiviral applications. In *MedChemComm* (Vol. 1, Issue 3). <https://doi.org/10.1039/c0md00119h>
- Tuncbag, N., Gosline, S. J. C., Kedaigle, A., Soltis, A. R., Gitter, A., & Fraenkel, E. (2016). Network-Based Interpretation of Diverse High-Throughput Datasets through the Omics Integrator Software Package. *PLoS Computational Biology*, 12(4). <https://doi.org/10.1371/journal.pcbi.1004879>
- Turkez, H. (2008). Effects of boric acid and borax on titanium dioxide genotoxicity. *Journal of Applied Toxicology*, 28(5), 658–664. <https://doi.org/10.1002/jat.1318>
- Turkez, H., & Geyikoglu, F. (2010). Boric acid: a potential chemoprotective agent against aflatoxin b(1) toxicity in human blood. *Cytotechnology*, 62(2), 157–165. <https://doi.org/10.1007/s10616-010-9272-2>
- Turkez, H., Geyikoglu, F., Tatar, A., Keles, M. S., & Kaplan, I. (2012). The effects of some boron compounds against heavy metal toxicity in human blood. *Experimental and Toxicologic Pathology*, 64(1–2), 93–101. <https://doi.org/10.1016/j.etp.2010.06.011>
- Turkez, H., Tatar, A., Hacimuftuoglu, A., & Ozdemir, E. (2010). Boric acid as a protector against paclitaxel genotoxicity. *Acta Biochimica Polonica*, 57(1), 95–97.
- Ulusik, I., Kaya, A., Fomenko, D. E., Karakaya, H. C., Carlson, B. A., Gladyshev, V. N., & Koc, A. (2011). Boron stress activates the general amino acid control mechanism and inhibits protein synthesis. *PLoS ONE*, 6(11). <https://doi.org/10.1371/journal.pone.0027772>
- Ulusik, I., Kaya, A., Unlu, E. S., Avsar, K., Karakaya, H. C., Yalcin, T., & Koc, A. (2011). Genome-wide identification of genes that play a role in boron stress response in yeast. *Genomics*, 97(2), 106–111. <https://doi.org/10.1016/j.ygeno.2010.10.006>
- Ustündağ, A., Behm, C., Föllmann, W., Duydu, Y., & Degen, G. H. (2014). Protective effect of boric acid on lead- and cadmium-induced genotoxicity in V79 cells.

- Archives of Toxicology*, 88(6), 1281–1289. <https://doi.org/10.1007/s00204-014-1235-5>
- Wei, Y., Yuan, F. J., Zhou, W. B., Wu, L., Chen, L., Wang, J. J., & Zhang, Y. S. (2016). Borax-induced apoptosis in HepG2 cells involves p53, Bcl-2, and Bax. *Genetics and Molecular Research*, 15(2). <https://doi.org/10.4238/gmr.15028300>
- Weir, R. J., & Fisher, R. S. (1972). Toxicologic studies on borax and boric acid. *Toxicology and Applied Pharmacology*, 23(3), 351–364. [https://doi.org/10.1016/0041-008X\(72\)90037-3](https://doi.org/10.1016/0041-008X(72)90037-3)
- Whorton, D., Haas, J., & Trent, L. (1994). Reproductive effects of inorganic borates on male employees: Birth rate assessment. *Environmental Health Perspectives*, 102(SUPPL. 7), 129–132.
- Wilson, N. K., Foster, S. D., Wang, X., Knezevic, K., Schütte, J., Kaimakis, P., Chilarska, P. M., Kinston, S., Ouwehand, W. H., Dzierzak, E., Pimanda, J. E., De Bruijn, M. F. T. R., & Göttgens, B. (2010). Combinatorial transcriptional control in blood stem/progenitor cells: Genome-wide analysis of ten major transcriptional regulators. *Cell Stem Cell*, 7(4). <https://doi.org/10.1016/j.stem.2010.07.016>
- Winker, R., Roos, G., Pilger, A., & Rüdiger, H. W. (2008). Effect of occupational safety measures on micronucleus frequency in semiconductor workers. *International Archives of Occupational and Environmental Health*, 81(4), 423–428. <https://doi.org/10.1007/s00420-007-0229-5>
- Wong, L. C., Heimbach, M. D., Truscott, D. R., & Duncan, B. D. (1964). Boric acid poisoning: Report of 11 cases. *Canadian Medical Association Journal*, 90, 1018–1023.
- Yamaguchi, K., Yang, L., McCall, S., Huang, J., Xing, X. Y., Pandey, S. K., Bhanot, S., Monia, B. P., Li, Y. X., & Diehl, A. M. (2007). Inhibiting triglyceride synthesis improves hepatic steatosis but exacerbates liver damage and fibrosis in obese mice with nonalcoholic steatohepatitis. *Hepatology*, 45(6). <https://doi.org/10.1002/hep.21655>
- Ying, X., Cheng, S., Wang, W., Lin, Z., Chen, Q., Zhang, W., Kou, D., Shen, Y., Cheng, X., Rompis, F. A., Peng, L., & Lu, C. Z. (2011). Effect of boron on osteogenic differentiation of human bone marrow stromal cells. *Biological Trace Element Research*, 144(1–3), 306–315. <https://doi.org/10.1007/s12011-011-9094-x>
- Young, E. G., Smith, R. P., & MacIntosh, O. C. (1949). Boric acid as a poison: Report of six accidental deaths in infants. *Canadian Medical Association Journal*, 61(5), 447.

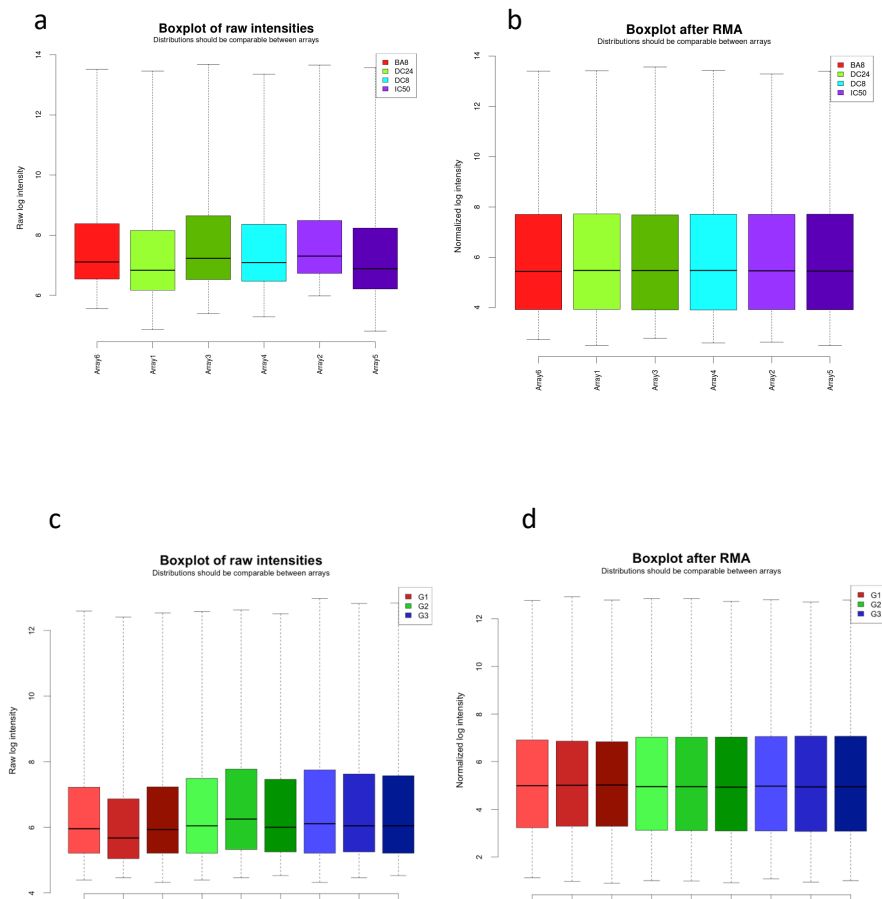
Zatloukal, K., Stumtner, C., Fuchsbichler, A., & Denk, H. (2006). Keratins as Targets in and Modulators of Liver Diseases. In *Intermediate Filaments*. https://doi.org/10.1007/0-387-33781-4_9

Zhao, X., Xiaoli, Zong, H., Abdulla, A., Yang, E. S. T., Wang, Q., Ji, J. Y., Pessin, J. E., Das, B. C., & Yang, F. (2014). Inhibition of SREBP transcriptional activity by a boron-containing compound improves lipid homeostasis in diet-induced obesity. *Diabetes*, *63*(7), 2464–2473. <https://doi.org/10.2337/db13-0835>

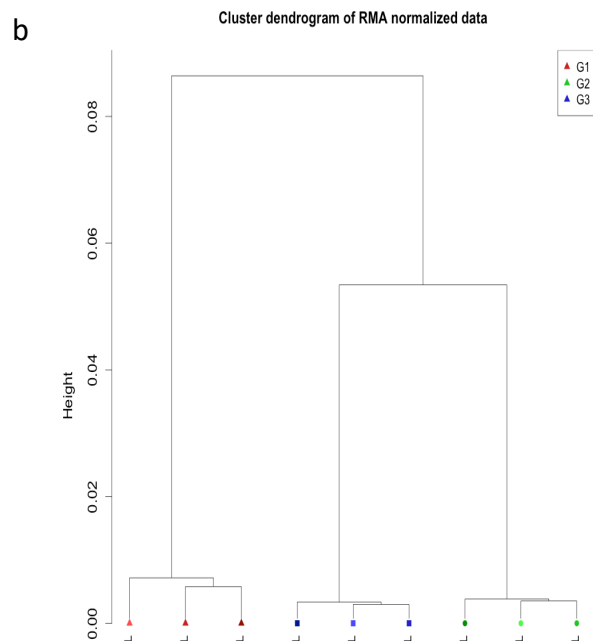
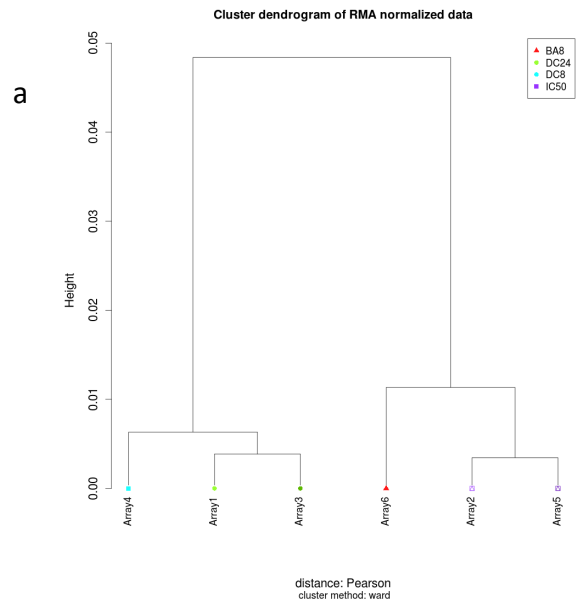
APPENDIX

App. Table 1: RNA concentrations and quality metrics before Microarray hybridizations

RNA Sample	RNA concentration (ng/uL)	Total amount (ug)	A_{260}/A_{280}	A_{260}/A_{230}
IC25-1	51.0	5.0	2.00	1.43
IC25-2	180.0	17.6	1.97	1.80
IC25-3	209.4	20.5	2.00	1.85
IC12.5-1	432.0	42.3	1.94	2.12
IC12.5-2	48.6	4.8	2.06	1.76
IC12.5-3	92.7	9.1	2.01	1.88
Control-1	118.9	11.7	2.03	1.57
Control-2	164.5	16.1	1.94	2.05
Control-3	172.5	16.9	2.01	2,05

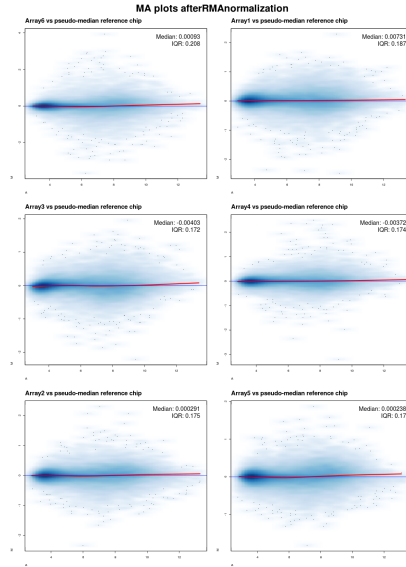


App. Figure 1: Boxplots of microarray log-signal intensities a, b) Raw and RMA normalized intensities of IC₅₀ and control samples (Dataset 1) c, d) Raw, RMA normalized intensities of IC₂₅, IC_{12.5} and control samples (Dataset 2)

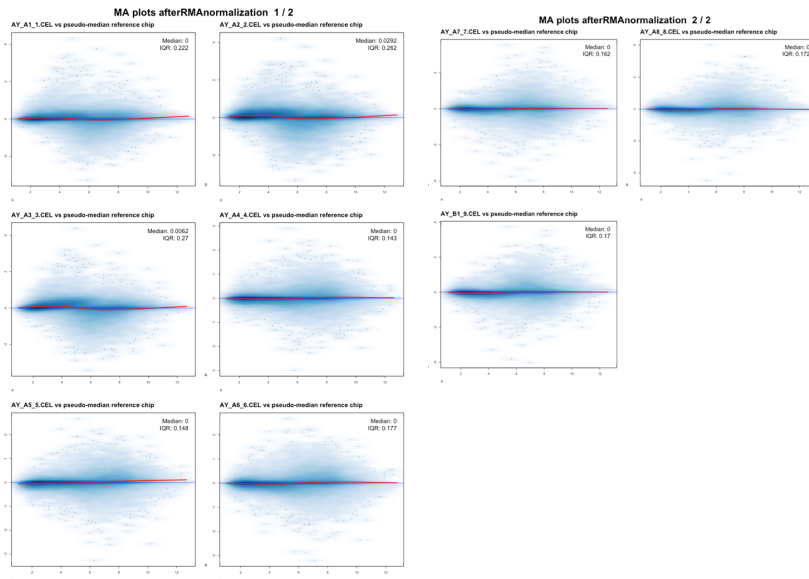


App. Figure 2: Cluster dendograms of a) IC₅₀ and control samples (Dataset 1)
b) IC₂₅, IC_{12.5} and control samples (Dataset 2)

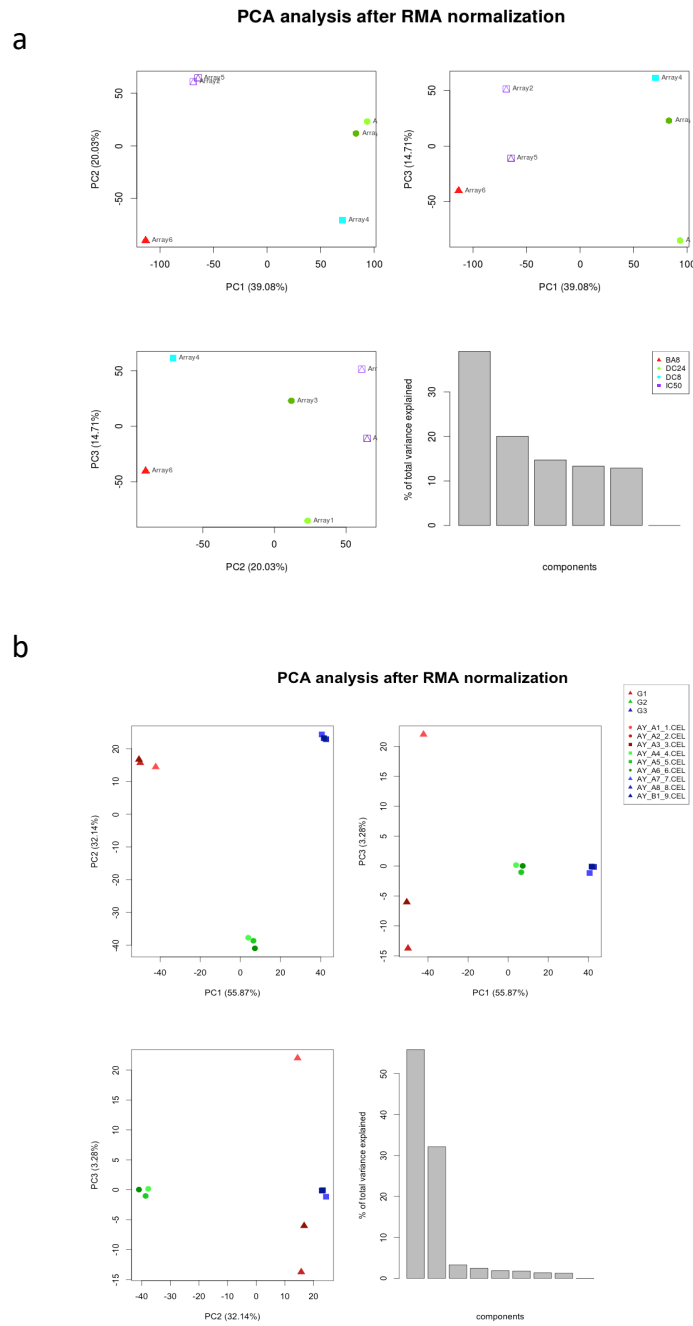
a



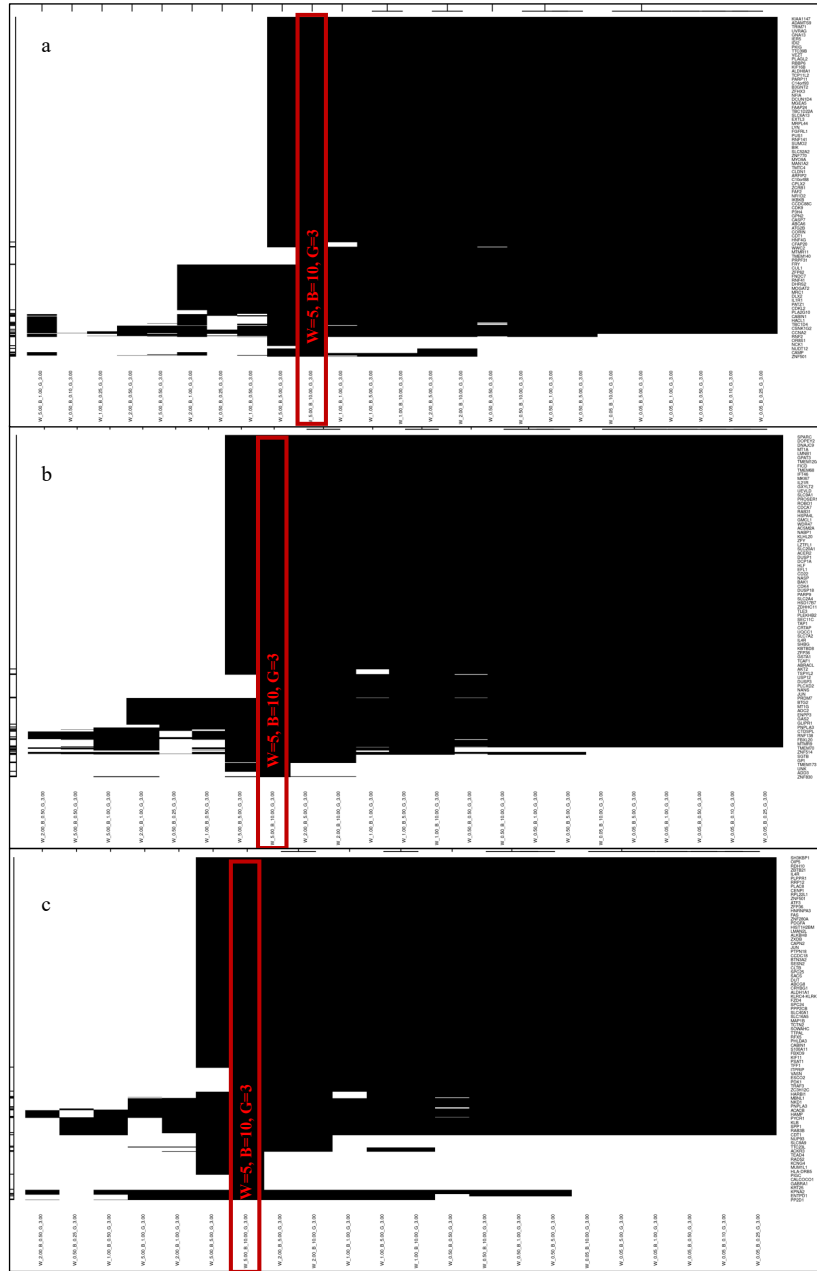
b



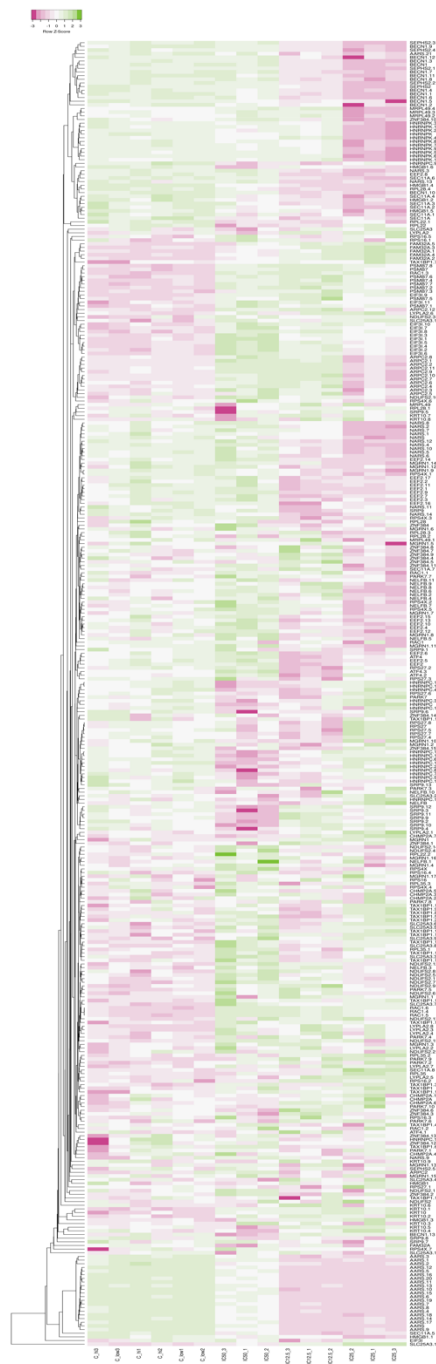
App. Figure 3: MA plots of a) IC₅₀ and control samples (Dataset 1) b) IC₂₅, IC_{12.5} and control samples (Dataset 2)



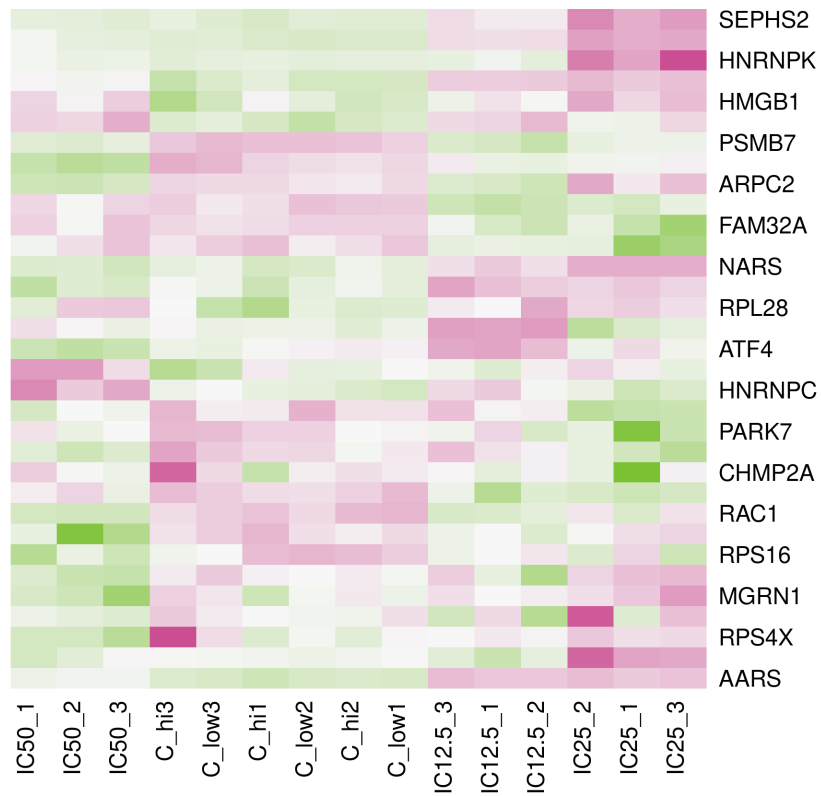
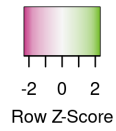
App. Figure 4: PCA plots of a) IC₅₀ and control samples (Dataset 1) b) IC₂₅, IC_{12.5} and control samples (Dataset 2)



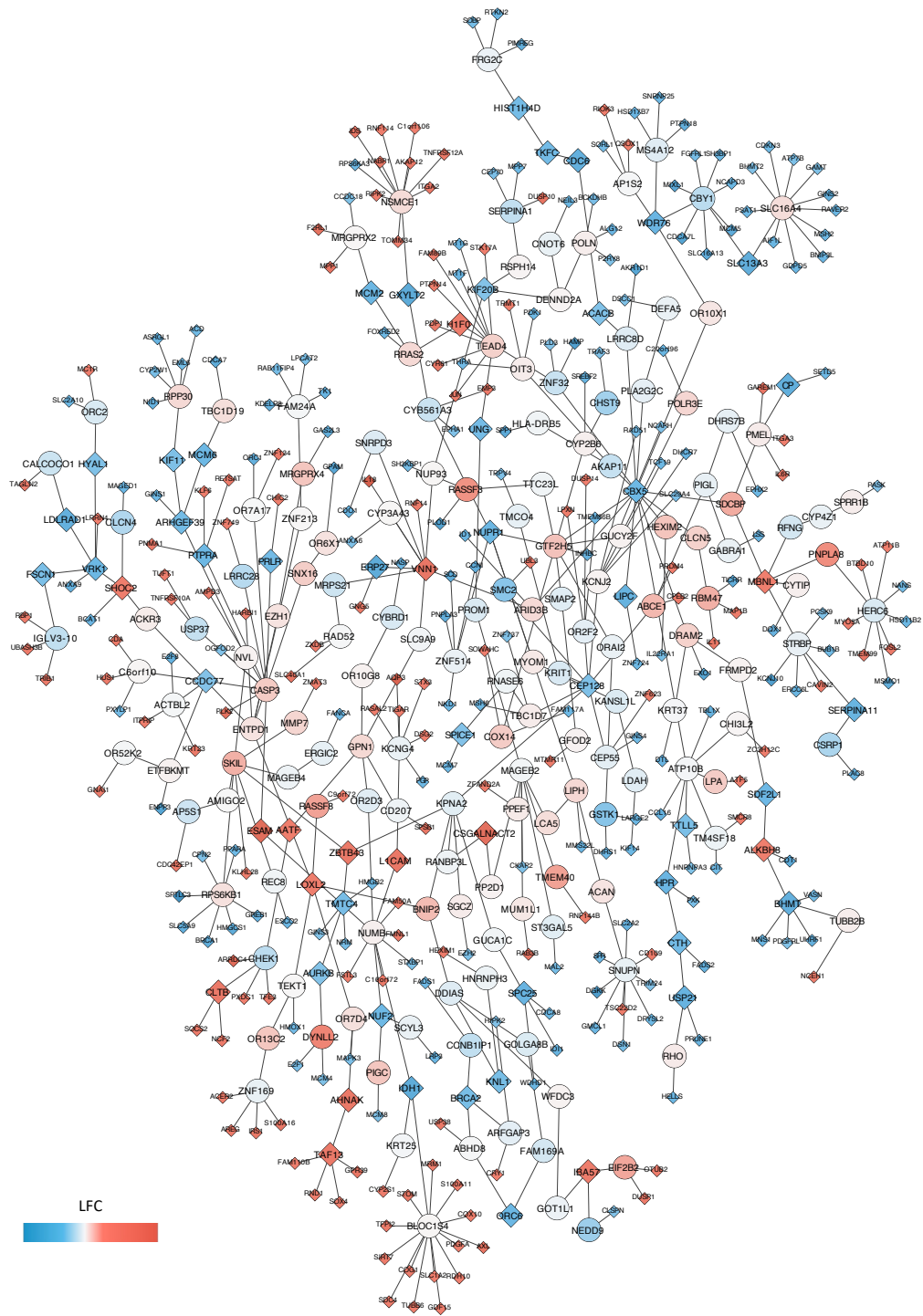
App. Figure 5: Parameter selection at the construction of optimal coregulatory subgraphs



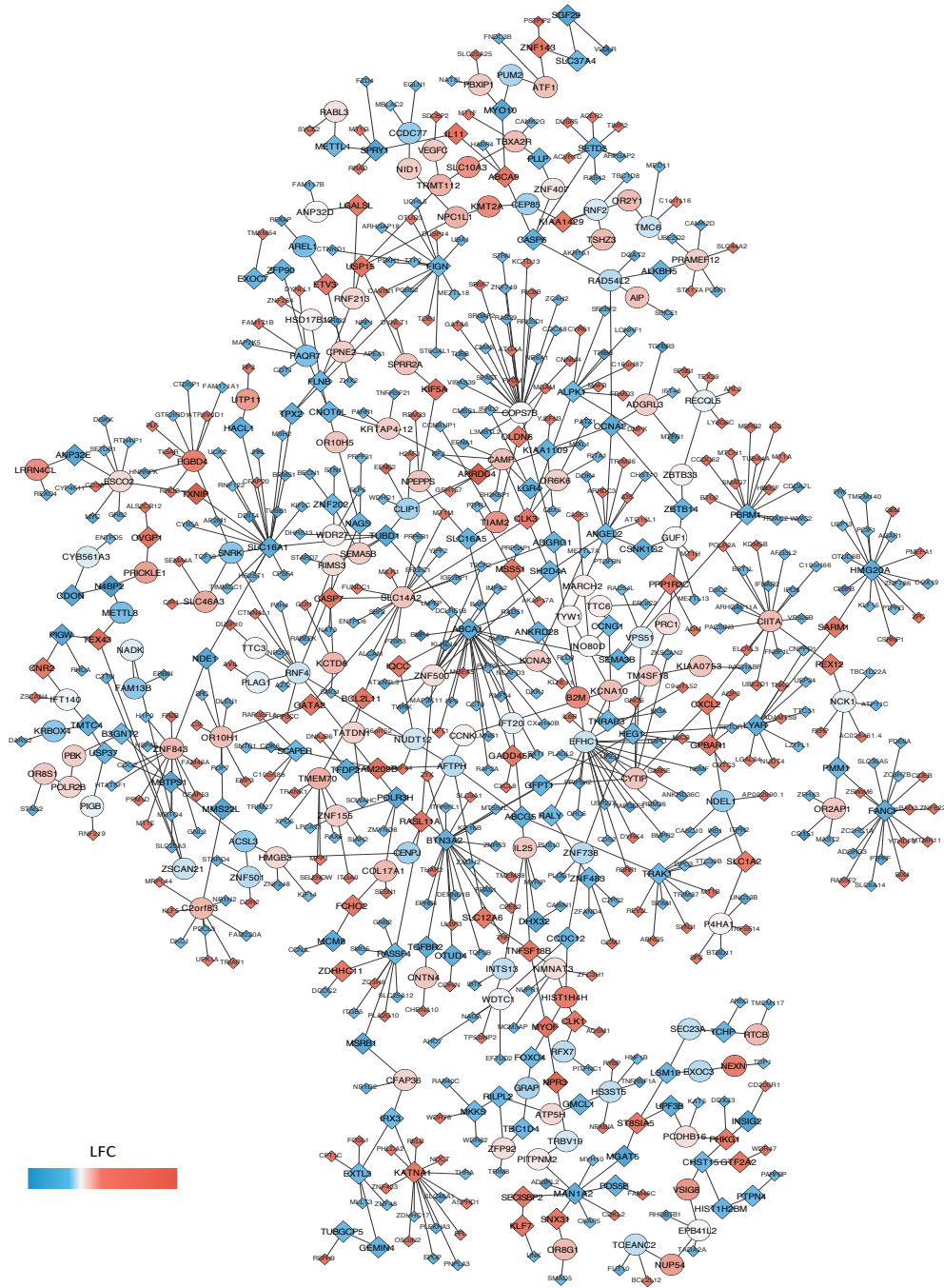
App. Figure 6: Heatmap of the top 2500 genes with the highest variance in fRMA normalized microarray samples



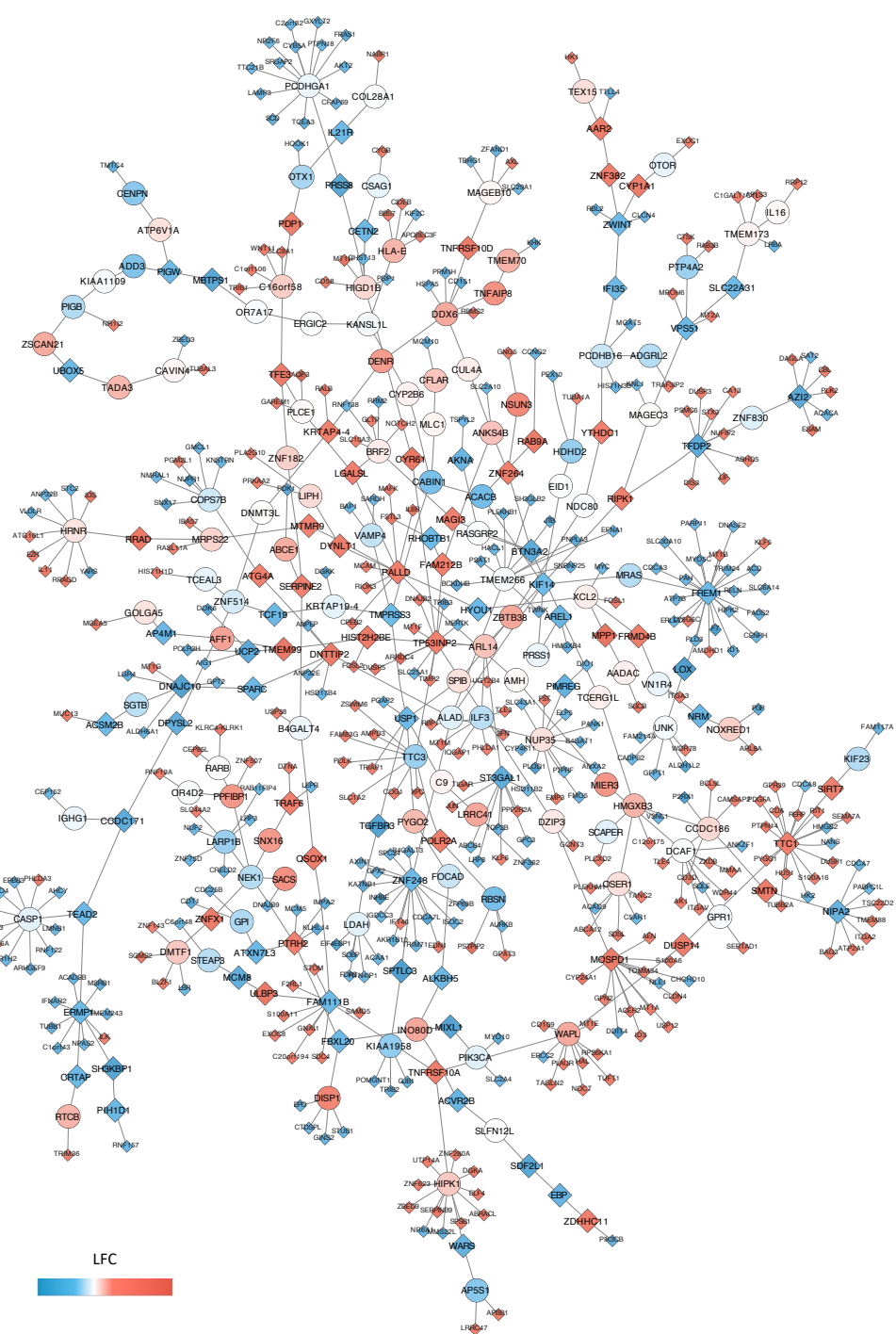
App. Figure 7: Heatmap of the known housekeeping genes of fRMA normalized microarray samples



App. Figure 8: Optimal coregulatory graph at IC_{50} , o: Steiner, \diamond : Terminal, LFC: $[-3.4, 4]$



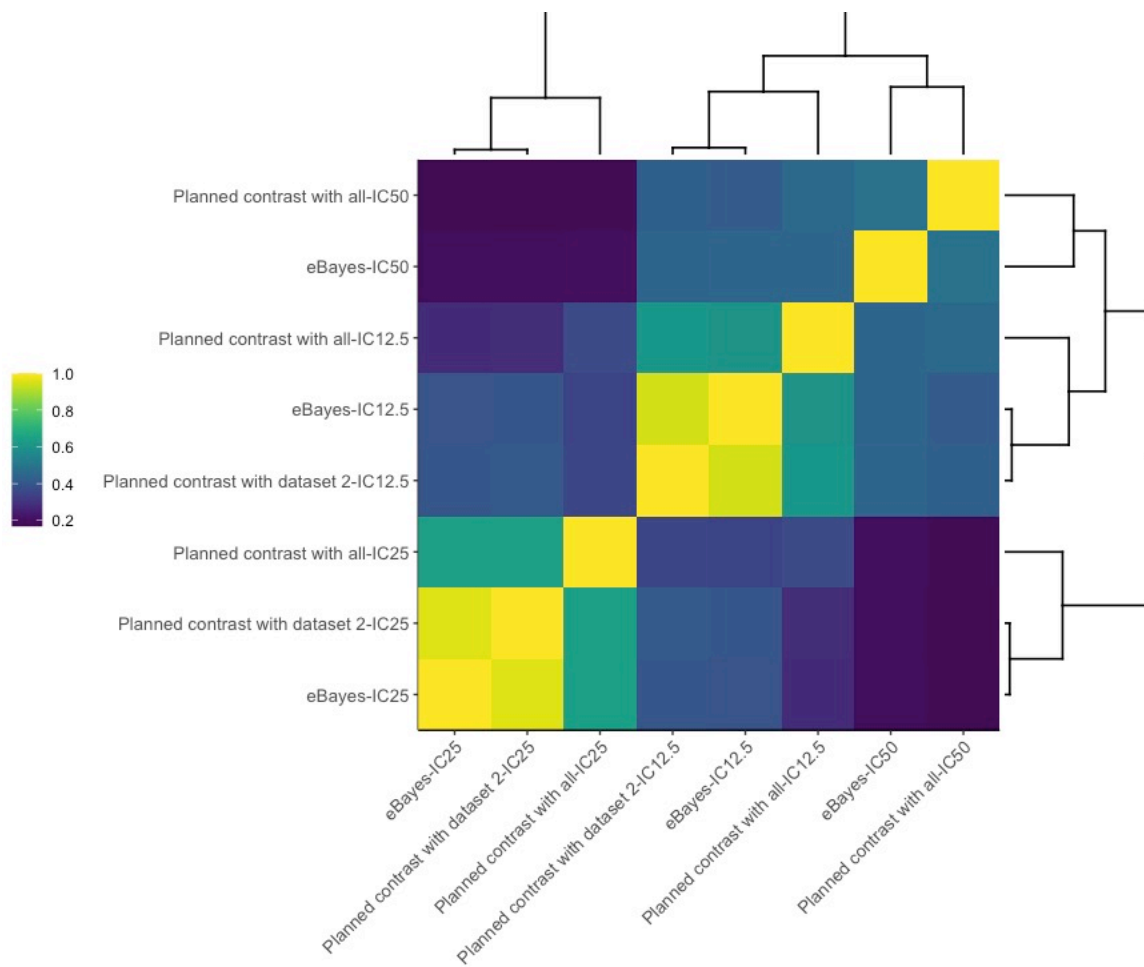
App. Figure 9: Optimal coregulatory graph at IC₂₅, ○: Steiner, ◇: Terminal, LFC: [-3.5,5.6]



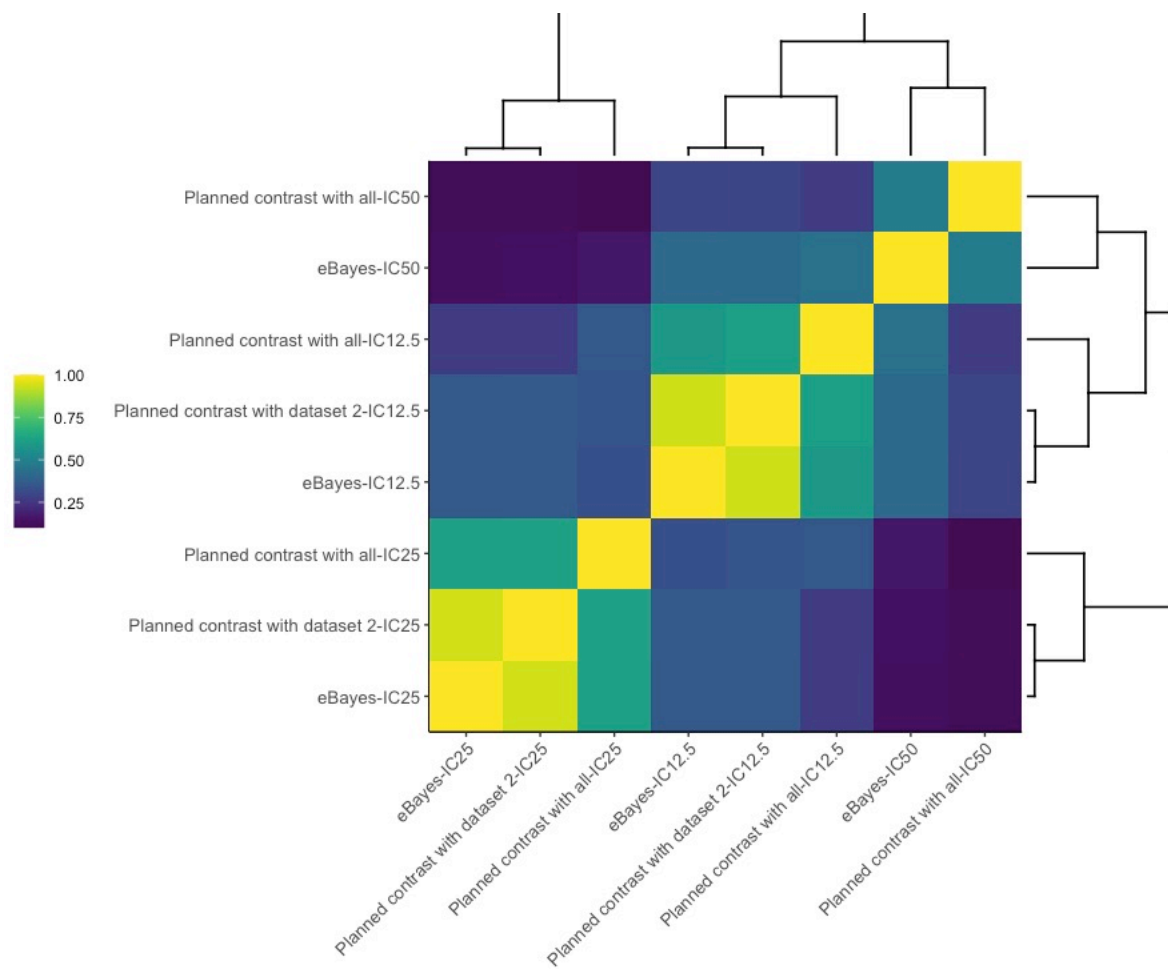
App. Figure 10: Optimal coregulatory graph at IC_{12.5}, o: Steiner, \diamond : Terminal, LFC: [-3, 4.2]

App. Table 2: A summary of the statistical tests used for validation

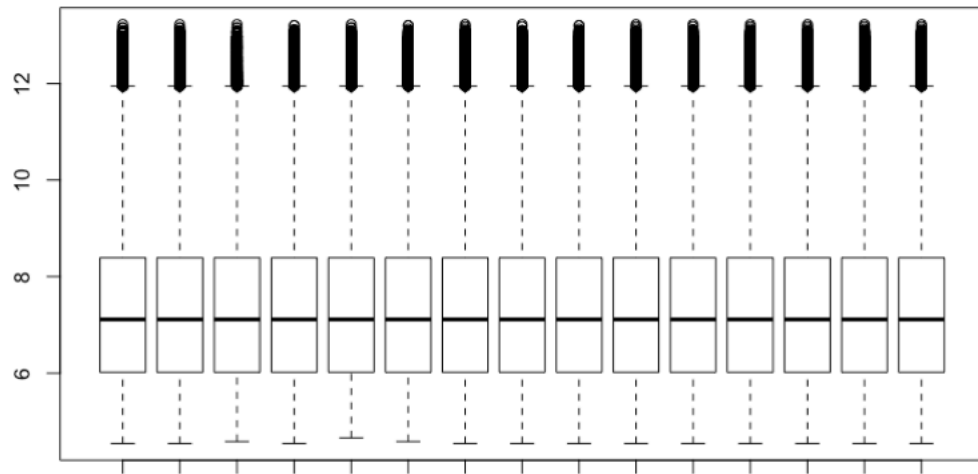
Test	Reading files	Preprocessing	Contrasts	Multiple hypothesis testing	Number of DE transcripts (IC ₅₀)	Number of DE transcripts (IC ₂₅)	Number of DE transcripts (IC _{12.5})
ANOVA for all three (Method 1)	AffyBatch + hugene10sthsenstcdf	vsrma + quantile normalization	IC ₅₀ -Control, IC ₂₅ -Control, IC _{12.5} -Control	1)Separate	2103(D) + 1295 (U) = 3398 transcripts	5893 (D)+3694 (U) = 9587 transcripts	4031 (D)+3078 (U) =7109 transcripts
ANOVA for all three (Method 2)	AffyBatch + hugene10sthsenstcdf (V23)	vsrma + quantile normalization	IC ₅₀ -Control, IC ₂₅ -Control, IC _{12.5} -Control	2)Global	2110(D) + 1295 (U) =3405 transcripts	5980 (D) +3693 (U) = 9673 transcripts	4031 (D) +3177 (U)= 7208 transcripts
eBayes separately for all	oligo + pd.hugene10sthsenst (V23)	rma	–	–	4311(D) + 2805 (U) =7116 transcripts	13652 (D) + 6372 (U) = 20024 transcripts	8586(D)+ 5446 (U)=14032 transcripts
ANOVA for IC₂₅ and IC_{12.5} batch (repetition - thesis)	oligo + pd.hugene10sthsenst (V23)	rma	IC ₂₅ -IC _{12.5} , IC ₂₅ -Control, IC _{12.5} -Control	Separate	–	13425 (D) +6218 (U) = 19643 transcripts	8489 (D) + 5326 (U) = 13815 transcripts



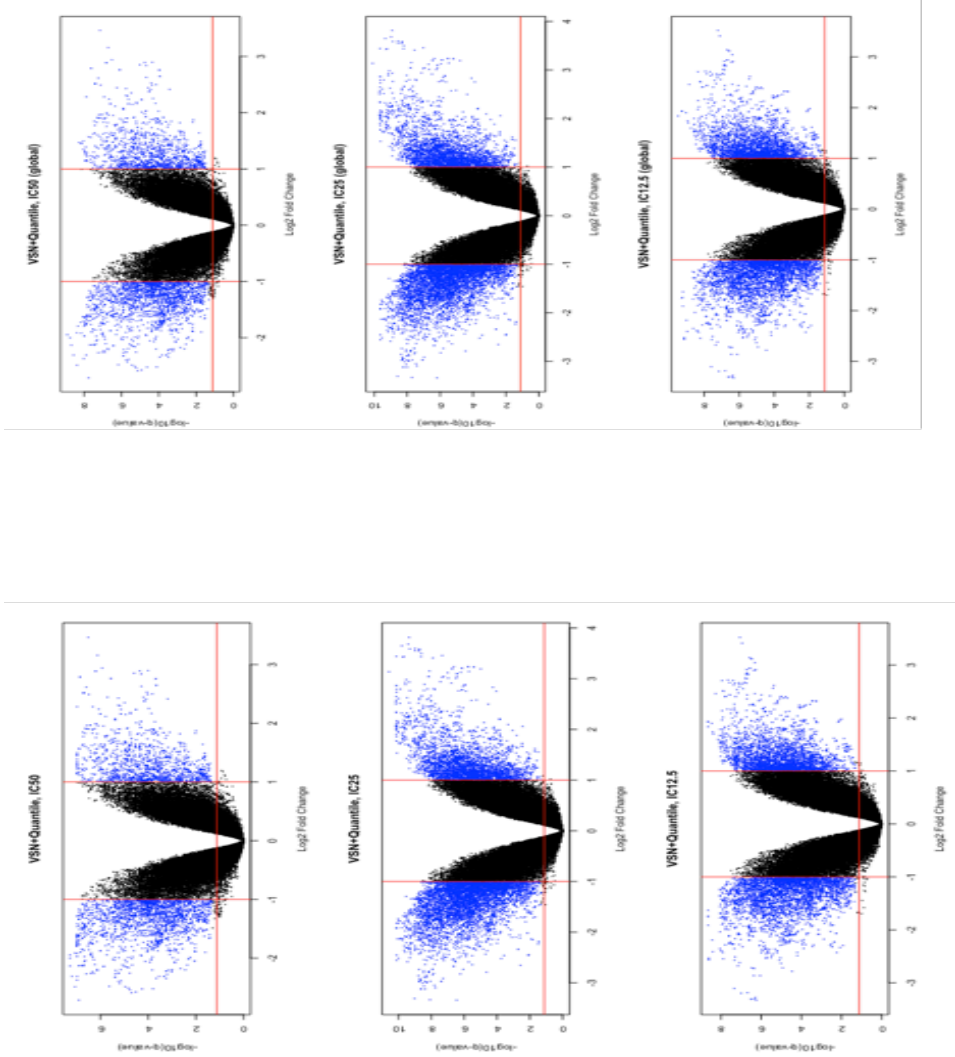
App. Figure 11: Map of downregulated gene lists found in the statistical tests



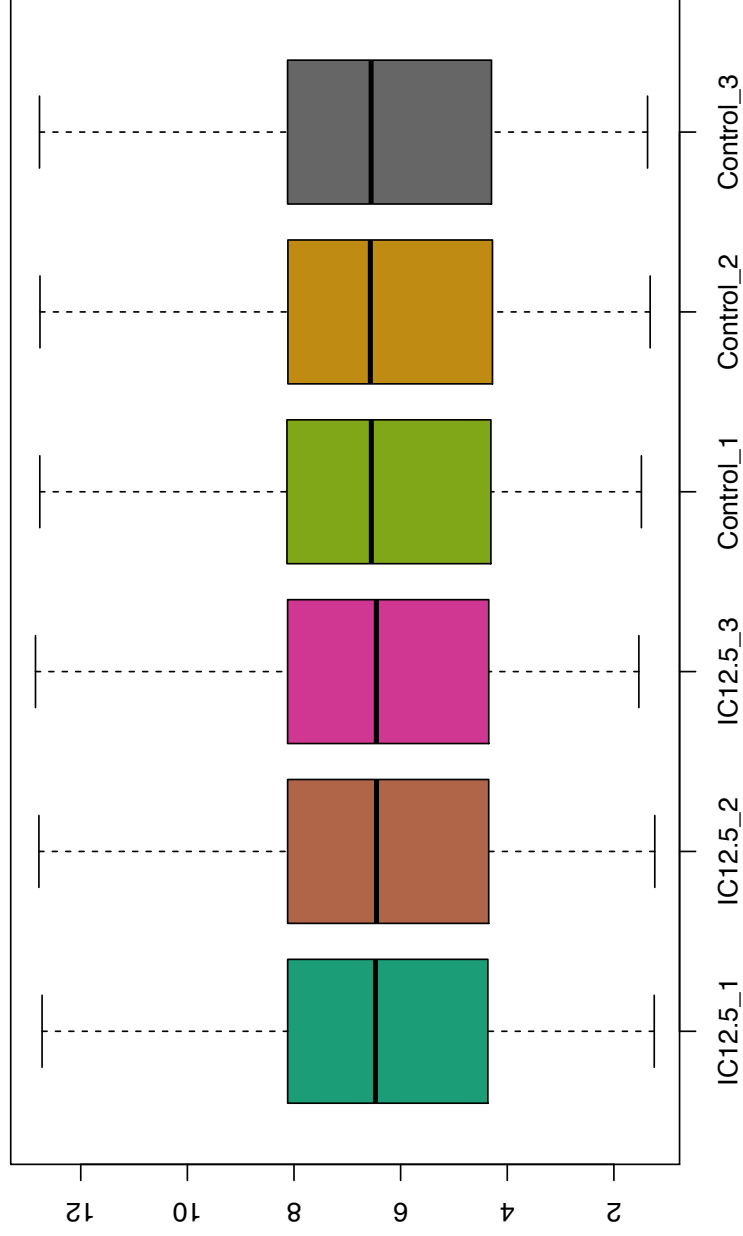
App. Figure 12: Map of upregulated gene lists found in the statistical tests



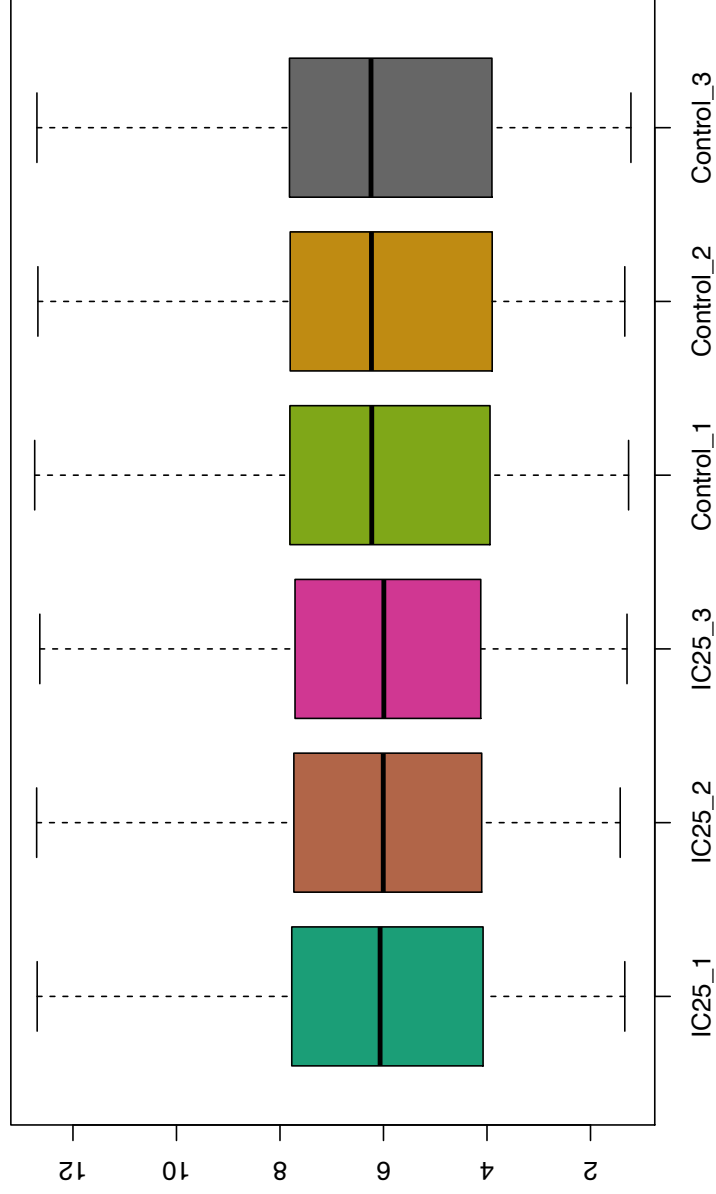
App. Figure 13: Boxplots of microarrays after vsn+quantile normalization



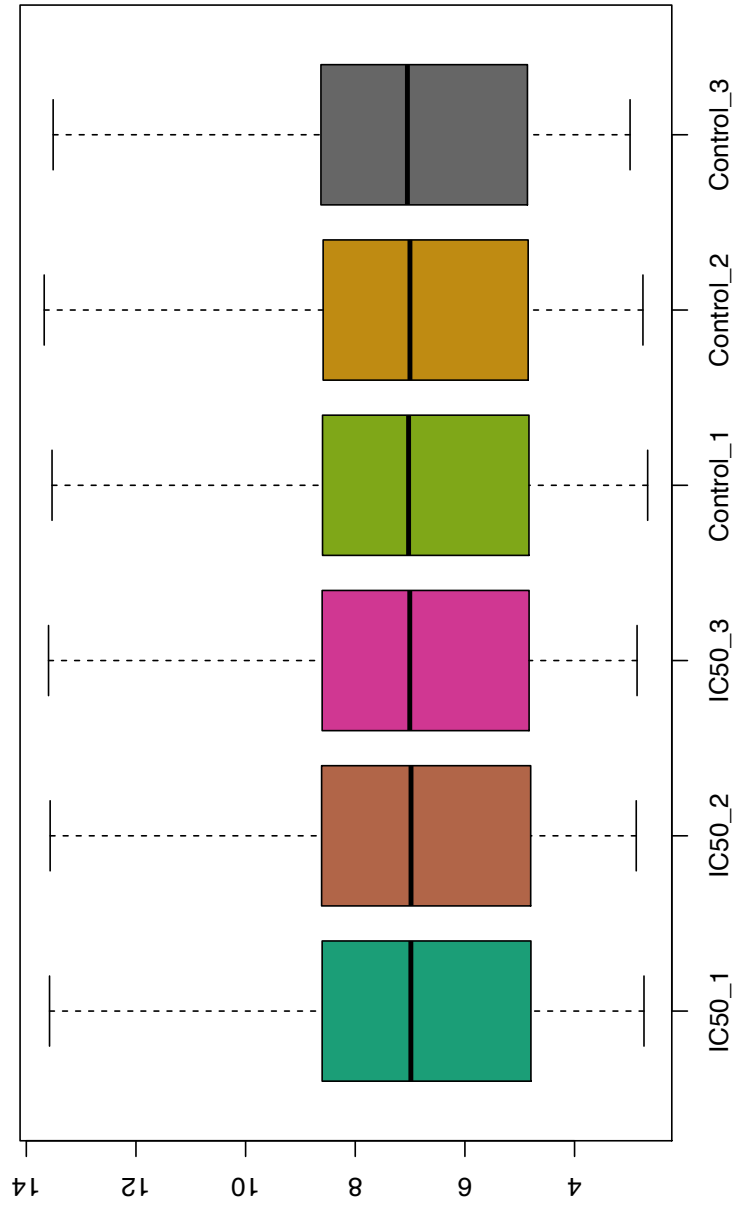
App. Figure 14: Volcano plots obtained from VSN+quantile normalized datasets



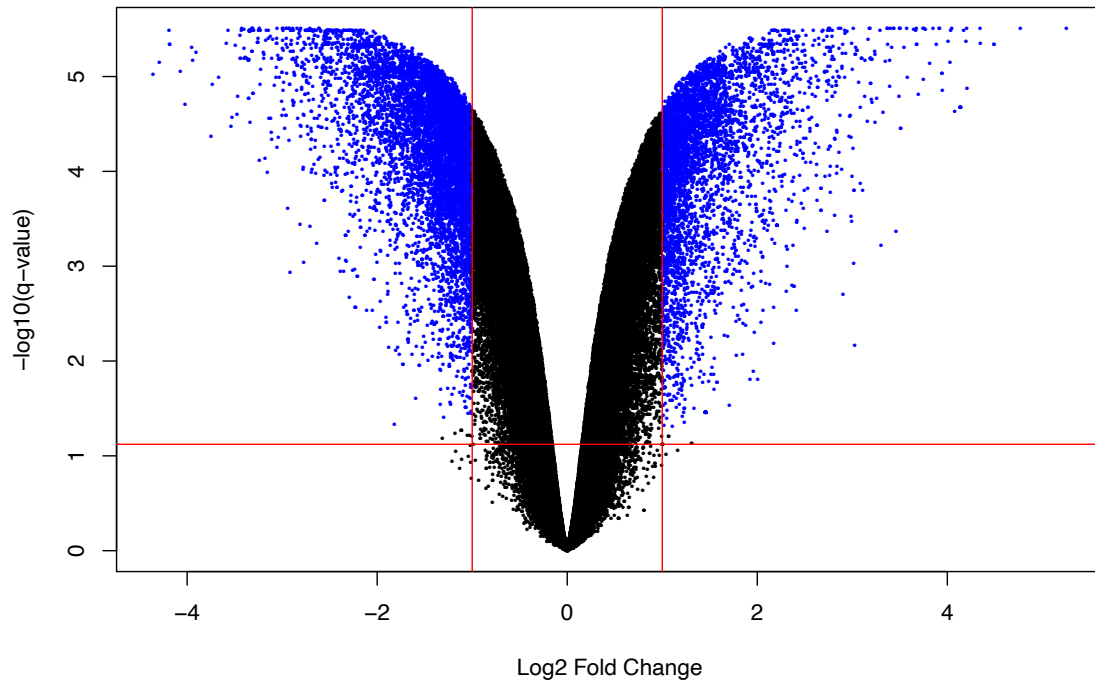
App. Figure 15: Boxplots of IC_{12.5} dataset after rna normalization (standalone eBayes test)



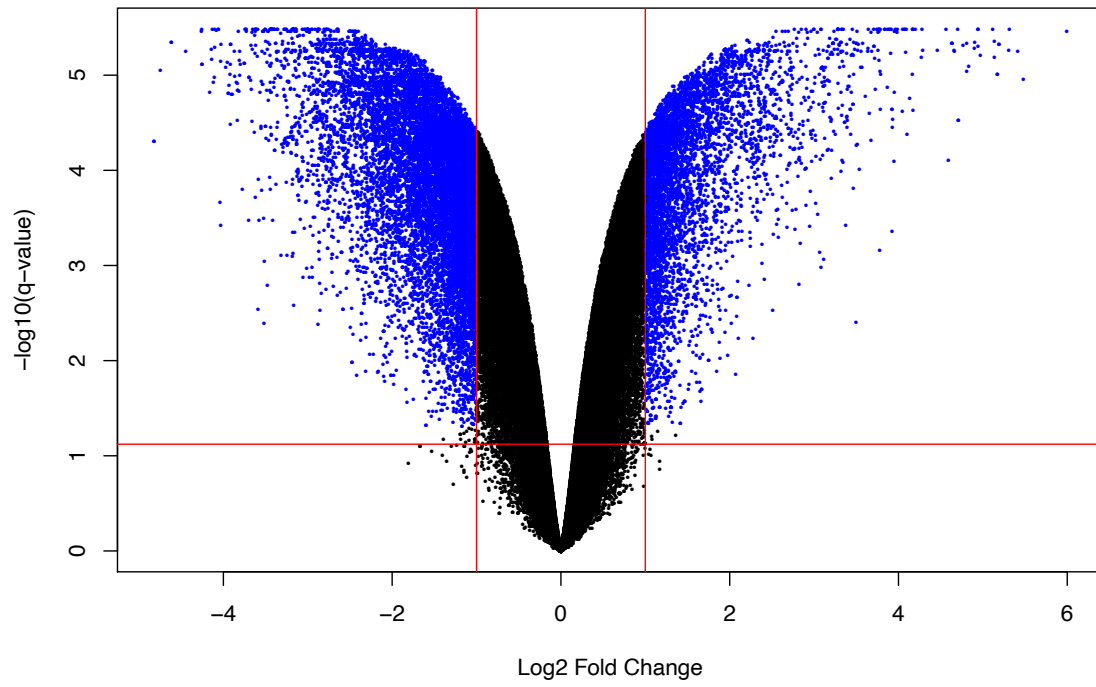
App. Figure 16: Boxplots of IC₂₅ dataset after rma normalization (standalone eBayes test)



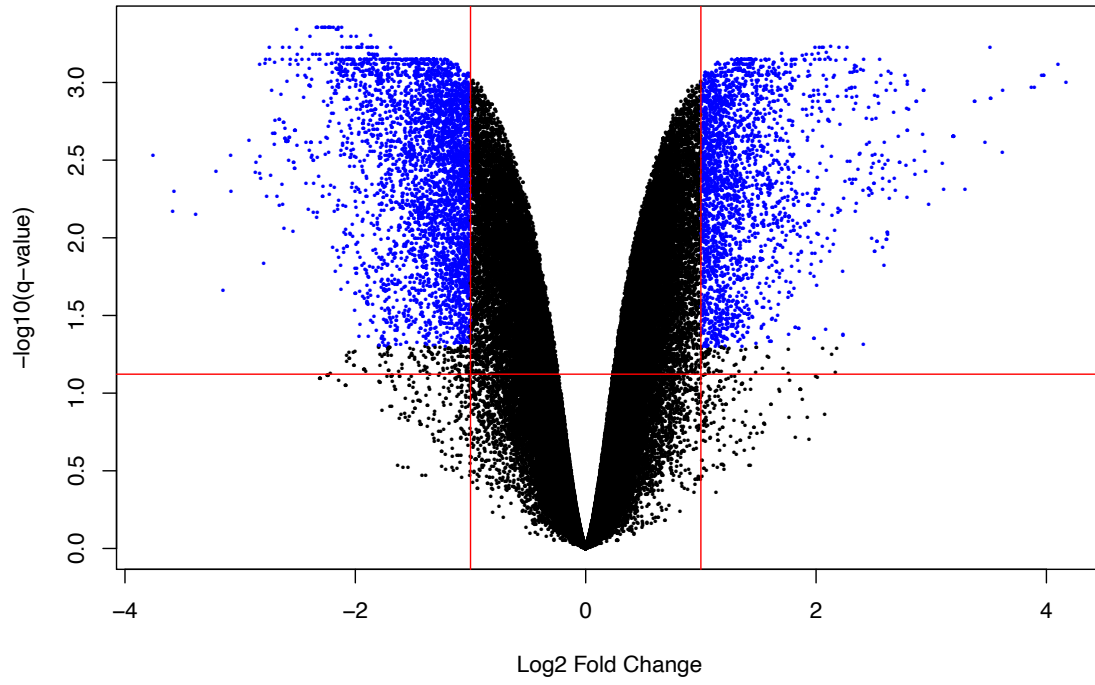
App. Figure 17: Boxplots of IC₅₀ dataset after rma normalization (standalone eBayes test)



App. Figure 18: Volcano plot of the eBayes test results of $IC_{12.5}$



App. Figure 19: Volcano plot of the eBayes test results of IC₂₅



App. Figure 20: Volcano plot of the eBayes test results of IC₅₀

CURRICULUM VITAE

PERSONAL INFORMATION

Surname, Name: Tombulođlu Ayşegül
email: aysegultombuloglu@gmail.com

EDUCATION

Degree	Institution	Year of Graduation
MS	Ihsan Dogramaci Bilkent University	2012
BS	Istanbul Technical University	2009

RESEARCH EXPERIENCE

Year	Position
2019-2022	Project Manager of Fast Support Project funded by TUBITAK
2015-2021	Research Assistant at Middle East Technical University
2009-2012	Research Assistant at Ihsan Dogramaci Bilkent University

HIGHLIGHTED PUBLICATION

- In vitro effects of boric acid on human liver hepatoma cell line (HepG2) at the half-maximal inhibitory concentration, Tombuloglu, A, Copoglu, H, Aydin-Son, Y, & Guray, NT, Journal of Trace Elements in Medicine and Biology, 2020, 126573.

FOREIGN LANGUAGES

Native Turkish, Advanced English, Beginner German